TU Delft

Delft University of Technology

Chenier Dynamics

Tas, S.A.J.

DOI
10.4233/uuid:d4c0062c-9191-40e4-805a-72fe7afde7bd

Publication date
2022

Document Version
Final published version

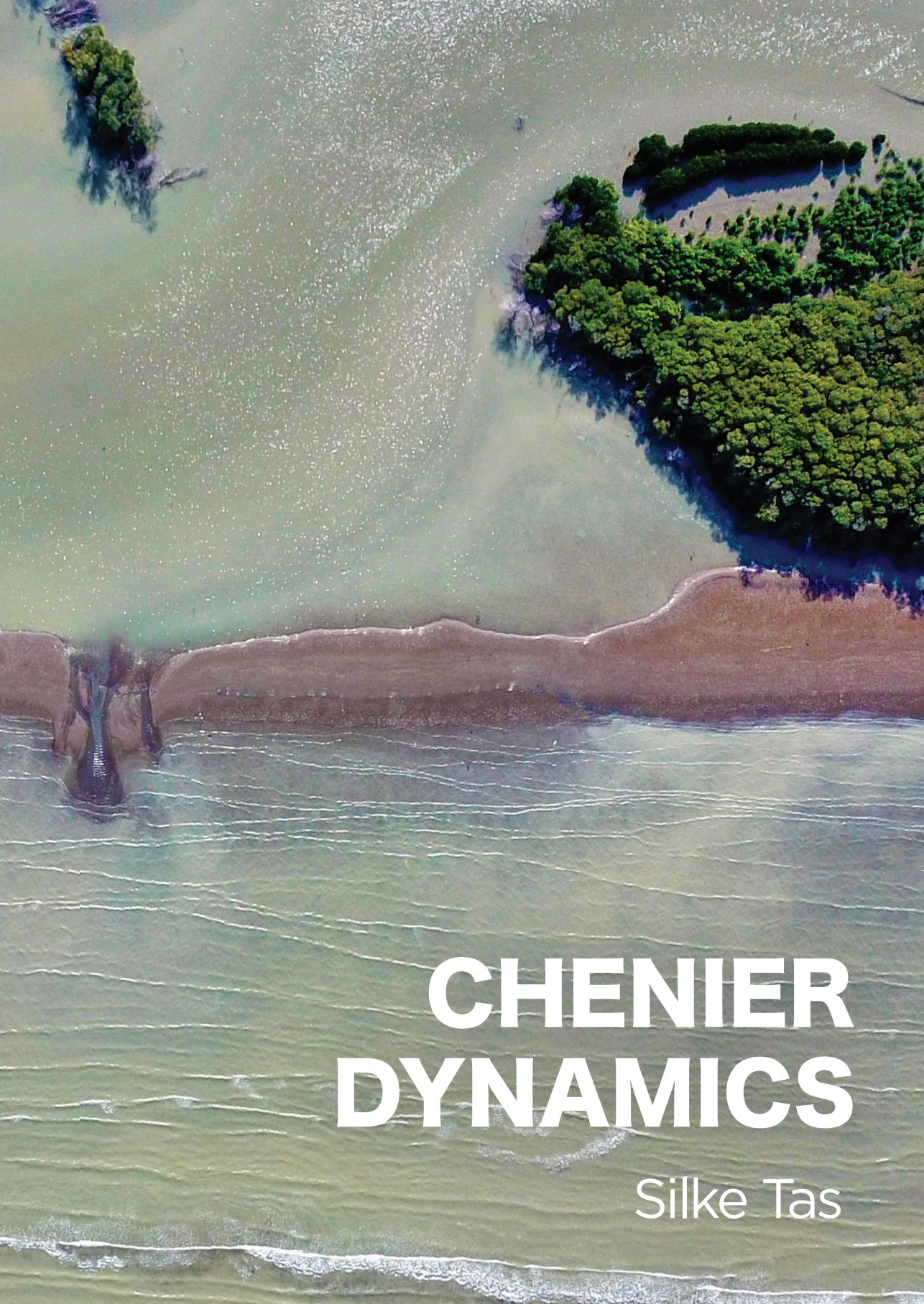
Citation (APA)
Tas, S. A. J. (2022). *Chenier Dynamics*. [Dissertation (TU Delft), Delft University of Technology]. https://doi.org/10.4233/uuid:d4c0062c-9191-40e4-805a-72fe7afde7bd

Important note
To cite this publication, please use the final published version (if applicable).
Please check the document version above.

Copyright
Other than for strictly personal use, it is not permitted to download, forward or distribute the text or part of it, without the consent of the author(s) and/or copyright holder(s), unless the work is under an open content license such as Creative Commons.

Takedown policy
Please contact us and provide details if you believe this document breaches copyrights.
We will remove access to the work immediately and investigate your claim.

This work is downloaded from Delft University of Technology.
For technical reasons the number of authors shown on this cover page is limited to a maximum of 10.



CHENIER DYNAMICS

Silke Tas

Chenier Dynamics

Silke Tas

Chenier Dynamics

DISSERTATION

for the purpose of obtaining the degree of doctor
at Delft University of Technology
by the authority of the Rector Magnificus,
prof. dr. ir. T.H.J.J. van der Hagen,
chair of the Board for Doctorates
to be defended publicly on
Monday 4 July 2022 at 10:00 o'clock

by

Silke Andrea Judith TAS

Civil Engineer,
Delft University of Technology, the Netherlands
born in Ghent, Belgium.

This dissertation has been approved by the promotor.

Composition of the doctoral committee:

Rector Magnificus,	chairperson
Prof. dr. ir. A.J.H.M. Reniers	Delft University of Technology, promotor

Independent members:

Prof. dr. ir. S.G.J. Aarninkhof	Delft University of Technology
Prof. dr. E.J. Anthony	Aix-Marseille University & CEREGE, France
Prof. dr. P. Hoekstra	Utrecht University
Dr. M. Helmi	Universitas Diponegoro, Indonesia
Prof. dr. ir. W.S.J. Uijttewaal	Delft University of Technology, reserve member

Other members:

Prof. dr. D.S. van Maren	East China Normal University, Delft University of Technology & Deltares
Prof. dr. ir. J.C. Winterwerp	Delft University of Technology

This work is part of the BioManCO project with project number 14753, which is (partly) financed by NWO Domain Applied and Engineering Sciences, and co-financed by Boskalis Dredging and Marine Experts, Van Oord Dredging and Marine Contractors bv, Deltares, Witteveen+Bos and Wetlands International. The BioManCO project is a collaboration between TU Delft, NIOZ and UNDIP and makes use of the framework set up by Building with Nature Indonesia, a programme by Ecoshape, Wetlands International, the Indonesian Ministry of Marine Affairs and Fisheries (MMAF), the Indonesian Ministry of Public Works and Housing (PU) and other partners.

Keywords: chenier, morphodynamics, modelling, sediment transport, mangroves

Cover: photo by Silke Tas, design by Jana Onzo

Printing: Ridderprint

ISBN 978-94-6366-576-6

Copyright ©2022 by Silke Tas

All rights reserved. No part of the material protected by this copyright notice may be reproduced or utilized in any form or by any means, electronic or mechanical, including photocopying, recording or by any information storage and retrieval system, without the prior permission of the author.

Typeset by the author with the LaTeX Documentation System.

Contents

	Summary	v
	Samenvatting	vii
	Ringkasan	ix
1	Introduction	1
2	Study area: Demak, Indonesia	9
3	Observations of cross-shore chenier dynamics	19
4	Drivers of cross-shore chenier dynamics	41
5	Chenier formation through wave winnowing and tidal transport	67
6	The role of cheniers in stabilising mangrove-mud coasts	89
	Bibliography	99
	List of symbols	117
	Acknowledgements	121
	List of Publications	123
	Curriculum Vitae	125

Summary

Over the last decades, mangrove forests have suffered immense and rapid losses worldwide. In recognition of their important socio-economic and environmental functions, many attempts have been made to both protect the remaining mangrove coastlines and restore eroding sites. Unfortunately, many rehabilitation attempts have failed, lacking a thorough system understanding of mangrove-mud coasts.
Some mangrove-mud coasts are protected on their seaward side by sandy ridges (called 'cheniers'). They protect against wave attack and can help to protect vulnerable mangrove-mud coastlines. In order to sustainably restore mangrove coasts, chenier dynamics need to be understood at the temporal and spatial scales relevant for mangrove establishment (daily to yearly variability driven by waves and tides). This dissertation aims to advance our understanding of chenier dynamics within the context of an eroding mangrove-mud coast. The severely eroded coastline of Demak, Indonesia, is used as a case study.
We started with a field campaign in Demak, observing the cross-shore dynamics of a single chenier. The observations revealed that cheniers can be very dynamic in relatively calm conditions. Using velocity moments as a proxy for the sediment transport, we have explored the role of tides and waves in the observed chenier dynamics. Tides drive the chenier landward, especially when the water depth over the chenier crest is low (high crest level relative to mean sea level). Waves only generate substantial sediment transport when the chenier is submerged. Overall, the cross-shore chenier dynamics are very sensitive to the timing of tides and waves: most transport takes place when high water levels coincide with (relatively) high waves.
While our observations showed the chenier to be highly dynamic in the short term, satellite images reveal that over longer timescales the position of the chenier remains more or less stable within the intertidal zone. This is in contrast to cheniers described in literature, which only migrate landward until they reach a stable position above tidal influences. We have developed an idealised chenier model to explore this dynamically stable position. The model simulates cross-shore chenier dynamics under daily wave and tidal influences and is able to predict both onshore and offshore migration. Onshore migration is mainly driven by wave action, while offshore migration is induced by a tidal phase lag or storms. This phase lag is caused by drowning of the coastal plain due to subsidence. For certain combinations of waves and tides, the model predicts a dynamically stable chenier. In the absence of a phase lag and storm season effect, the model yields a 'classic' stable chenier that welds onto the shoreline by onshore migration.

We used Delft3D to explore the formation of cheniers through wave winnowing (the sorting of sand and mud by waves). We have identified three phases of chenier development: (1) a winnowing phase, during which mud is washed out of the seabed initially consisting of a mixture of sand and mud, (2) a sand transport phase, when the sand in the upper layer is transported onshore, and (3) a crest formation phase, during which a chenier crest rapidly develops at the landward limit of onshore sediment transport. The main mechanism driving onshore sand transport is wave asymmetry. During calm conditions, sand transport takes place within a narrow band limiting the volume of sand delivered nearshore, and therefore no chenier develops. In contrast, average storm conditions mobilise sufficient sand for a crest to develop. Our results thus reveal that chenier formation through wave winnowing does not require extreme storm conditions. Our study also shows that chenier formation through wave winnowing is a relatively slow process, with the largest time scales associated with the the first two phases of chenier development: winnowing and sand transport.

Overall, this dissertation contributes to our understanding of cross-shore chenier dynamics. While very dynamic in the short term, cheniers can maintain a stable position in the intertidal zone for certain combinations of waves and tides. As such, they can contribute to mangrove rehabilitation by creating windows of opportunity for mangrove establishment. Due to its rapid subsidence rates, the coast of Demak provides an analogue for a global drowning of coastlines under anticipated accelerated sea level rise. In fact, cheniers may form a natural defense mechanism of drowning coastal plains. As a result, small changes to the coastal plain (e.g. constructing a dike) could have a significant impact, disturbing the chenier dynamics and interrupting their negative feedback on coastal erosion. This work has illustrated the complexity and interconnectedness of coastal systems, a crucial notion in designing successful protection strategies for mangrove-mud coasts.

Samenvatting

Het wereldwijde oppervlak van mangrovebossen is de afgelopen decennia drastisch gedaald. Mangrovebossen spelen een belangrijke rol op sociaaleconomisch en milieutechnisch vlak, en daarom zijn er veelvuldige pogingen ondernomen om de overgebleven mangrovekusten te beschermen en geërodeerde gebieden te herstellen. Helaas zijn veel van deze pogingen mislukt, vaak door een gebrek aan grondige kennis over mangrovekusten.
Sommige mangrovekusten worden aan hun zeezijde beschermd door zandruggen ('cheniers' genaamd). Deze cheniers verminderen de golfslag en dragen daardoor bij aan de bescherming van de kwetsbare mangrovekusten. Om mangrovekusten op een duurzame manier te kunnen herstellen, is het nodig de dynamiek van cheniers te begrijpen op een tijd- en ruimteschaal die relevant is voor de groei van mangroves (dagelijkse tot jaarlijkse variatie gedreven door golven en getij). Dit proefschrift heeft als doel een beter begrip te ontwikkelen van chenierdynamiek binnen de context van eroderende mangrovekusten. Hiervoor hebben we de extreem geërodeerde kust van Demak in Indonesië gebruikt als studiegebied.
We zijn het onderzoek begonnen met veldwerk in Demak, waar we de dynamiek loodrecht op de kust van een enkele chenier hebben geobserveerd. Deze metingen lieten zien dat cheniers heel dynamisch kunnen zijn in relatief kalme omstandigheden. We hebben de rol die het getij en de golven spelen in de waargenomen chenierdynamiek bestudeerd aan de hand van snelheidsmomenten, als benadering voor sedimenttransport. Het getij stuwt de chenier landwaarts, met name bij een kleine waterdiepte boven de chenier (dus een hoge cheniertop ten opzichte van gemiddeld zeeniveau). Golven genereren alleen substantieel sedimenttransport wanneer de chenier volledig onder water staat. De chenierdynamiek loodrecht op de kust is zeer gevoelig voor de timing van golven en het getij: het meeste sediment wordt getransporteerd wanneer hoog water samenvalt met (relatief) hoge golven.
Hoewel onze waarnemingen lieten zien dat de chenier zeer dynamisch was op korte termijn, tonen satellietbeelden dat de chenier op de lange termijn vrij stabiel blijft in het intergetijdengebied. Dit staat haaks op de algemene chenierliteratuur, waarin beschreven wordt dat cheniers uitsluitend landwaarts migreren, tot ze stabiliseren op de kust, boven de hoogwaterlijn. We hebben een geïdealiseerd chenier model ontwikkeld om deze dynamische evenwichtspositie in het intergetijdengebied verder te onderzoeken. Het model simuleert chenierdynamiek loodrecht op de kust onder invloed van golven en getij, en is in staat om zowel landwaartse als zeewaartse cheniermigratie te voorspellen. Landwaartse migratie

wordt hoofdzakelijk gestuurd door golven, terwijl zeewaartse migratie veroorzaakt wordt door een fasedraaiing van het getij of door stormen. Deze fasedraaiing is ontstaan door bodemdaling van het volledige kustgebied. Het model voorspelt een dynamisch stabiele chenier voor bepaalde combinaties van getij en golven. Zonder fasedraaiing en stormen vertoont het model het 'klassieke' cheniergedrag, waarbij de chenier landwaarts migreert en stabiliseert boven de waterlijn.
We hebben Delft3D gebruikt om het ontstaan van cheniers uit een zand-slibbodem te bestuderen. Dit gebeurt in drie fases: (1) het uitspoelen van slib uit het zand-slibmengsel in de bodem door golfwerking, (2) de zandtransportfase, wanneer het zand in de bovenste laag van de bodem landwaarts wordt getransporteerd, en (3) de accumulatiefase, waarbij de cheniertop zich heel snel ontwikkelt. Onze resultaten laten zien dat cheniervorming door zand-slibscheiding geen uitzonderlijke stormcondities vereist, maar ook al optreedt tijdens rustigere omstandigheden. Maar de golfcondities bepalen de grootte van het gebied waarover zand wordt gemobiliseerd, en dus het volume zand dat wordt afgeleverd bij de kust. Enkel wanneer er voldoende zand beschikbaar is dicht bij de kust, kan de cheniertop zich ontwikkelen. Onze modelstudie laat ook zien dat cheniervorming door zand-slibscheiding een redelijk traag proces is, waarbij de eerste twee fases van cheniervorming (het uitspoelen van slib en het zandtransport) het langst duren.
Dit proefschrift heeft bijgedragen aan ons begrip van chenierdynamiek loodrecht op de kust. Hoewel zeer dynamisch op korte termijn, kunnen cheniers op langere termijn een stabiele positie vasthouden in het intergetijdengebied, voor bepaalde combinaties van getij en golven. Op deze manier kunnen ze bijdragen aan het herstel van mangrovekusten, door de juiste gelegenheden te bieden voor mangrovegroei. Cheniers kunnen zelfs een natuurlijk beschermingsmechanisme zijn van zinkende kustgebieden. Dit betekent dat kleine ingrepen in het kustgebied (bv. de aanleg van een dijk) verregaande gevolgen kunnen hebben, wanneer ze de chenierdynamiek verstoren en daarbij de remmende werking van cheniers op de kusterosie verbreken. Dit werk toont eens te meer de complexiteit en onderlinge verbondenheid van kustsystemen aan, cruciaal bij het ontwerpen van succesvolle beschermingsstrategieën voor mangrovekusten. Dit is relevant voor kustgebieden waar nu bodemdaling optreedt, maar in de toekomst voor veel meer gebieden omdat de extreem snelle bodemdaling in Demak een mogelijk toekomstscenario voor kustgebieden onder versnelde zeespiegelstijging schetst.

Ringkasan

Selama beberapa dekade terakhir, hutan mangrove telah mengalami pengurangan luas yang cepat di seluruh dunia. Sebagai pengakuan atas fungsi sosial-ekonomi dan lingkungan yang esensial, telah dilakukan berbagai upaya untuk melindungi garis pantai dengan mangrove yang tersisa dan merehabilitasi mengrove yang tererosi. Sayangnya, banyak upaya rehabilitasi yang gagal, menunjukkan perlunya pemahaman sistem yang menyeluruh tentang pesisir lumpur bermangrove.
Beberapa pantai berlumpur yang ditumbuhi mangrove dilindungi pada sisi ke arah laut oleh gosong pasir (disebut 'cheniers'). Kehadiran gosong pasir berfungsi sebagai penyangga alamiah terhadap serangan gelombang dan dapat membantu melindungi garis pantai yang rentan dan pesisir lumpur bermangrove. Untuk merestorasi pesisir lumpur bermangrove secara berkelanjutan, dinamika gosong pasir perlu dipahami pada skala temporal dan spasial yang relevan untuk pembentukan mangrove (variabilitas harian hingga tahunan yang didorong oleh gelombang dan pasang surut). Disertasi ini bertujuan untuk mendorong pemahaman kita tentang dinamika gosong pasir dalam konteks pesisir lumpur bermangrove yang tererosi. Garis pantai Demak, Indonesia, yang tererosi parah dijadikan sebagai studi kasus. Kami mulai dengan sosialisasi atau kampanye lapangan di Demak, mengamati dinamika lintas pantai sebuah gosong pasir. Pengamatan mengungkapkan bahwa gosong pasir dapat sangat dinamis dalam kondisi yang relatif tenang. Menggunakan momen kecepatan sebagai proksi untuk transportasi sedimen, kami telah mengeksplorasi peran pasang surut dan gelombang dalam dinamika gosong pasir yang diamati. Pasang surut mendorong gosong pasir ke daratan, terutama ketika puncak gosong pasir relatif tinggi terhadap permukaan air. Gelombang hanya menghasilkan transportasi sedimen yang substansial ketika gosong pasir terendam. Secara keseluruhan, dinamika gosong pasir lintas pantai sangat sensitif terhadap waktu pasang surut dan gelombang: sebagian besar transportasi terjadi ketika permukaan air yang tinggi bertepatan (relatif) dengan gelombang tinggi.
Sementara pengamatan kami menunjukkan gosong pasir menjadi sangat dinamis dalam waktu singkat, citra satelit mengungkapkan bahwa gosong pasir kurang lebih dapat mempertahankan posisinya yang stabil dalam jangka panjang. Hal ini berbeda dengan gosong pasir yang dijelaskan dalam literatur, yang diketahui hanya bermigrasi ke darat sampai mereka stabil di garis pantai. Kami telah mengembangkan model gosong pasir yang ideal untuk mengeksplorasi posisi yang stabil secara dinamis ini. Model ini mensimulasikan dinamika gosong pasir lintas pantai di bawah gelombang harian dan pengaruh pasang surut serta mampu memprediksi dengan baik migrasinya ke darat maupun lepas pantai. Migrasi dekat

pantai (onshore migration) terutama didorong oleh aksi gelombang, sedangkan migrasi lepas pantai (offshore migration) disebabkan oleh perbedaan fase pasang surut atau efek dari musim badai. Perbedaan fase pasang surut (tidal phase lag) disebabkan oleh tenggelamnya dataran pantai karena penurunan muka tanah. Untuk kombinasi gelombang dan pasang surut tertentu, model memprediksi kestabilan dinamis lebih baik. Dengan tidak adanya perbedaan fase dan efek musim badai, model menghasilkan gosong pasir stabil 'klasik' yang menyatu ke garis pantai oleh migrasi dekat pantai.

Kita menggunakan Delft3D untuk mengeksplorasi formasi dari gosong pasir melalui sortasi pasir dan lumpur (winnowing) oleh gelombang. Kami telah mengidentifikasi tiga fase pembentukan gosong pasir: (1) sortasi pasir dan lumpur, di mana lumpur dibersihkan dari campuran pasir-lumpur dasar laut, (2) transportasi pasir, ketika pasir di lapisan atas diangkut ke darat, terutama oleh asimetri gelombang, dan (3) pembentukan puncak, pertumbuhan cepat dari puncak gosong pasir. Hasil kami mengungkapkan bahwa pembentukan gosong pasir melalui sortasi pasir dan lumpur tidak memerlukan kondisi badai yang ekstrem, tetapi juga terjadi selama kondisi yang lebih tenang. Namun, kondisi gelombang menentukan area di mana pasir dimobilisasi, dan karenanya volume pasir dikirim ke dekat pantai. Hanya ketika pasir yang cukup tersedia di dekat pantai, puncak gosong pasir akan berkembang. Studi model kami juga menunjukkan bahwa pembentukan gosong pasir melalui sortasi pasir dan lumpur (winnowing) adalah proses yang relatif lambat, dengan skala waktu terbesar yang terkait dengan dua fase pertama pengembangan gosong pasir: sortasi pasir dan lumpur (winnowing) dan pengangkutan pasir.

Secara keseluruhan, disertasi ini berkontribusi pada pemahaman kita tentang dinamika gosong pasir lintas pantai. Meskipun sangat dinamis dalam jangka pendek, gosong pasir dapat mempertahankan kestabilan posisi di zona intertidal untuk kombinasi gelombang dan pasang surut tertentu.

Dengan demikian, gosong pasir dapat berkontribusi pada rehabilitasi mangrove dengan menciptakan peluang untuk penanaman mangrove. Mempelajari pesisir Demak telah memberikan kami mengintip ke masa depan dari dampak kenaikan permukaan laut, karena kenaikan muka laut yang relatif ekstrim akan dialaminya. Faktanya, gosong pasir mungkin merupakan mekanisme pertahanan alami untuk menenggelamkan dataran pantai. Akibatnya, perubahan kecil pada dataran pantai (misalnya membangun tanggul) dapat berdampak signifikan, mengganggu dinamika gosong pasir dan mengganggu umpan balik negatifnya terhadap erosi pantai. Sekali lagi, karya ini telah mengilustrasikan kompleksitas dan keterkaitan sistem pantai, gagasan penting dalam merancang strategi perlindungan yang berhasil untuk pesisir lumpur bermangrove.

Chapter 1

Introduction

Worldwide, around 680 million people live in low-lying coastal zones (below 10 m elevation) and this number is expected to exceed one billion by 2050 (Intergovernmental Panel on Climate Change, 2019). These areas are extremely vulnerable to coastal hazards and the increasing impact of sea level rise. Along sheltered coastlines in the (sub)tropics, coastlines are typically occupied by mangrove forests. While mangrove forests fulfil many important socio-economic and environmental functions (Alongi, 2008; Temmerman et al., 2013), they are under increasing (anthropogenic) pressure and disappearing rapidly (Worthington et al., 2020). Protecting the remaining mangrove coasts, as well as restoring eroded mangrove coastlines, requires a thorough system understanding of both healthy and degraded mangrove-mud coasts.
Some mangrove-mud coasts are protected at their seaward side by sandy ridges (called 'cheniers'). Their presence acts as a natural buffer against wave attack and can help to protect vulnerable mangrove coastlines. Most chenier studies have approached the topic from a geological point of view, looking at the temporal and spatial scales of an entire chenier plain. However, in order to sustainably develop and restore mangrove-mud coasts, chenier dynamics need to be understood at much smaller spatial and temporal scales (daily to yearly variability driven by waves and tides), as these are the scales at which mangrove establishment takes place. This thesis aims to advance our understanding of chenier dynamics focusing on the drowning mud coast of Demak, Indonesia, which is flanked at its seaward side by dynamic cheniers.
In the following sections, some background information is given on mangrove coasts and cheniers, before introducing the research objectives and the outline of this dissertation.

1.1 Mangrove coasts

Mangroves are a group of trees and shrubs that grow in tidal, saline wetlands along sheltered tropical and subtropical coasts (Duke, 1992; Blasco et al., 1996). The term mangrove is also used to describe the habitat in which these plants

1

are found (Miththapala, 2008). In fact, they are the only trees that are able to survive at the boundary between land and water, where water levels, salinity, oxygen, sediment and other environmental conditions are constantly varying (López-Angarita et al., 2016; Kathiresan and Bingham, 2001; Hogarth, 2015). To survive in these challenging circumstances, they have developed special adaptations: aerial root systems (to breathe above ground when the waterlogged soils lack oxygen, see Figure 1.1), viviparous embryos (i.e. the seeds germinate while still attached to the tree), tidal dispersal of propagules, efficient nutrient retention mechanisms and physiological mechanisms for salt toleration. The three most abundant mangrove species in Demak, Indonesia are *Avicennia marina* (Figure 1.1b), *Avicennia alba* and *Rhizophora mucronata* (Figure 1.1a) (van Bijsterveldt et al., 2022). The *Avicennia* species are pioneer species, which means they are the first mangrove species to colonise bare mudflats and are usually found at the seaward fringe of mangrove forests.

Mangrove forests provide a wide range of ecosystem services (i.e. benefits to humans provided by ecosystems). They provide natural coastal protection, through wave and flow attenuation (Temmerman et al., 2013; Bao, 2011; Quartel et al., 2007; van Santen et al., 2007), and they are able to grow with sea level rise through sediment trapping (Alongi, 2008). Mangroves not only mitigate some consequences of climate change (sea level rise), but they can also mitigate its causes through carbon sequestration and storage (Friess, 2016; Nam et al., 2016; Donato et al., 2011).

Despite their resilience and adaptability, mangrove forests are suffering immense and rapid losses, with only 137.600 km^2 of the more than 200.000 km^2 of original mangrove forest remaining in 2010 (Bunting et al., 2018; Worthington et al., 2020). The main causes of deforestation are urbanisation, aquaculture, agriculture, (over)exploitation of resources, pollution and erosion (Alongi, 2009; Worthington et al., 2020; Richards and Friess, 2016; Thomas et al., 2017; Duke, 2016; Carugati et al., 2018).

In recognition of the importance of mangrove forests, and following the design philosophy of Building with Nature, many attempts have been made to slow down the continuing loss of mangroves, as well as to restore lost areas. However, many rehabilitation attempts have (partially) failed (Lewis, 2005; Wodehouse and Rayment, 2019; Winterwerp et al., 2020), often because the rehabilitation area was not a suitable mangrove habitat.

Even when a suitable habitat in the form of an intertidal mudflat is present, mangrove establishment is not evident; often there are thresholds in the form of spatially and temporally varying disturbances. Seedling establishment requires periods when these disturbances are absent or low, these periods are called 'windows of opportunity' (Romme et al., 1998; Proisy et al., 2009). Balke et al. (2011) identified three thresholds for successful seedling establishment of *Avicennia alba*: (1) an inundation-free period to develop roots that can withstand flooding, (2) root development that allows the seedling to withstand forces induced by waves and currents, and (3) further root development to survive high energy events



Figure 1.1: Two different mangrove species commonly found in Demak, Indonesia: **(a)** *Rhizophora mucronata* and **(b)** *Avicennia marina*. Note the different types of pneumatophores, *Rhizophora* species have 'stilt roots' growing down from the stem, while *Avicennia* species have aerial roots growing up from the roots below ground (photos by S.A.J. Tas).

which are accompanied by sheet erosion. The presence of a chenier in the intertidal zone could create such a window of opportunity, by sheltering the mudflat on its landward side from waves. This is confirmed by van Bijsterveldt et al. (in prep.b), who analysed the probability of mangrove response (retreat, stable or



Figure 1.2: Example of a chenier off the coast of Demak, Indonesia (photo by S.A.J. Tas).

expansion) for various mudflat widths and chenier presence. Without a chenier, mangrove retreat was found more likely (ca. 70% probability); if a chenier is present during one year, the probability of mangrove retreat decreased (ca. 55%) and the probability of mangrove expansion increased (from ca. 20% to 30%). If a chenier is present seaward of the mangrove edge for 2 years or longer, the probability of mangrove retreat became equal to mangrove expansion (both ca. 40%).

1.2 Cheniers

Cheniers are ridges consisting of wave-reworked coarse-grained sediments, resting on top of muddy sediment, separated from the shoreline by a mudflat (Augustinus, 1989; Otvos and Price, 1979). Figure 1.2 shows an example of a chenier off the coast of Demak, Indonesia.

The word ‘chenier’ originated in Louisiana, where oaks (called ‘chêne’ in French) grew on relict cheniers inland, and was first described in literature by Russell and Howe (1935). Since then, there has been some debate regarding the exact definition of cheniers. Most authors agree that a chenier consists of coarser particles (sand, gravel, shells, ...) and that it is a shallow-based ridge forming a sharp contrast to the underlying fine-grained deposits. However, Otvos and Price (1979) proposed a stricter definition, requiring that a chenier is surrounded by tidal mudflats on both its landward and seaward sides and is therefore sheltered from daily wave and tidal processes. Later, Otvos (2019) further restricted this

definition, adding that cheniers occur in multiple sets of ridges, inland from the shoreline, forming a so-called 'chenier plain'. On the other hand, many authors also use the term for active cheniers, i.e. ridges that are still under influence of regular wave and tidal processes, or for single bands of cheniers which are not part of a multi-membered chenier plain. Some examples of active cheniers can be found along the coast of the Guianas (Anthony et al., 2010, 2013, 2019; Nardin and Fagherazzi, 2018; Augustinus, 1980; Brunier et al., 2019), in Gomso Bay, Korea (Lee et al., 1994; Ryu et al., 2008), in the Firth of Thames, New Zealand (Woodroffe et al., 1983) and near Saltés Island, Spain (Morales et al., 2014). In this dissertation, we adopt the more general interpretation of the term 'chenier' to include the active sandy ridges overlying a muddy substrate.

Since cheniers are by definition only found along muddy coastlines, chenier coasts are characterised by mildly sloping foreshores and low to moderate wave environments (Augustinus, 1989). Cheniers may occur in tidal regimes ranging from microtidal (e.g. Demak, Indonesia (Tas et al., 2020) or Louisiana, USA (Mcbride et al., 2007)) through mesotidal (e.g. Gulf of Carpentaria, Australia (Rhodes, 1982) or Firth of Thames, New Zealand (Woodroffe et al., 1983)) to macrotidal (e.g. Mont-Saint-Michel Bay, France (Weill et al., 2012) or Gomso Bay, Korea (Lee et al., 1994)).

Although cheniers require a specific balance between sediment availability and wave action, they can be found in many different locations around the world (see Figure 1.3b). Cheniers are azonal, i.e. they are not restricted to a certain climate zone, in contrast to mangroves, which are only found in the tropics and subtropics (Giri et al., 2011), delineated by the 20°C isotherm of seawater in winter (Alongi, 2009) (see Figure 1.3a).

Within the tropics and subtropics, cheniers can be found along mangrove-mud coasts, for example in the Guianas (Anthony et al., 2019), in Vietnam (Quartel et al., 2007), in Australia (Woodroffe and Grime, 1999). In fact, the presence of mangroves may even facilitate chenier formation, by trapping sediment around high tide (Augustinus, 1989). While cheniers may adversely impact mangroves when their landward migration leads to asphyxiation of the trees by covering the aerial roots under a layer of sand (Anthony et al., 2019), they also provide a protecting barrier. Along the coasts of the Guianas, sediment discharged by the Amazon River is transported alongshore in large mud banks. These mud banks protect the shoreline from wave attack, creating opportunities for accretion and mangrove expansion (Anthony et al., 2010). Between the passage of two mud banks, during the 'inter-bank' phase, the waves are able to erode the coastline, and, where sand is available locally, cheniers are formed. These cheniers then protect their back-barrier by dissipating wave energy.

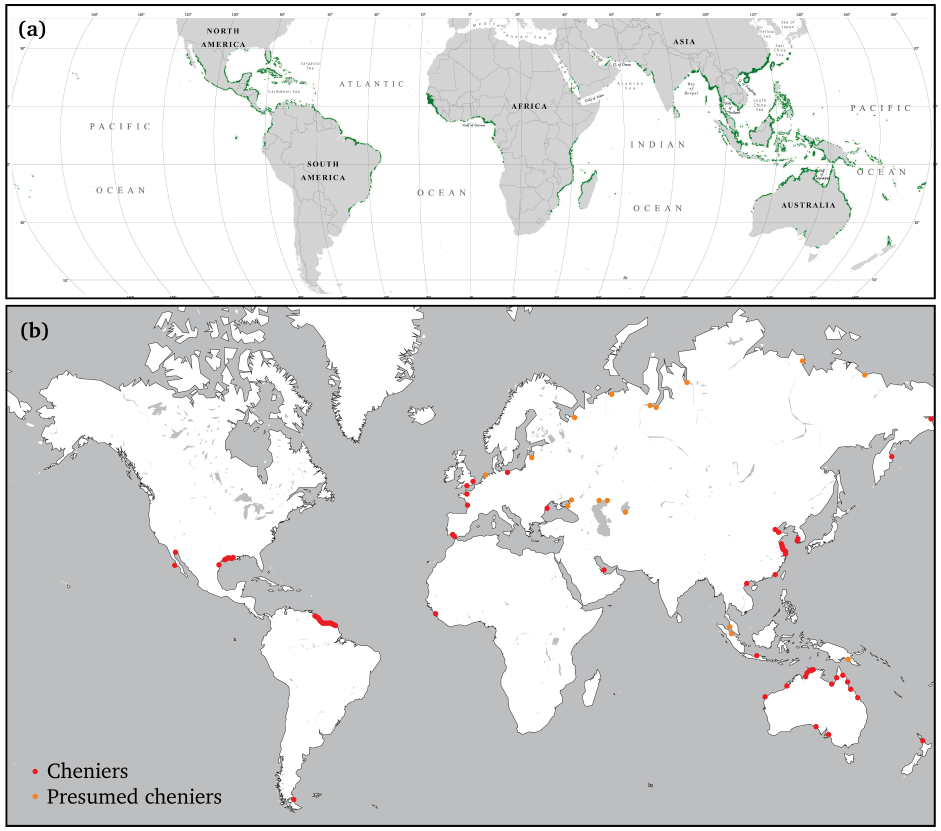


Figure 1.3: **(a)** Map of mangrove habitat worldwide (reproduced from Giri et al. (2011)). **(b)** Map of known chenier locations (extended from Augustinus (1989); Holland and Elmore (2008); Horne et al. (2014)). See Supplementary Table 1.1 for overview of papers reporting all cheniers indicated with a red dot. Presumed cheniers (orange dots) are classified as cheniers by Augustinus (1989) but lack profile data demonstrating they are 'true' cheniers (sand on top of mud).

1.3 Research objective

The aim of this thesis is to improve the understanding of chenier dynamics within the context of eroding mangrove-mud coasts. We will focus on cross-shore dynamics at time scales of hours to months (governed by wave-driven and tidal transport). To study the chenier dynamics, three research questions have been formulated:

- Which processes control the cross-shore dynamics of a chenier during calm conditions? (Chapter 3)
- Which processes are responsible for the dynamic equilibrium of cheniers on a drowning coastal plain? (Chapter 4)

- How are cheniers formed through wave winnowing and tidal and wave-driven sediment transport? (Chapter 5)

1.4 Thesis outline

Chapter 2 provides key background information on the study area of Demak, Indonesia.
Chapter 3 presents the field observations of a chenier in Demak. Despite the relatively calm conditions, the chenier was highly dynamic, migrating surprisingly fast in the landward direction. Using velocity moments as a proxy for the sediment transport, the role of the tide and waves on the cross-shore chenier dynamics is investigated.
Chapter 4 explores the cross-shore chenier dynamics and possible stable states under daily wave and tidal influences. In literature, only one stable state is described, when cheniers migrate strictly onshore until their crest level reaches above tidal influences. Observations in Demak, however, suggest the existence of an alternative stable state, when a chenier is highly dynamic in the short term, moving both onshore and offshore, but dynamically stable in the long term. We developed an idealised chenier model to investigate these dynamics and stable states.
Chapter 5 analyses the formation of a chenier through wave winnowing and tidal transport. Starting from a fully mixed bed, the different phases of chenier development are identified using Delft3D. The processes responsible for each phase are identified, as well as the conditions required for chenier development.
Chapter 6 synthesises the different chapters of this thesis and discusses their implications for the future of eroding mangrove-mud coasts. The chapter concludes with some recommendations for further research.

Supplementary Table 1.1: Supporting Figure 1.3b. Literature overview of papers reporting cheniers around the world (extended from Augustinus (1989); Holland and Elmore (2008); Horne et al. (2014)). This is a non-exhaustive list, especially in regions where cheniers have been studied at length (e.g. Louisiana, the Guianas), this list contains only a few example references.

Continent	**Country/Region**	**References**
Africa	Sierra Leone	Anthony (1989)
America	Argentina	Isla et al. (1991); Vilas et al. (1999)
	Guianas	Augustinus (1980); Prost (1989); Daniel (1989); Anthony et al. (2010, 2013, 2019); Toorman et al. (2018); Brunier et al. (2019); Jolivet et al. (2019)
	Mexico	Thompson (1968); Meldahl (1995)
	USA	Russell and Howe (1935); Thompson (1968); Penland and Suter (1989); Huh et al. (2001); Draut et al. (2005); Mcbride et al. (2007); Anderson et al. (2014); Hijma et al. (2017)
Asia	China	Cangzi and Walker (1989); Wang and Ke (1989); Yan et al. (1989); Zhao (1989); Saito et al. (2000); Wang et al. (2004)
	Indonesia	Marfai et al. (2016); Winterwerp et al. (2020); Tas et al. (2020); van Bijsterveldt et al. (in prep.b)
	Qatar	Shinn (1973)
	Republic of Korea	Park et al. (1996); Yang et al. (2005); Ryu et al. (2008); Kim et al. (2020)
	Vietnam	Quartel et al. (2007); van Santen et al. (2007); Tamura et al. (2010)
Europe	France	Pontee et al. (1998); Weill et al. (2012)
	Spain	Morales et al. (2004); Rodríguez-Ramírez and Yáñez-Camacho (2008); Morales et al. (2014)
	UK	Greensmith and Tucker (1969); Neal et al. (2002, 2003)
Oceania	Australia	Cook and Polach (1973); Rhodes (1982); Belperio et al. (1988); Short (1989); Chappell (1993); Woodroffe and Grime (1999); Nanson et al. (2013); Horne et al. (2014, 2015)
	New Zealand	Schofield (1960); Woodroffe et al. (1983); Dougherty and Dickson (2012)

Chapter 2

Study area: Demak, Indonesia

The coastline of Demak, Indonesia is used as a case study to investigate chenier dynamics along eroding mangrove-mud coasts. This chapter provides relevant background information (site description, climate) and context (project framework). We begin by introducing how this dissertation is embedded within the BioManCO project and providing a short overview of the contributions of parallel studies within this project. Next, a short overview of the history of Demak's coastal zone is given. The chapter concludes with an introduction to the climate and hydrodynamics of Demak.

2.1 The BioManCO project

This dissertation is part of the BioManCO project, which stands for Bio-morphodynamic modelling of Mangrove-mud COasts. The aim of the project is to unravel key mechanisms responsible for the dynamics of (eroding) mangrove-mud coasts. The project team is formed by 3 PhD candidates: (1) Celine van Bijsterveldt, investigating mangrove ecology, (2) Silke Tas, studying chenier dynamics, and (3) Alejandra Gijón Mancheño, researching permeable structures for mangrove restoration (see Figure 2.1).
Celine van Bijsterveldt studied the different drivers of mangrove dynamics in Demak (van Bijsterveldt, in prep). Linking back to the topic of this dissertation, she showed how important cheniers are for the mangrove stability (van Bijsterveldt et al., in prep.b). Furthermore, she studied natural mangrove regeneration in abandoned aquaculture ponds for greenbelt creation (van Bijsterveldt et al., 2020) and in which situations planting can facilitate mangrove restoration (van Bijsterveldt et al., 2022). She also investigated the impact of indirect anthropogenic stressors on mangrove survival, such as plastic pollution (van Bijsterveldt et al., 2021) and land subsidence (van Bijsterveldt et al., in prep.a).
Alejandra Gijón Mancheño addressed how permeable structures should be designed to restore mangrove habitat (Gijón Mancheño, in prep). She studied how the structures influence currents (Gijón Mancheño et al., 2021c), waves (Gijón Mancheño et al., 2021b) and sediment transport (Gijón Mancheño et al., in prep.).

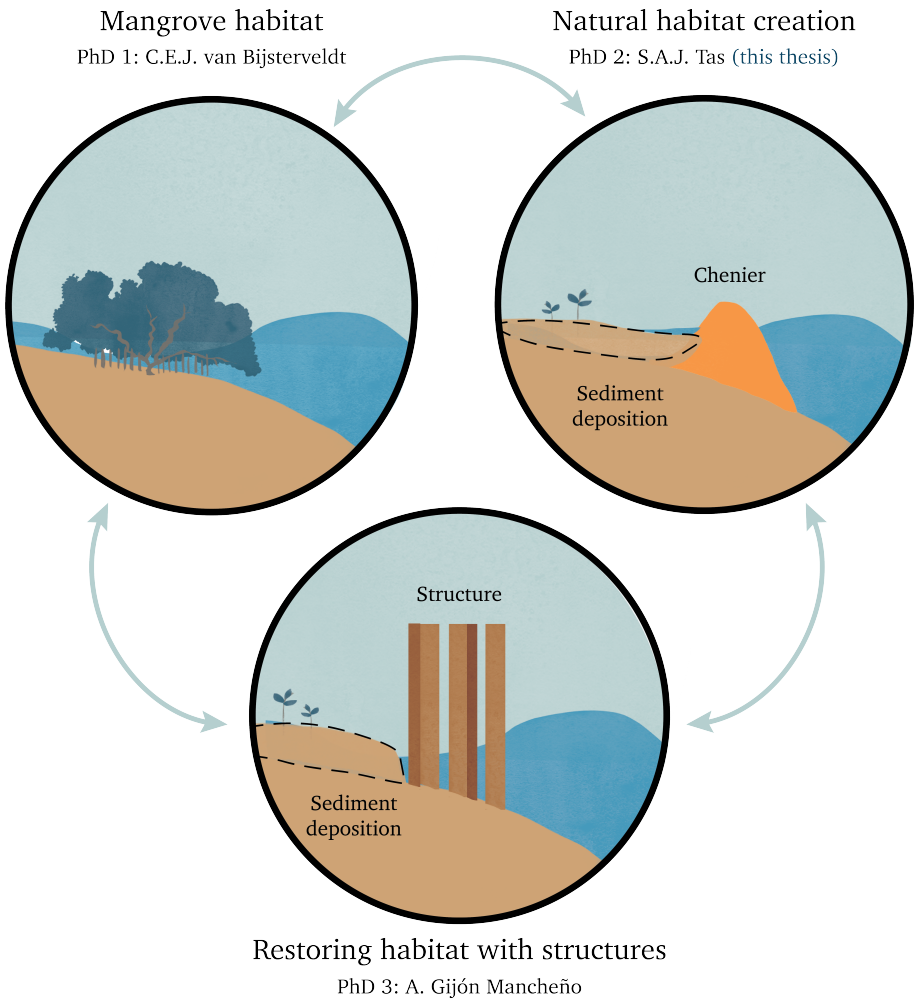


Figure 2.1: Conceptual figure of the connection and coherence between the three PhD studies within the BioManCO project (figure reproduced with permission from Gijón Mancheño (in prep)). This dissertation reports the work of PhD 2.

For the latter, a new modelling tool was developed: XMgrove (Reniers and Gijón Mancheño, in prep.). Furthermore, she developed a tool for feasibility studies that identify mangrove opportunities in data-scarce areas, applying it to Bangladesh (Gijón Mancheño et al., 2021a).
Lessons learned in Indonesia, during the BioManCO project and the Building with Nature Indonesia projects, as well as during other restoration efforts in Guyana, Suriname, Thailand and Vietnam, on how to manage erosion of mangrove-mud coasts using permeable structures, were presented in Winterwerp et al. (2020).
The BioManCO research project is embedded in the framework set up by Building with Nature Indonesia, which was a programme by Ecoshape, Wetlands Inter-

national, the Indonesian Ministry of Marine Affairs and Fisheries (MMAF), and the Indonesian Ministry of Public Works and Housing (PU), and other partners. The philosophy behind Building with Nature is to harness the forces of nature to benefit economy, society and the environment; in this case to restore a healthy mangrove coast which enables vulnerable coastal communities to prosper and be more resilient against coastal hazards. MMAF selected Demak as location for the pilot project, not only because of its high coastal vulnerability, but also because of the socio-economic context and the high level of local support.

2.2 Demak, Indonesia

Demak is a coastal district along the north coast of Central Java, see Figure 2.2a. It borders the Java Sea and is located just north of Semarang, the capital and largest city of Central Java. The coastline used to be completely covered by mangroves (yellow shaded zone in Figure 2.2b), but already in the nineteenth century most of the area landward of the mangrove greenbelt and some parts of the mangrove forest itself (closer to Semarang) had been converted into sawahs (rice paddies). By the end of the twentieth century, nearly all mangrove cover, as well as many rice fields had been replaced by fish ponds (Figure 2.2c). In the following 25 years, Demak has experienced extreme coastal erosion (Ervita and Marfai, 2017), with coastal retreat of more than 4 km (compare Figures 2.2c-d).
On top of the mangrove removal, the vulnerability was further increased by land subsidence due to ground water extraction by industry in Semarang. Subsidence rates of 13.5 cm/y (measured between 2008 and 2009) are reported by Chaussard et al. (2013), up to 16.5 cm/y (measured between 1997 and 2000) by Marfai and King (2007), and 14-19 cm/y (measured between 1999 and 2011) by Abidin et al. (2013). All analyses show a spatial variation in subsidence rates, with the highest rates in the north and northeast part of the city, where most industrial activity is concentrated.

2.3 Monsoon climate and local site effects

Demak features a tropical monsoon climate (Am) following the Köppen-Geiger climate classification (Peel et al., 2007). The SE monsoon (dry season) generally runs from April to October, and the NW monsoon (wet season) from December to March (see Figure 2.3 and Figure 2.4). Due to the orientation of the coastline of Demak, winds during the SE monsoon are directed offshore, creating very calm conditions nearshore, while the winds during the NW monsoon are directed onshore, generating higher waves, and storms occur regularly during the NW monsoon, resulting in even higher wave conditions.
Besides the dominant monsoon directions (NW and SE), a third peak direction occurs during the SE monsoon (from the north, see Figure 2.4a) which can be attributed to sea breezes. A sea breeze is the result of a local circulation system

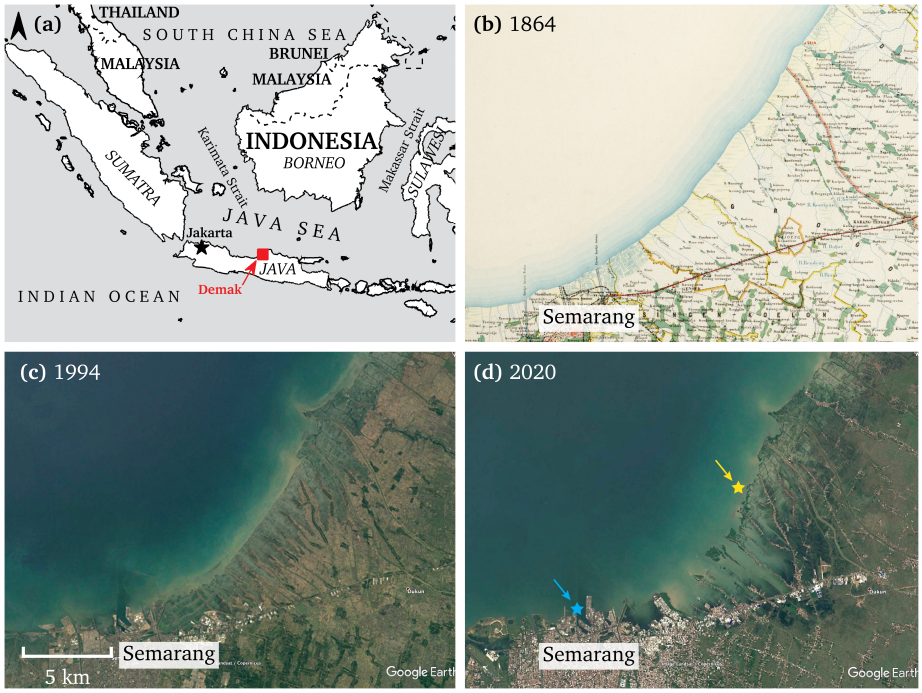


Figure 2.2: **(a)** Map of Indonesia, with the Demak coastline indicated by the red arrow. **(b)** Topographic map of the coastline of Demak in 1864 (Beijerinck and von Schierbrand, 1871). **(c-d)** Satellite image of the coastline of Demak in 1994 (c) and 2020 (d) (Google Earth, 2021). The location of the chenier observed during field work is indicated in (d) by the yellow arrow and star, the location of the water level monitoring station in Semarang is indicated by the blue arrow and star.

induced by temperature differences between sea and land (during the day, the air above land heats up quicker than the air above sea) and therefore, its dynamics depend greatly on local characteristics (Haurwitz, 1947; Miller et al., 2003). While less frequent than other winds during the dominant SE monsoon, the sea breeze is much stronger (generally $u_{10} > 4$ m/s and the only wind during the SE monsoon season that exceeds 6 m/s, see Figure 2.3). In Demak, the wind direction shifts from SE (monsoon) to N (sea breeze) between 12h and 14h (local time), then remains N for approximately 6 hours before returning SE again (see Figure 2.4c). Due to the orientation of the coast and the higher wind speeds, the sea breeze generates significantly higher waves than the prevailing SE monsoon wind.

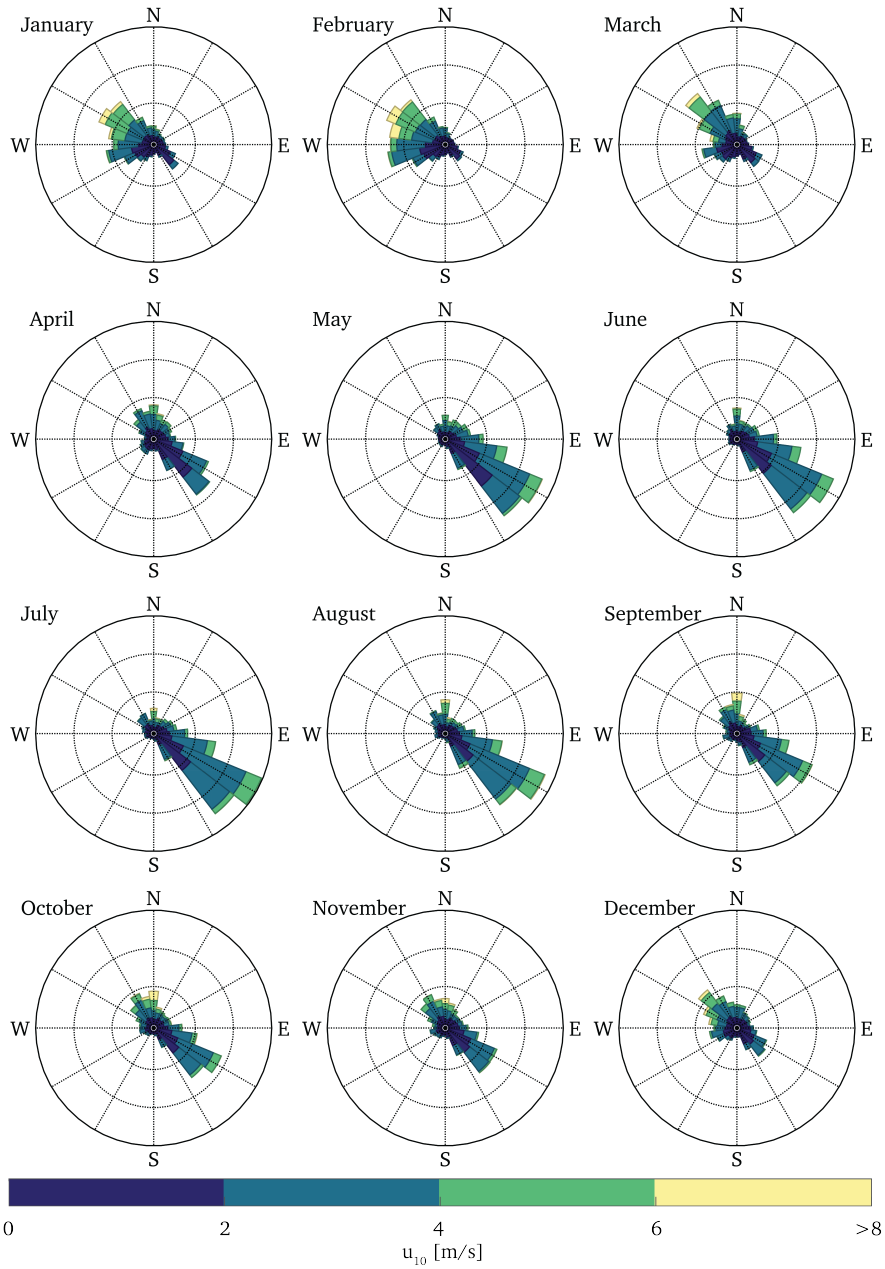


Figure 2.3: Monthly wind climate, based on measurements between 2015 and 2018 in the port of Semarang (Badan Meteorologi Klimatologi dan Geofisika, 2020). The colors represent the wind speed, the radius the frequency of time that the wind blows from each direction (circles at 7, 14 and 21%).

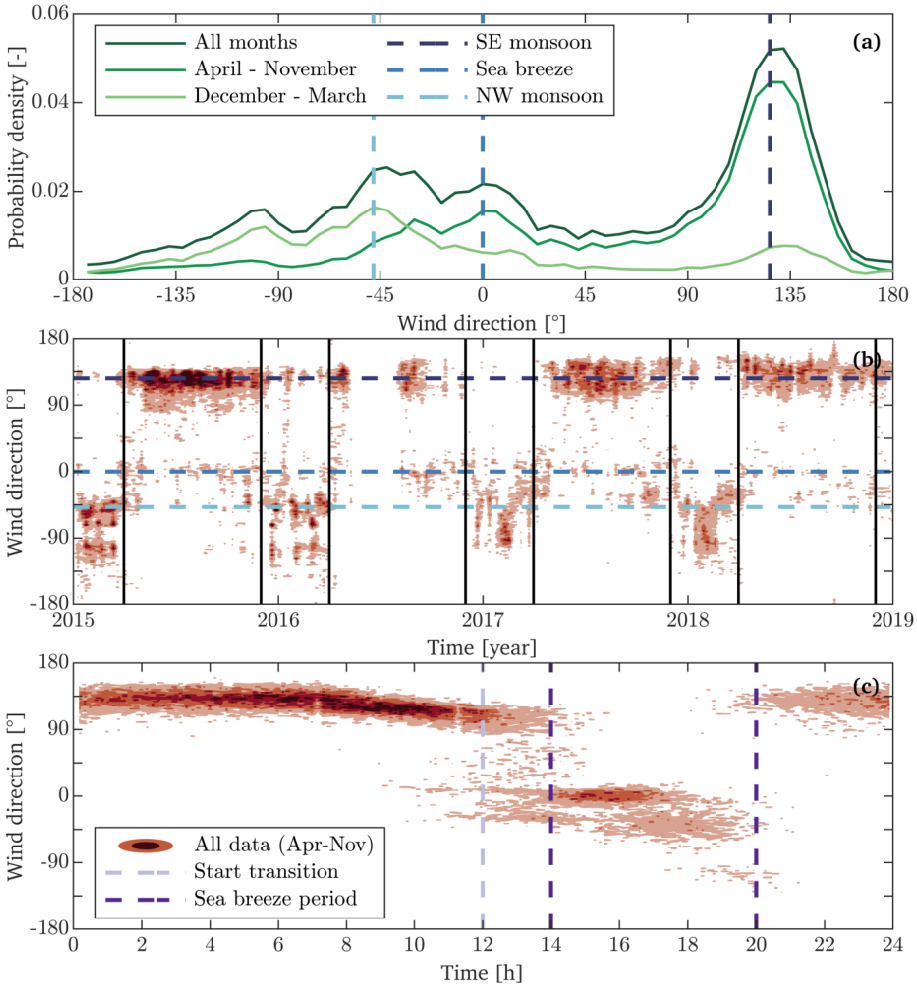


Figure 2.4: **(a)** Probability density function of the wind direction over the entire year (dark green) and the two monsoon seasons separately (lighter green lines). The peak directions of the two monsoon seasons (NW and SE) and the secondary peak direction of the sea breeze are indicated with blue dashed lines. **(b)** Density distribution of the wind directions over the period 2015-2018. The same peak directions as in panel (a) are indicated with the blue dashed lines. The different monsoon seasons are separated by the black lines. **(c)** Density distribution of the wind directions over the day during the SE monsoon season. The sea breeze period (and transition period) are indicated by purple dashed lines. All data in this plot is based on measurements between 2015 and 2018 in the port of Semarang (Badan Meteorologi Klimatologi dan Geofisika, 2020).

2.4 Hydrodynamics

2.4.1 Waves

The wave climate off the coastline of Demak is generally mild, especially during the SE monsoon season, when the general wind direction (SE) is offshore. Wave data was collected with a WaveDroid®directional wave buoy during three periods: 29 July 2017 - 8 August 2017 (SE monsoon season), 19 November 2017 - 30 December 2017 (NW monsoon season) and 25 October 2018 - 9 December 2018 (SE monsoon season transitioning to NW monsoon season). The wave buoy was anchored at a water depth of 12 m[1], 5.5 km offshore of the chenier in Demak (location S0 in Figure 3.1). Figures 2.5a-c show the wave climate during the three measurement periods.
Note that the waves originating from southeasterly directions are generated over the short fetch length separating the wave buoy from the coast; close to the chenier these waves are non-existent. During the third campaign, the monsoon was transitioning, so the first waves from the NW started arriving as well. This means that during the first (Figure 2.5a) and third (Figure 2.5c) measurement periods, most waves in the nearshore originate from the north, i.e. the sea breeze direction.
To show that the waves from the north are indeed the result of a sea breeze circulation, the wave direction distribution over the day is plotted in Figure 2.5d (for the third measurement period). The three main wind directions (SE monsoon, NW monsoon and N sea breeze) are visualised by the blue dashed lines. Two clear patterns can be distinguished, corresponding to the two monsoon seasons. The SE monsoon season pattern shows waves coming from the SE for most of the day, except during the afternoon, when waves come from the north due to the sea breeze. Similar to the wind direction distribution over the day (see Figure 2.4c, the transition from SE to N occurs between 12h and 14h, however, the transition back to SE is less abrupt, with the northerly sea breeze-induced waves persisting until well into the night, while the SE monsoon-induced waves pick up again after 20h. Next, there is the NW monsoon season pattern, with waves coming from the NW throughout the entire day.

2.4.2 Tide

The tidal constituents have been determined by performing a tidal harmonic analysis (Foreman and Henry, 1989) on a water level time series measured between 2016 and 2018 at monitoring station in the port of Semarang (Flanders Marine Institute (VLIZ) and Intergovernmental Oceanographic Commission (IOC), 2021) using UTide (Codiga, 2011). The main constituents are given in Table 2.1.
The tidal form factor is 1.72, therefore the tide can be classified as mixed, mainly diurnal (Pugh, 1987). Despite the diurnal character, the spring-neap variation is

[1]During the first deployment, the wave buoy was anchored closer to the coast at a depth of 6 m.

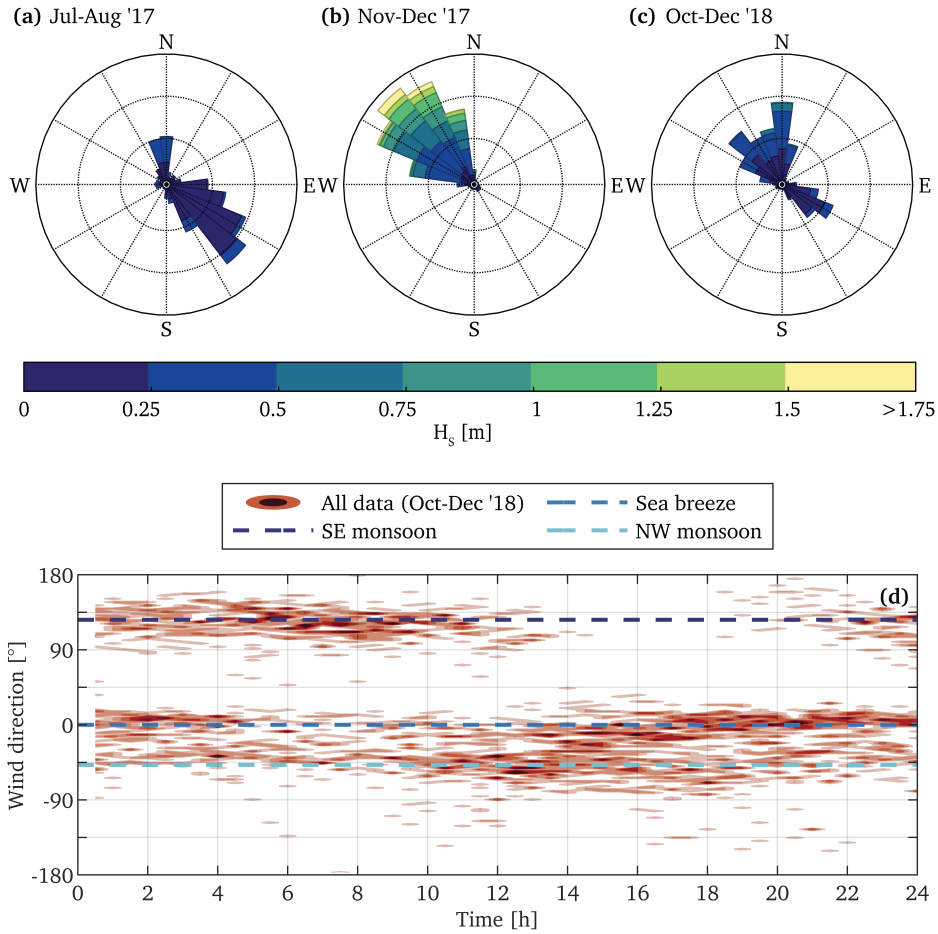


Figure 2.5: Wave climate measured during three periods: **(a)** 29 July 2017 - 8 August 2017, **(b)** 19 November 2017 - 30 December 2017 and **(c)** 25 October 2018 - 9 December 2018. **(d)** Density distribution of wave directions over the day during the third measurement period (25 October 2018 - 9 December 2018). The blue dashed lines indicate the peak wind directions: SE monsoon (126°, darkest blue), sea breeze (0°, middle blue) and NW monsoon (-48°, lightest blue).

dominated by the semidiurnals (due to the large difference in amplitude between O1 and K1 but small difference between S2 and M2). The spring tidal range is usually around 1 m.

The sea level monitoring station in Semarang is located 12 km southeast of the measurement location in Demak (see Figure 2.2d). In Figure 2.6, a measured water level time series in Demak (at location S1, see Figure 4.2d) is compared to the tidal constituents in Semarang. The measured and calculated water levels are in close agreement, therefore the tidal constituents of Semarang are also applicable in Demak.

Table 2.1: Main tidal constituents Semarang

Constituent	Name	Period [hr]	Amplitude [m]	Phase [deg]
K1	Lunar-solar declinational (diurnal)	23.93	0.226	245
M2	Principal lunar (semidiurnal)	12.42	0.103	55
S2	Principal solar (semidiurnal)	12.00	0.083	308
O1	Principal lunar (diurnal)	25.82	0.079	132
P1	Principal solar (diurnal)	24.07	0.071	247
SSA	Solar (semiannual)	4383	0.047	156
N2	Lunar elliptical (semidiurnal)	12.66	0.042	18
K2	Lunar-solar declinational (semidiurnal)	11.97	0.035	347
S1	Solar (diurnal)	24.00	0.022	64

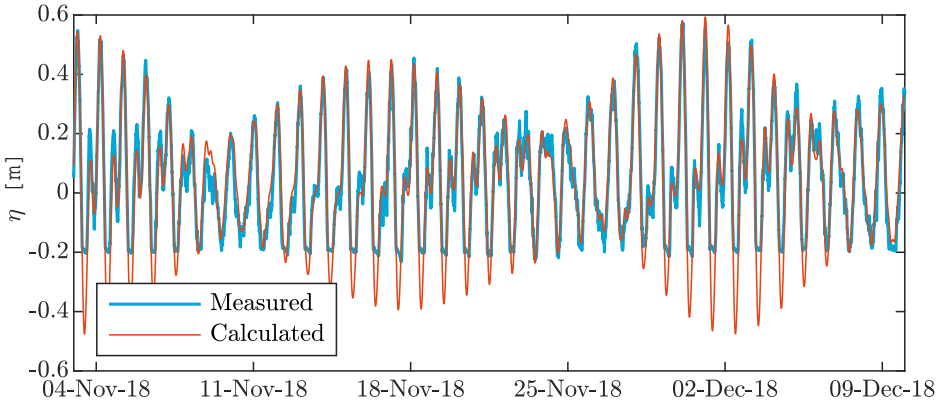


Figure 2.6: Water levels measured in Demak (blue line) and water level calculated with the tidal constituents of Semarang (orange line). The pressure sensor was installed at MSL -0.2 m, hence no lower water levels were measured.

Besides the tidal constituents, the tidal analysis also yielded a linear slope in mean water level, which suggests that the station has been sinking. Between 2012 and 2016, the relative water level increased at a rate of 7.9 cm/year. After a gap in the data of several months, the linear trend decreased to 3.9 cm/year. While it is unknown what happened to the station during the downtime, we speculate that the station may have been anchored to a deeper bed layer. For comparison, a tidal analysis on the data between 2012 and 2016 yielded similar amplitudes and phases for the tidal constituents.

Chapter 3

Observations of cross-shore chenier dynamics in Demak, Indonesia

Abstract

Cheniers are important for stabilising mud-dominated coastlines. A chenier is a body of wave-reworked, coarse-grained sediment consisting of sand and shells overlying a muddy substrate. In this chapter we present and analyse a week of field observations of the dynamics of a single chenier along the coast of Demak, Indonesia. Despite relatively calm hydrodynamics during the one-week observational period, the chenier migrated surprisingly fast in the landward direction. The role of the tide and waves on the cross-shore chenier dynamics is explored using velocity moments as a proxy for the sediment transport. This approach shows that both tide and waves are capable of transporting the sediment of the chenier system. During calm conditions (representative for the southeast monsoon season), the tides generate a landward-directed sediment transport when the chenier crest is high relative to mean sea level. Waves only generate substantial sediment transport (direct, via skewness, and indirect, via stirring) when the chenier is submerged during periods with higher waves. The cross-shore chenier dynamics are very sensitive to the timing of tide and waves: most transport takes place when high water levels coincide with (relatively) high waves.

This chapter has been published as: Tas, S.A.J., van Maren, S.D. & Reniers, A.J.H.M. (2020). Observations of Cross-Shore Chenier Dynamics in Demak, Indonesia. *Journal of Marine Science and Engineering*. 8(972). doi:10.3390/jmse8120972.

The measurement data is available in the repository of 4TU.ResearchData, with doi:10.4121/13177388.

3.1 Introduction

A chenier is a beach ridge, resting on silty or clayey deposits, which becomes isolated from the shore by a band of tidal mudflats (Otvos and Price, 1979; Augustinus, 1989). Cheniers play an important role in stabilising the coast (for example, along the Amazon-Orinoco coast, where large mud banks migrate alongshore, cheniers mitigate erosion in inter-mudbank areas (Anthony et al., 2019)). Cheniers can be part of an inactive delta plain (the so-called chenier plain, a multi-membered, progradational ridge/interridge mudflat sequence (Augustinus, 1989)) or manifest itself as active barriers. Chenier plains are associated with prograding littoral environments (Otvos and Price, 1979) or deltas (Augustinus, 1989) with a sufficient supply of fine sediments of which the relative importance varies in time (Otvos and Price, 1979; Augustinus, 1989); winnowing of the fine sediment deposits gives rise to the sandy barriers. Chenier plain shores are generally characterised by low to moderate wave conditions, tides may range from micro-tidal to macro-tidal and periods of wave dominance alternate with periods of high sediment supply (Otvos and Price, 1979). Nardin and Fagherazzi (2018) demonstrate that chenier plains may also develop in areas with persistent high waves and without alternating periods as long as a specific balance between sediment availability and wave action exists. Chenier plain formation along actively prograding river mouths has indeed been observed along e.g., the Red River Delta, where formation of barriers is triggered by cyclic growth of the delta front under constant river supply (van Maren, 2005). The most extensive and most studied chenier plains are those in Louisiana (e.g., Russell and Howe (1935); Mcbride et al. (2007)) and along the Suriname–Guyana coastline (Augustinus, 1989; Anthony et al., 2019). Less well investigated examples include the chenier plains in China (Cangzi and Walker, 1989) and West Africa (Anthony, 1989, 1995).

A poorly documented example of an active chenier system can be found along the coastline of Demak, a region along the north coast of Central Java in Indonesia. Cheniers are observed along stretches of the rapidly eroding mangrove-mud coast. Their formation may therefore result of sand winnowing from the muddy substrate, analogous to classical chenier plain formation. However, a chenier plain cannot be seen in the landscape. This could mean that the cheniers have only recently formed, possibly connected to the trend of coastal erosion starting in the early 2000s. Another explanation may be that older cheniers have disappeared due to sand mining, since sand is a commodity in a mud-dominated coast. While cheniers are traditionally observed in the proximity of large rivers (such as the Mississippi River for the cheniers along the coastline of Louisiana, or the Amazon River for the cheniers along the Suriname–Guyana coastline), the Demak coastline does not feature rivers of such size. The Wulan River at the northern border of Demak only has a fraction of the discharge of these large rivers, which suggests that the observed cheniers are not directly related to river supply. Although their origin is unknown, their presence is pivotal for the protection of the eroding coastline: van

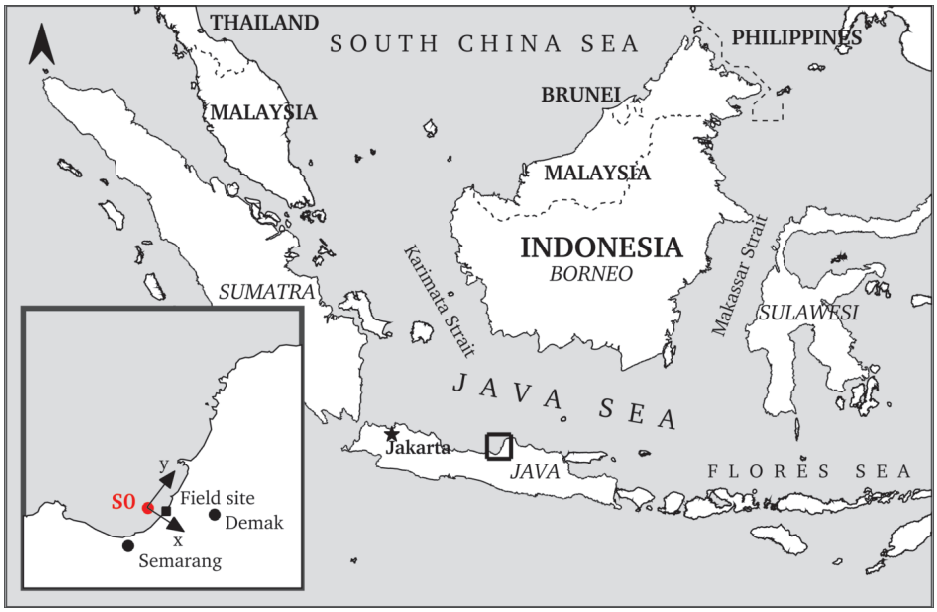


Figure 3.1: Map of the Java Sea. The box indicates the location of the inset map, showing the coastline of Demak on the north coast of Central Java, where the field study was conducted. The red dot on the inset map shows the position of S0, a WaveDroid measuring the offshore wave conditions.

Bijsterveldt (2015); van Bijsterveldt et al. (in prep.b) show that 92% of mangrove cover in Demak in 2014 was situated east, southeast or south of the nearest chenier, which means the mangroves are sheltered from the northwest (NW) monsoon wind and resulting waves. This confirms that mangroves (stabilising the coastline) mainly grow in areas sheltered by cheniers. As such, knowledge of their formation, dynamics and fate is crucial.

Demak borders the Java Sea, a shallow and sheltered basin, see Figure 3.1. The region features a tropical monsoon climate, bordering on a tropical rain forest climate (Lohmann et al., 1993). During the wet monsoon season, usually November to April, the dominant wind direction is northwest, and reverses to southeast during the dry season (Putranto and Rüde, 2016).

Old Dutch colonial maps indicate that the coastal area of Demak used to be completely covered by mangroves (Lang, 1869). By the turn of the 21st century, almost all mangrove cover had been replaced by fish ponds, and the area had also started suffering from land subsidence due to groundwater extraction, natural consolidation and added load of constructions (Marfai and King, 2007). By this time, large-scale coastal erosion had started, leading to coastal retreat of more than a kilometre in some locations along the coastline of Demak by 2010. Satellite images show the appearance of cheniers in the same period. Whether they are a new phenomenon, or whether they have always been present in this system is unknown. However, there seems to be a relation between the presence of cheniers

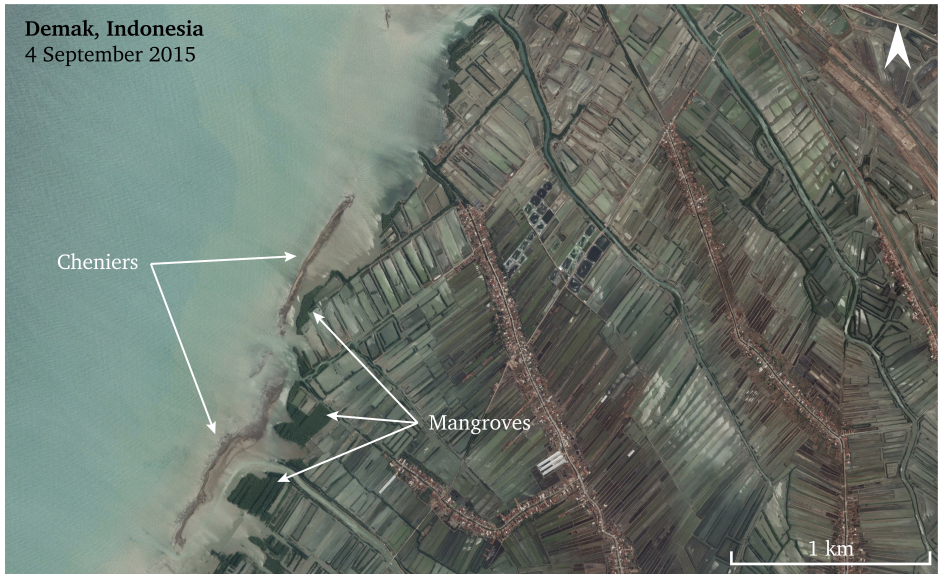


Figure 3.2: Google Earth image (Google Earth, 2020) taken on 4 September 2015 shows two cheniers off the coastline of Demak. Behind those cheniers, some small patches of mangrove forest are visible. North of the cheniers, where the coastline is unprotected, barely any mangrove tree persists.

and mangrove cover (van Bijsterveldt, 2015; van Bijsterveldt et al., in prep.b). The Google Earth image (Google Earth, 2020) in Figure 3.2 confirms this, showing more mangroves along chenier-sheltered sections of the coastline and erosion of exposed areas. However, the cheniers are very dynamic, so their impact on longer time scales remains unknown.

Closer examination of Google Earth satellite images (Google Earth, 2020) over time reveals a relation between chenier dynamics and the monsoon period (Figure 3.3). During the calm and dry southeast (SE) monsoon season, the chenier migrates in an onshore direction, as seen in Figures 3.3b-c. There are no satellite images during the wet NW monsoon season, but the first image after the wet season reveals that the chenier has migrated in the offshore direction compared to the location before the start of the wet season (Figures 3.3a and 3.3d). This suggests that calm conditions induce landward migration of the chenier, while storm conditions result in a seaward migration of the chenier.

Observations (this chapter) of chenier dynamics along the north coast of Central Java reveal that they are extremely dynamic and rapidly migrating in the cross-shore direction. The relative role of tides, waves and sediment supply in their dynamics is up to now insufficiently understood. Our aim is therefore to identify the physical processes that drive the dynamics of an existing chenier in the cross-shore direction. To that end we carried out an extensive field experiment capturing the hydrodynamics and morphology of one chenier over a period of six weeks. In this chapter, we focus on the last week of observations, a period during which the

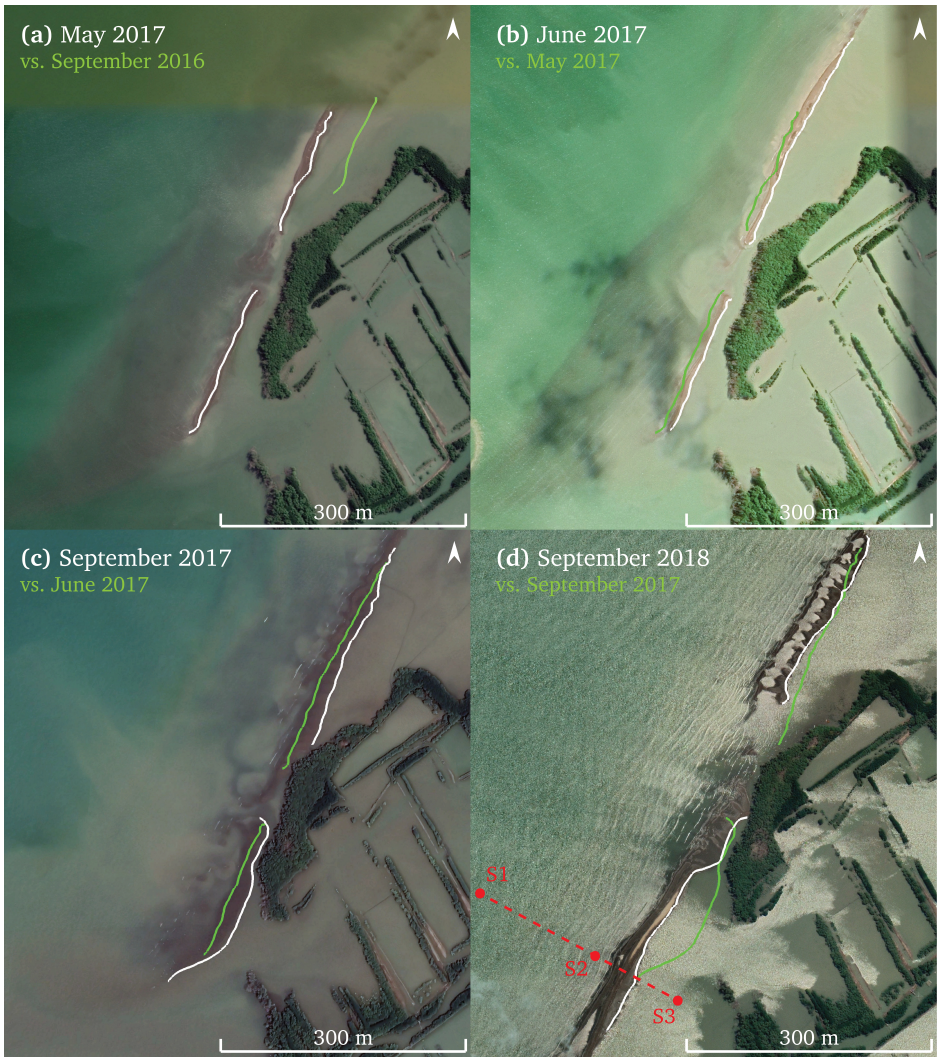


Figure 3.3: Google Earth images (Google Earth, 2020) illustrating that the chenier migrates landward during the calm and dry southeast (SE) monsoon season, and seaward over the wet northwest (NW) monsoon season. The white line follows the landward edge of the chenier crest at the time the image was taken, while the green line shows the location of the chenier at the time of the previous image. The red dashed line in (d) is the location of our observation transect in Figure 3.4, with S1–S3 depicting the location of instruments.

chenier became very dynamic.
The structure of this chapter is as follows. The methodology is introduced in Section 3.2. In Section 3.3 we present the field observations (Section 3.3.1) and analyse the mechanisms driving the cross-shore chenier dynamics, using velocity moments as a proxy for the sediment transport (Section 3.3.2) and Section 3.4 discusses the influence of the hydrodynamic conditions, the importance of the sea breeze and draws an analogue with breaker bars. The conclusions are summarised in Section 3.5.

3.2 Methods

In order to investigate the cross-shore chenier dynamics in more detail, a field study was conducted at one chenier in front of the coastal village of Timbulsloko between 25 October and 10 December 2018. The chenier is only connected to the shore at its northern extremity, where it borders a mangrove patch (the lower chenier in Figure 3.3). The chenier creates a bay between itself and the (severely) eroded coast. This measurement period was chosen such that it would cover the end of the (calm) SE monsoon season and the start of the NW monsoon season, with higher waves. Unfortunately, the NW monsoon season started later than usual, so throughout the entire field campaign, the SE monsoon conditions persisted. Therefore, the wave height remained low, except during afternoons when a sea breeze generated local wind waves.
Several high-resolution topographic surveys were conducted using Trimble 5700 DGPS (Differential Global Positioning System) receivers, one serving as fixed base station and the other a mobile sensor to measure the coordinates and elevation of points on the chenier. Due to problems with the base station, the absolute height of each measured profile is unknown. However, the relative height of each profile with respect to each other could be determined using data of erosion pins at the emerged part of the profile. Profiles were collected between 8 November and 8 December 2018. Additional bathymetric profiles were collected using a rod and a handheld GPS. These data were further supplemented with detailed measurements of bed level changes using erosion pins at 8 points along the transect.
Water level information was collected using three OSSI-010-003C-01 Wave Loggers, at S1, S2 and S3 (see Figure 3.3d), sampling at a frequency of 10 Hz. The pressure signal of the sensors was used to calculate wave spectra over intervals of 30 minutes, with a frequency resolution of 0.01 Hz. The sensors were placed 15 cm above the bed and the sensors at S2 and S3 emerged partly through the tidal cycle. Offshore wave data were collected using a WaveDroid®directional wave buoy, which was deployed at a water depth of 12 m, 5.5 km offshore of the chenier (location S0, see Figure 3.1). Current velocities were obtained using an Acoustic Doppler Velocimeter (ADV), deployed at the seaside of the chenier at S1 (see Figure 3.3d), measuring at a frequency of 4 Hz. The measuring volume was situated 30 cm above the bed, and the sensor emerged partly through the tidal cycle.

Sediment transport was not directly measured, but can be approximated using the flow velocity, assuming the sediment is mainly transported by bed load (Bowen, 1980; Bailard and Inman, 1981; Roelvink and Stive, 1989; Thornton et al., 1996). The time-averaged cross-shore sediment flux S is assumed to be proportional to the third power of the flow velocity (Bailard and Inman, 1981), see Equation 3.1:

$$\overline{S} \sim \overline{u^3}, \tag{3.1}$$

where u is the instantaneous velocity and the overbar denotes time-averaged (over a period of 30 min). Next, the velocity is decomposed into three components, $\overline{u}$ the time-averaged velocity, $\widetilde{u}$ the velocity due to the short wave motion and u_{ig} the velocity due to the infragravity waves. The frequency cut-off for the infragravity waves is set at 0.05 Hz, as longer swell and wind waves are not expected in the shallow and sheltered Java Sea. This gives:

$$\begin{aligned}\overline{S} &\sim \overline{(\overline{u}+\widetilde{u}+u_{ig})^3} \\ &\sim \overline{\overline{u}^3+\widetilde{u}^3+{u_{ig}}^3+3\overline{u}^2\widetilde{u}+3\overline{u}^2u_{ig}+3\overline{u}\widetilde{u}^2+3\overline{u}{u_{ig}}^2+3\widetilde{u}^2u_{ig}+3\widetilde{u}{u_{ig}}^2+6\overline{u}\widetilde{u}u_{ig}}\end{aligned} \tag{3.2}$$

Solving the third power in this equation splits the right hand side into 10 velocity moments, following Bowen (1980). By time-averaging the individual moments, some are reduced to zero, leaving four individual moments given by:

1. $\overline{u}^3$ representing the sediment transport driven by the mean current,
2. $\overline{\widetilde{u}^3}$ associated with the skewness of the short waves,
3. $3\overline{\overline{u}\widetilde{u}^2}$ due to the stirring by the short waves and subsequent transport by the mean current, and
4. $3\overline{u_{ig}\widetilde{u}^2}$ representing the transport by long waves.

The above method can be applied directly to the measured velocities at S1. However, the estimation of wave-related velocity moments from the pressure recordings at location S2 (where velocity was not measured) requires an extra step through which the instantaneous pressure is translated into horizontal velocities. Here we follow the approach of de Wit et al. (2019) using linear wave theory and assuming that the wave reflection is minimal. This approach is explained in more detail in Appendix 3.A. Comparing the velocity moments obtained from the measured velocities by the ADV with the co-located pressure recordings at location S1 shows good agreement (on 2 December, the median root mean square error (RMSE) is 16% of the median measured velocity). This suggests that pressure recordings at other locations can be used to estimate the corresponding wave-related velocity moments.

As only pressure is measured at site S2, the mean flow velocity at this location is estimated using the concept of continuity. Here, it is assumed that the cross-shore flux of water at S1 due to the rising and falling of the tide is equal to the volume

of water flowing over the chenier crest when it is submerged. This means that $\overline{u}$ can be estimated by scaling the current velocity measured by the ADV to the ratio of the water depth at the location of the ADV over the water depth on top of the chenier.
For the calculation of both the pressure- and continuity-derived velocity moments, a minimum water depth of 10 cm has been applied to avoid erroneous velocity estimates due to inherent measurement uncertainty of the bed profile at the chenier top.

3.3 Results

3.3.1 Observations

Bathymetry

Figure 3.4 shows the profiles measured between 28 November 2018 and 4 December 2018. Mean Sea Level corresponds to $z = 0$, the origin of the x-axis is situated at the WaveDroid offshore (S0), and the coastline is around $x = 5800$. The landward end of the measured transect represents the edge of the sand body, which is separated from the coastline by a mudflat of 200 m wide (see Figure 3.3). An estimate of the bathymetry of the mudflat, based on point measurements using a rod and handheld GPS, is shown by the dashed line in Figure 3.4. The three frames on which instruments were mounted are also indicated, S1 seaward of the chenier, at a submerged bar (around $x = 5425$) with an ADV and a wave logger, S2 just seaward of the chenier crest (around $x = 5520$), with a wave logger and S3 landward of the chenier (around $x = 5620$) with a wave logger.
Despite relatively mild hydrodynamic conditions, the chenier migrated surprisingly fast in the landward direction. The emerged part of the chenier ($5550 < x < 5590$) migrated approximately 20 m landward between 1 and 2 December 2018. However, the submerged part of the chenier remained relatively stable, notably the two submerged bars around $x = 5420$ and $x = 5450$. This quick migration took place during spring tide conditions, but also during relatively high wave conditions, as is elaborated in the following sections.

Hydrodynamics

Water levels were measured with pressure sensors at S1, S2 and S3. The mean spring tidal range is around 1 m (Figure 3.5a), so the tidal regime can be classified as micro-tidal (Pugh, 1987). Tidal analysis (using UTide (Codiga, 2011)) provided tidal constituents revealing that the form factor is 1.72. Therefore, the tide can be classified as mixed, mainly diurnal characterized by two distinct spring-neap cycles overlapping two times per year (Pugh, 1987; van Maren and Gerritsen, 2012). Despite the diurnal dominance, the relatively large difference between O1 (0.08 m) and K1 (0.22 m) leads to a limited spring-neap variation of the diurnals,

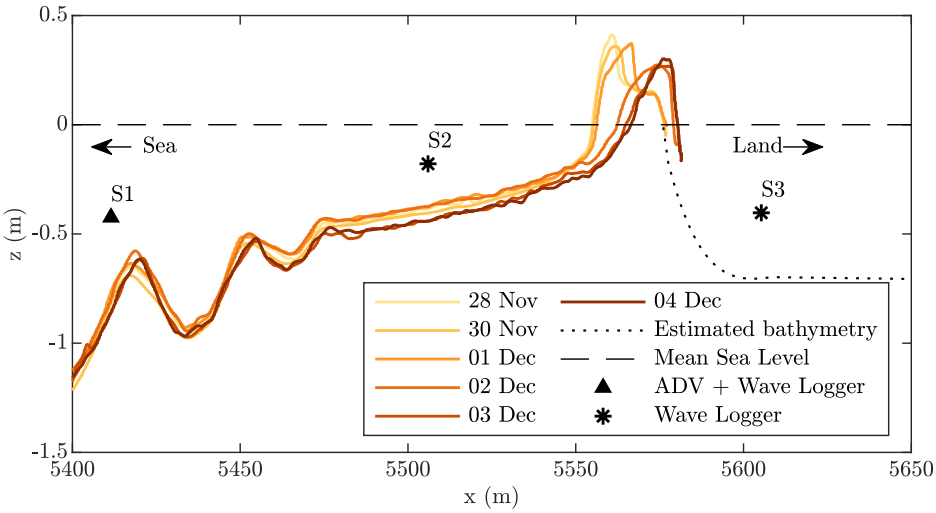


Figure 3.4: Profiles (see Figure 3.3d for location) measured daily with a Differential Global Positioning System (DGPS) between 28 November 2018 and 4 December 2018. The black dotted line gives an estimate of the bathymetry of the mudflat landward of the chenier. The two black asterisks indicate the location of two wave loggers, the black triangle of the frame with the Acoustic Doppler Velocimeter (ADV) and a wave logger. Mean Sea Level (black dashed line) corresponds to $z = 0$. The origin of the x-axis is the location of the WaveDroid offshore (S0, see Figure 3.1 for location), and the coastline is around $x = 5800$.

whereas the small difference between S2 (0.08 m) and M2 (0.10 m) leads to a pronounced spring-neap variation of the semi-diurnals.
The measured wave height was generally low (Figure 3.5b). The highest waves typically occur in the afternoon, when the prevailing weak southeast monsoon wind is overruled by a stronger onshore sea breeze (the purple dots in Figure 3.5d show the wind direction measured at a monitoring station in Semarang (Badan Meteorologi Klimatologi dan Geofisika, 2020)). The sea breeze generates higher, longer and onshore directed waves. One exception to this daily trend can be observed on 2 December 2018, a period when higher, onshore waves, were observed during the early hours.
Figure 3.5e gives the cross-shore velocity, where positive is onshore directed, while Figure 3.5f shows the alongshore velocity, positive in northeastern direction, away from Semarang. The blue line gives the instantaneous signal, whereas the orange line represents a moving average with a window of 30 min, representing the mean current.

3.3.2 Analysis

The observed cross-shore migration of the chenier is relatively fast and varying over time. The top of the chenier migrates landward with a maximum speed of 8 m/day. In order to explain the rapid onshore migration (see Figure 3.4), we

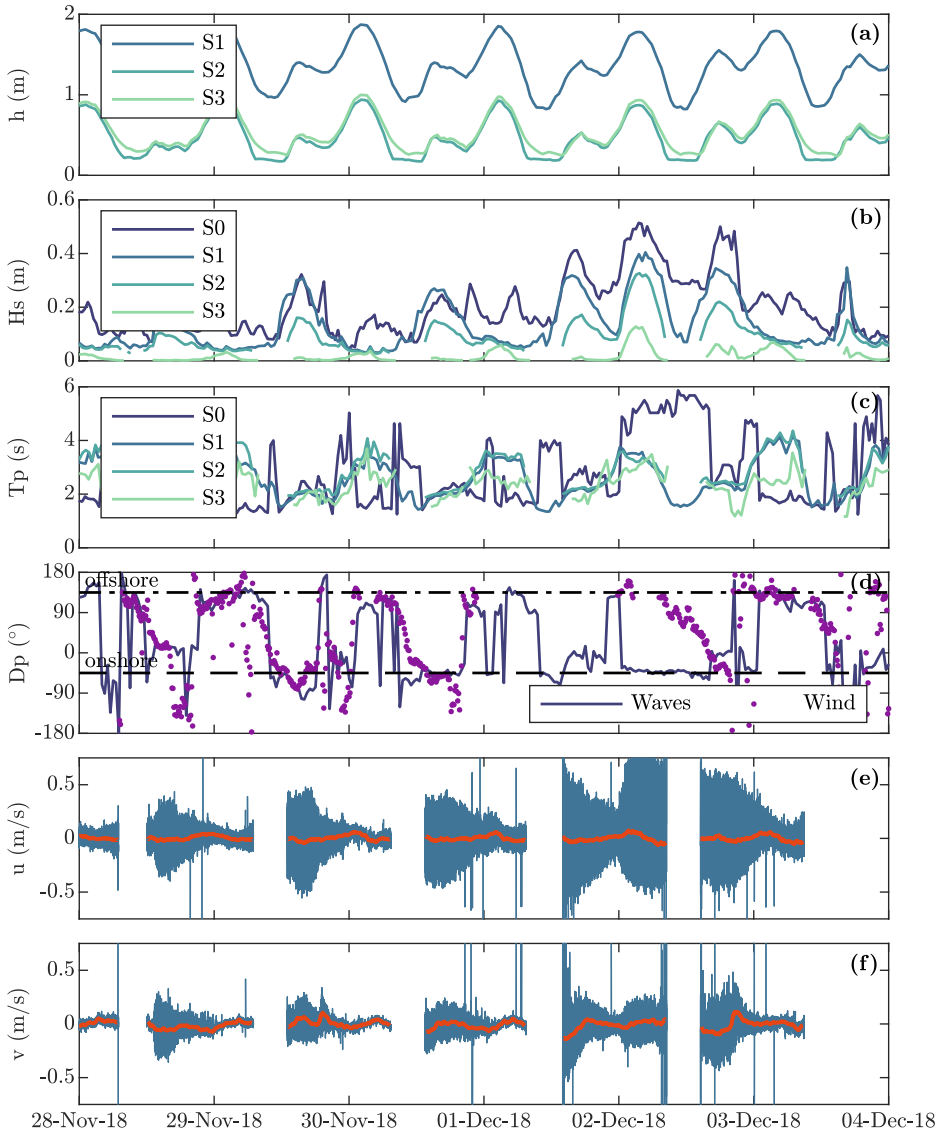


Figure 3.5: Hydrodynamic conditions between 28 November and 4 December 2018: **(a)** water depth, **(b)** significant wave height, **(c)** peak wave period, **(d)** peak wave and wind direction (wrt north), **(e)** cross-shore velocity (positive in onshore direction) and **(f)** longshore velocity (positive in northeastern direction, away from Semarang). The locations of the sensors are indicated in Figure 3.1 (S0, offshore station) and Figure 3.4 (S1-S3). The wave direction in (d) is measured by the WaveDroid at S0 and the wind direction is retrieved from a monitoring station in Semarang (Badan Meteorologi Klimatologi dan Geofisika, 2020). The velocities (e-f) are measured with an ADV at S1.

decompose the observed hydrodynamic data into velocity moments (see Section 3.2).
The cross-shore displacements of both the chenier crest (red) and the submerged bar (blue) are shown in Figure 3.6a. During the first 2–3 days, the profile is fairly stable. After 1 December, the chenier crest migrates landward rapidly (around 5 meter per day). The submerged bar is less dynamic, only on 2 and 3 December, a small landward displacement is observed. The water level at both locations is shown in Figure 3.6b. The dashed black line represents the height of the chenier crest, so when the water level exceeds this dashed line, the chenier is fully submerged (the periods when the chenier is fully submerged are shaded in gray in Figures 3.6b-f). Note that the submergence period depends on the tidal range, but also on the height of the chenier, which decreases over time (see also Figure 3.4).
Figures 3.6c-f show the velocity moments at two locations, in blue at the submerged bar, based on the ADV measurements, and in red on top of the chenier, estimations based on pressure recordings and continuity (see Section 3.2, Appendix 3.A and de Wit et al. (2019) for a detailed explanation of the followed approach). The cumulative velocity moments, which are a good proxy for the net sediment transport, are given in Figure 3.7. The bar is always submerged during these 6 days, so the cumulative velocity moment is calculated over a continuous period. The chenier is only submerged during parts of the 6 days. The cumulative velocity moments on top of the chenier are therefore only calculated for the periods when the chenier was completely submerged.

Sediment transport by mean current

Figure 3.6c gives $\overline{u}^3$, representing the sediment transport driven by the mean current (mainly tidal, but also including wind and wave-driven components). At the location of the submerged bar (blue line), $\overline{u}^3$ is insignificant. However, on top of the chenier, $\overline{u}^3$ becomes significant, especially when the water depth is small at the start and end of the submergence periods (indicated by the gray shaded areas). On 2 December, $\overline{u}^3$ is higher than on other days around the same time, probably due to an additional wave set-up.
The cumulative velocity moment (a proxy for the net sediment transport) due to the mean current is negligible at the location of the submerged bar, as the instantaneous velocity moments are small as well. The crest of the chenier experiences a net landward transport at each tidal cycle for the first couple of days. The last two days, however, the landward directed transport during the first hours of high tide is balanced by an offshore directed transport during the last hour of submergence. This flow reversal can be explained by the spatial variability of the chenier: when the chenier crest is high relative to the water level, the ebb tide mainly flows around the chenier (through an opening southwest of the chenier, see Figure 3.3). However, as the height of the chenier crest decreases (both in absolute terms because of morphological changes, but also relatively because of higher high water levels), part of the ebb tide flows back over the chenier, thereby transporting sediment offshore.

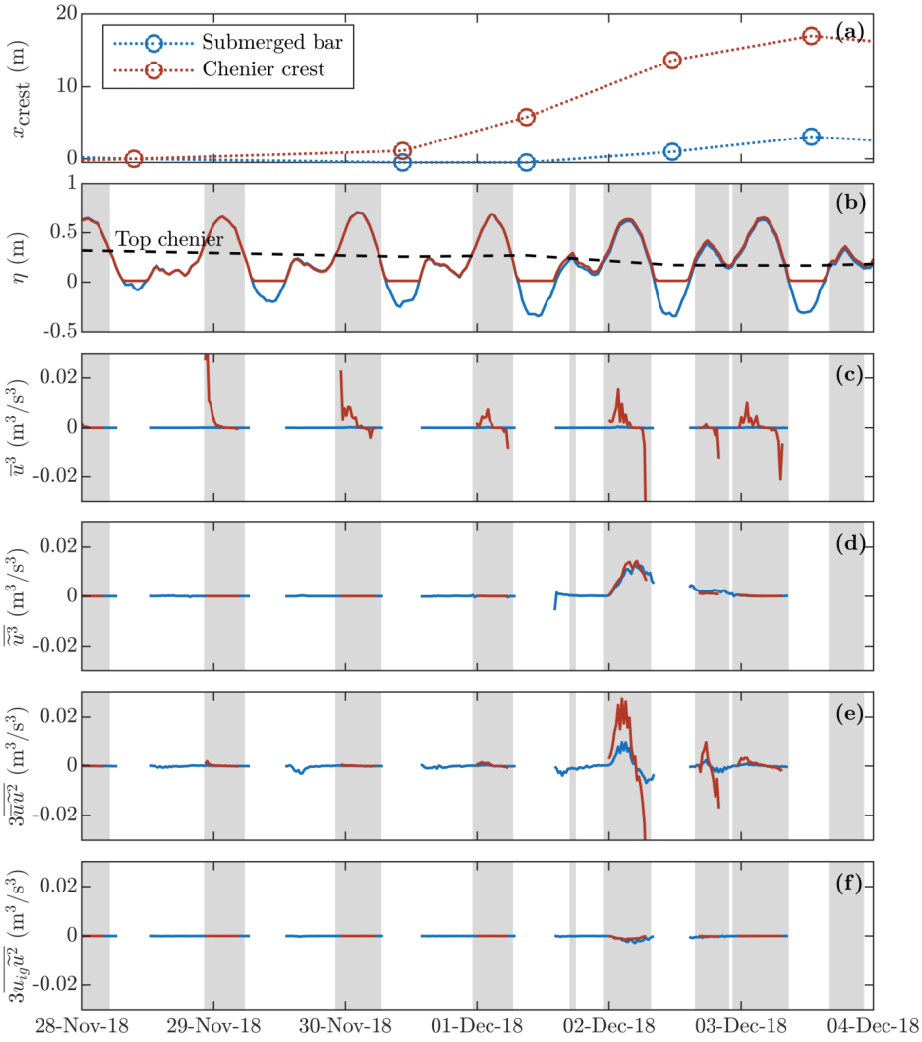


Figure 3.6: Time series at the submerged bar (blue) and chenier crest (red) of **(a)** the cross-shore coordinate of the bar/chenier crest; **(b)** water level; **(c)** $\overline{u}^3$, mean current; **(d)** $\overline{\widetilde{u}^3}$, short waves; **(e)** $3\overline{\widetilde{u}\widetilde{u}^2}$, stirring; **(f)** $3\overline{u_{ig}\widetilde{u}^2}$, infragravity waves.

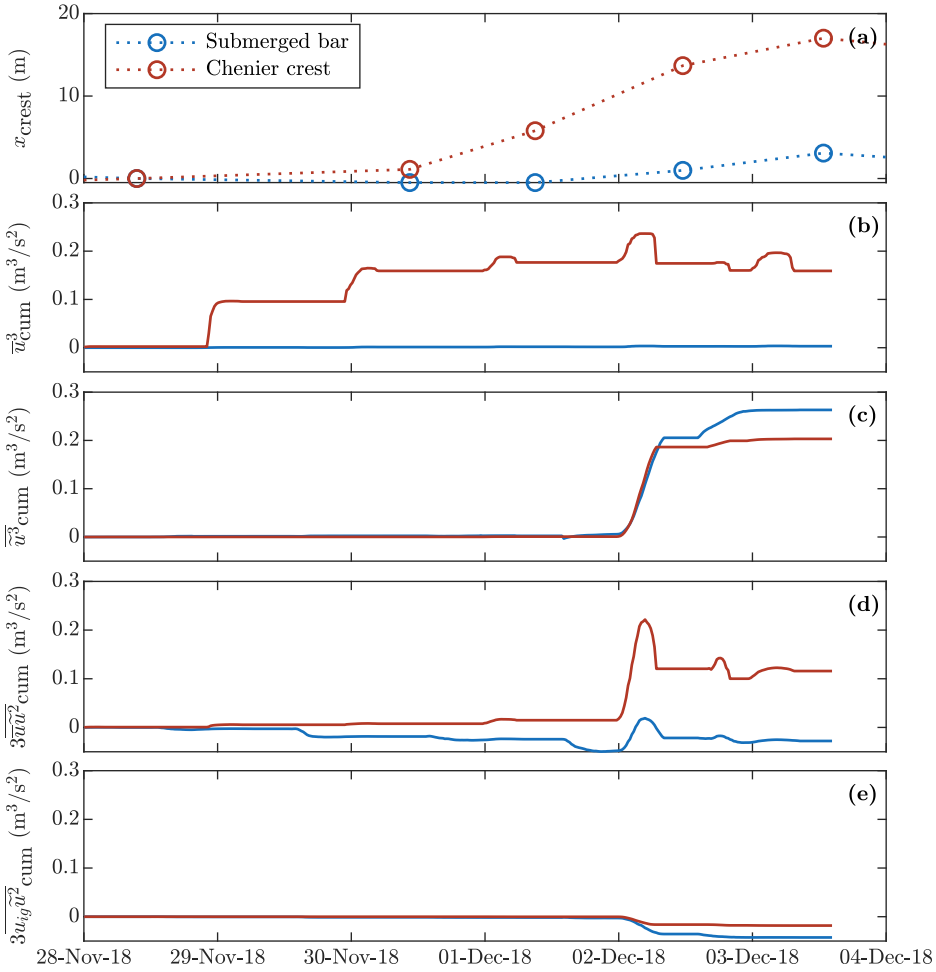


Figure 3.7: Cumulative velocity moments at the submerged bar (blue) and chenier crest (red). **(a)** the cross-shore coordinate of the bar/chenier crest; **(b)** $\overline{u}^3_{cum}$, mean current; **(c)** $\overline{\widetilde{u}^3}_{cum}$, short waves; **(d)** $3\overline{\widetilde{u}\widetilde{u}^2}_{cum}$, stirring; **(e)** $3\overline{u_{ig}\widetilde{u}^2}_{cum}$, infragravity waves.

Sediment transport by short waves

The first four days, the waves are low and therefore $\overline{\widetilde{u}^3}$ is zero (see Figure 3.6d). On 2 December, the waves are higher, resulting in positive velocity moments at both locations. While the wave height is lower on top of the chenier (see Figure 3.5), the water depth is lower as well, so the orbital velocities near the bed remain relatively high. During the afternoon of 2 December, the sea breeze-induced waves occur around mean sea level (MSL) and therefore the chenier is not fully submerged. By the time the chenier becomes fully submerged, the wave height has decreased, leading to smaller velocity moments.
The cumulative velocity moments (see Figure 3.7c) remain close to zero over the first four days. In the early hours of 2 December at high tide, a positive net sediment transport is generated at both observation locations. In the afternoon, during conditions with wind waves generated by the sea breeze, an additional positive sediment transport is generated at the location of the submerged bar. On top of the chenier, this transport starts later because the chenier is not submerged yet. However, as the wave height has decreased during the period of high tide, the wave-generated transport is much lower.
Short waves (when present) generally generate net positive sediment transport, due to relatively large skewness and negative asymmetry (not shown). During the week of field observations, the sea breeze coincided with tidal elevations around MSL, when the chenier crest was not submerged. Therefore, wave skewness plays a more important role in the sediment transport over the submerged bar, than over the top of the chenier.

Sediment transport by stirring

Stirring, shown in Figure 3.6e, is the combined effect of the mean current and short waves; the waves stir up the sediment from the bed and the mean current transports it. The transport direction is therefore identical to the transport by the mean flow (see Figure 3.6c). At the location of the submerged bar, $3\overline{\widetilde{u}\widetilde{u}^2}$ is mostly negligible up to 2 December, with a small but persistent negative value around MSL. This is consistent with the presence of a return flow to compensate for the wave-induced mass flux (Dyhr-Nielsen and Sorensen, 1970) at times of the sea breeze. This wave-related mean flow effect is absent on top of the submerged chenier as the waves are very small during high tide (see Figures 3.5a-b). On 2 December, $3\overline{\widetilde{u}\widetilde{u}^2}$ is large and landward directed during a time when the chenier is fully submerged, the tide is rising and the wave height is (relatively) high. The values are significantly larger at the chenier crest than at the submerged bar, which is due to a larger mean current due to the smaller water depth, while the orbital velocities near the bed are comparable at both locations. The velocity moment changes sign during the last hours of submergence of the chenier crest, because of the offshore-directed mean flow during ebbing consistent with the mean velocity moments discussed earlier.
The cumulative of $3\overline{\widetilde{u}\widetilde{u}^2}$ (see Figure 3.7d), representing the net sediment transport

due to stirring, reveals a small negative transport over the first four days at the submerged bar. The last two days, when the waves are higher, the net transport is more or less zero, because the transport rates during ebbing and flooding are nearly equal but opposite. On the chenier top, the cumulative effect is zero during the first days, because the waves are small at the time of submergence. On 2 December, the high waves combined with an onshore mean current generate a strong, positive sediment transport, which is only partially compensated during falling tide. This is different from the mean-flow moment and can be explained by the fact that although the mean flow reversal is symmetric, the waves are larger during the rising tide than during the falling tide (see Figures 3.5a-b). On December 3rd, the waves are more or less constant in height but smaller and the net transport is zero, consistent with the mean flow transport.

Sediment transport by infragravity waves

The infragravity waves are negligible during the first four days, therefore the velocity moments are zero as well (see Figure 3.6f). On the morning of 2 December, $3\overline{u_{ig}\widetilde{u}^2}$ is negative at both locations. This is the result of a negative correlation between the short wave envelope and the infragravity waves (Roelvink and Stive, 1989) consistent with the presence of bound infragravity waves.
The cumulative velocity moments (see Figure 3.7e) remain close to zero over the first four days. On the morning of 2 December, sediment transport is seaward at both locations. The cumulative transport over the submerged bar is two times higher than the transport over the chenier crest, but both contributions are relatively small, compared to the other transport mechanisms discussed earlier.

Combined sediment transport

Figure 3.8 shows the cumulative velocity moments of all processes combined on the right y-axis, and the displacement of the bed in the cross-shore direction on the left y-axis. Note that there is no difference in scaling between the two locations, so the net transport on top of the chenier is around twice the net transport at the submerged bar, whereas the displacement of the chenier crest is around three times the displacement of the submerged bar. With this constant scaling the cumulative velocity moments show a close correspondence to the cross-shore displacement of both the bar crest and the chenier top.
During relatively calm periods, the mean current transport is too small to influence the bottom profile at the submerged bar, but is the dominant contribution in sediment transport over the chenier when it is submerged. With a relatively high crest elevation this leads to a net onshore transport as the ebb currents are diverted by larger-scale topographic effects flowing around the chenier (see Figure 3.3). When the chenier becomes relatively lower, the ebb currents also partially flow over the chenier crest, resulting in equal ebb and flood transports and thereby negligible net sediment transport.

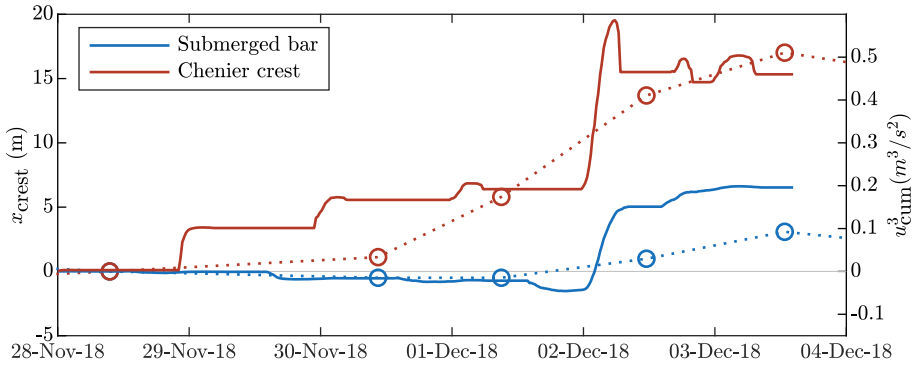


Figure 3.8: Crest displacements x_{crest} (left y-axis, circles connected by dotted lines) versus cumulative velocity moments $\overline{u^3}_{cum}$ (right y-axis, solid lines) at the submerged bar (blue) and chenier crest (red).

In the presence of relatively high waves when the chenier is emerged, a relatively small offshore-directed sediment transport occurs at the submerged bar, caused by stirring. When relatively high waves occur during a time when the chenier is submerged, relatively large landward-directed sediment transports occur both at the submerged bar and on top of the chenier. During these periods, skewness and stirring are the dominant mechanisms. Where skewness only generates landward transport, the net transport by stirring is determined by the timing of the waves and the (reversing) mean flow. Infragravity waves do not contribute significantly to the sediment transport at this location.

3.4 Discussion

3.4.1 Importance of local sea breeze

Our field observations were collected during the southeast monsoon season, a period during which the wind is persistently blowing from land to sea. Due to the resulting limited fetch length, the waves generated by the offshore monsoon wind are very short and only marginally stir up sediment. However, during this season a persistent sea breeze develops in the afternoon. The wind waves generated by this onshore wind are typically much larger than the SE monsoon-generated waves.

The first four days of the measurement period are a good representation of the typical conditions during the SE monsoon season. Despite the sea breeze generating higher waves, this does not lead to significant sediment transport. Most sediment transport takes place on 2 December, during a local wind event unrelated to the sea breeze. These waves contributed strongly to net displacement of the chenier, partly because the wave height is slightly larger than those resulting from the sea breeze, but mainly due to the phase shift between high waves and high

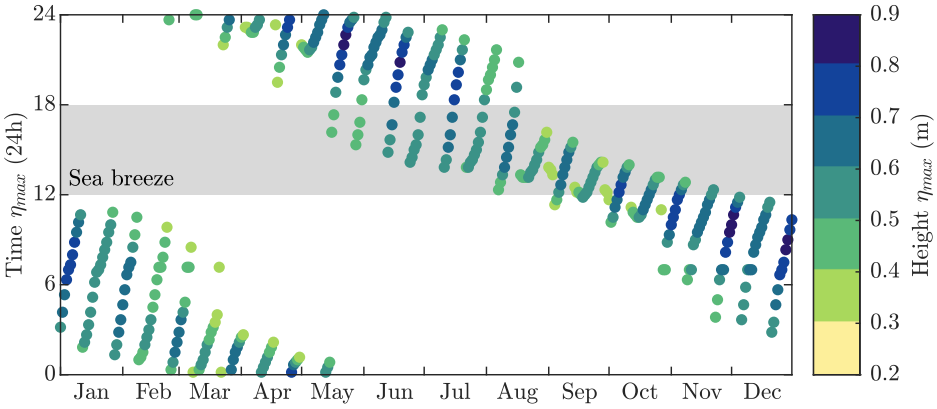


Figure 3.9: Time of the highest water level of the day for the year 2018 (reconstructed using UTide (Codiga, 2011)). The colour scale represents the height of the highest water level of the day. The shaded area indicates the period when the sea breeze occurs (between 12h00 and 18h00).

tide. The 2 December event generated high waves around high water, whereas the sea breeze resulted in high waves during the afternoon, when water levels are low (and therefore the chenier crest was not submerged).
While the timing of the sea breeze is the same throughout the entire SE monsoon season (the afternoon), the timing of the diurnal high tide shifts through the day. Figure 3.9 shows the time of the highest water level per day for the year 2018. During the months of June–September, the highest water level of the day occurs in the afternoon, coinciding with the sea breeze. This will likely lead to higher sediment transport and therefore to even more dynamic cheniers. However, most of the high tides are relatively low, which will reduce the sediment transport, as the chenier may not always be submerged at high tide, reducing the dynamics of the cheniers.

3.4.2 Analogue with breaker bars

The observed profiles reveal the presence of two submerged sand bars (see Figure 3.4) resembling breaker bars commonly observed at sandy coastlines. The dynamics of these breaker bars have been studied extensively (in contrast to the short-term dynamics of chenier bars), and therefore we evaluate to what extent the known dynamics of breaker bars also represent the dynamics of chenier bars. Ruessink et al. (2003) compared a large number of breaker bars, and concluded that the cross-shore bar length L_{bar} is exponentially related to the water depth above the bar h_{bar} as in:

$$L_{bar} = 100 \exp(0.27 \cdot h_{bar}), \tag{3.3}$$

which yields a length of $O(100)$ m using the bar depth near S1. This is slightly longer than observed, however their data set considered bar systems with larger bar depths, resulting in a less accurate description of breaker bar length at smaller depths. This suggests that these bars are indeed breaker bars that have been formed during storm conditions. Breaker bars are known to propagate onshore during mild non-breaking conditions due to wave skewness, asymmetry and boundary layer streaming effects (e.g., Gallagher et al. (1998); Hoefel and Elgar (2003); Henderson et al. (2004); Ruessink et al. (2007)). This is consistent with the current observations where the onshore displacement of the bar crest coincides with the presence of waves with significant skewness (see Figure 3.6). These higher waves coincide with high tide (see Figure 3.5), resulting in a wave height over water depth ratio of less than 0.3, consistent with non-breaking waves over the bar crest (e.g., Robertson et al. (2013)). It is expected that the breaker bars move offshore during storm conditions, consistent with the observed bar behaviour along open sandy coasts (e.g., Walstra et al. (2012)), but this cannot be supported by the current observations as only non-storm conditions were observed.

The cross-shore migration rate for the chenier top is much faster than for the submerged bars resulting in a much larger cross-shore displacement (see Figure 3.6a). This rapid onshore displacement coincides with the submergence of the chenier crest and as such is more in line with swash bars that have been observed to propagate rapidly onshore during mild submergence (Cohn and Ruggiero, 2016; Vos et al., 2020). This rapid displacement is attributed to the fact that waves propagate over the inter-tidal bar where the wave-related mass transport subsequently is seaward through lateral runnels (e.g., Vos et al. (2020)). Here, the presence of the bay behind the chenier acts like a runnel, preventing the wave-related mass flux to create a return current, thus enhancing the onshore mean flow over the chenier top. In that case both the stirring and wave non-linearity become very effective in transporting sediment onshore, resulting in a rapid onshore motion.

Note that the cross-shore displacement of both breaker bars and chenier crest are the result of cross-shore changes in the sediment transport. The analyses presented here are based on measurements close to the crest of the breaker bars and the chenier top where the locally maximum sediment transport is expected to occur. As such they are expected to be a good indicator of both the propagation direction and migration rate of these features (e.g., Gallagher et al. (1998); Hoefel and Elgar (2003)).

3.4.3 Influence of hydrodynamic conditions

This chapter presents a semi-quantitative approach using an energetics-based approach using velocity moments to estimate the sediment transport (Bowen, 1980; Bailard and Inman, 1981). However, with the field data alone, it is not possible to completely quantify the sediment transport, nor is it possible to estimate the sediment transport during other conditions. It was hypothesized that the phase

shift between the sea breeze (always in the afternoon) and the period of high tide (regulated by the phase inclination of the O1 and K1 tidal constituents) will lead to more dynamic bar behaviour during monsoon conditions. Also, counterbalancing mechanisms (leading to an offshore migration of the submerged bars and the chenier crest) have not yet been quantified, although satellite images (Figure 3.3) reveal offshore migration during the monsoon season. Also, the analogue with breaker bars suggests storms provide conditions for seaward migration.
As a next step, the sediment transport mechanisms during other hydrodynamic conditions will be explored in more detail using a numerical model. Such an approach will reveal to what extent the onshore migration during calm conditions is indeed counterbalanced by offshore migration during storm conditions. The model will then be utilized to determine to what extent the phasing of the high water levels (gradually shifting throughout the year) relative to the sea breeze influences the dynamics of the chenier during the SE monsoon season. Finally, such a numerical approach would allow us to analyse the influence of the tidal basin behind the chenier on chenier dynamics, by exploring various spring tide and storm set-up scenarios.

3.5 Conclusions

Cheniers can play an important role in stabilising a coastline. This chapter presents and analyses a week of field observations of a chenier along the coast of Demak, Indonesia. Under relatively calm hydrodynamic conditions, the chenier migrated landwards relatively fast (the chenier top moved at speeds between 0.5 and 8 m/day). Using velocity moments as a proxy for the sediment transport, the role of the tide and waves on the cross-shore chenier dynamics was investigated by means of a decomposition of the velocity in mean current, short wave and long wave contributions.
During calm conditions (representative for the SE monsoon season, Hs smaller than 0.5 m at deep water), the tide generates substantial sediment transport in very shallow water only. When the chenier is relatively high (height crest compared to high tide), this transport is landward-directed, because the ebb currents prefer to flow around instead of over the chenier.
Waves transport sediment directly through skewness and indirectly through stirring. In the SE monsoon season, most of the significant waves are generated by a sea breeze in the afternoon. However, during the field measurements, the chenier was not submerged in the afternoon (high tide was during the night). This resulted in a small net offshore sediment transport at the submerged bars and negligible transport at the chenier crest. On 2 December, a local wind event unrelated to the sea breeze took place during high tide. This caused significant (landward-directed) sediment transport due to waves, both through skewness and stirring.
The field observations show that both tide and waves transport sediment, thus driving the cross-shore chenier dynamics. Whereas the magnitude of both play

a role, it is mainly the timing of the higher waves and the higher water levels that is crucial for the cross-shore chenier dynamics. When the high waves occur during high tide, cheniers show behaviour similar to swash bars. Since the field observations took place during the calmer, SE monsoon season, they do not reveal mechanisms responsible for the cross-shore chenier dynamics during the NW monsoon season, including storm conditions. These conditions will be explored in more detail using a numerical model as part of future work.

3.A Estimate velocity from pressure signal

To obtain pressure-derived velocities use is made of linear wave theory following the approach of de Wit et al. (2019). The wave-related pressure for a monochromatic wave with radial frequency ω is given by:

$$p_{wave}(z,t) = \rho g a \frac{\cosh(k(h+z))}{\cosh(kh)} \cos(\omega t + \phi_p), \tag{3.4}$$

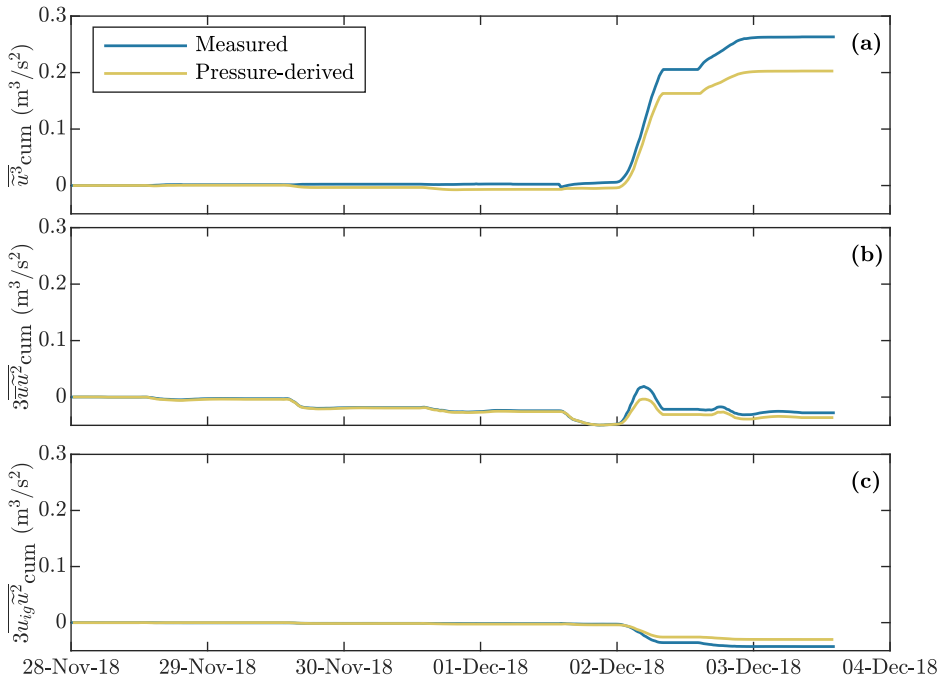
where z is the vertical elevation (defined positive upward from the mean water level), ρ the water density, g the gravitational constant, a the wave amplitude, h the local water depth, ϕ_p is a phase shift and the wave number k is obtained through the dispersion relation $\omega = \sqrt{gk\tanh(kh)}$. The corresponding expression for the horizontal orbital velocity is given by:

$$u_{wave}(z,t) = \omega a \frac{\cosh(k(h+z))}{\sinh(kh)} \cos(\omega t + \phi_u), \tag{3.5}$$

with ϕ_u a velocity phase shift. In case of progressive waves, the wave related pressure and velocity are in phase, hence $\phi_p = \phi_u$, and these two expressions can be combined to express the wave orbital velocity as function of the pressure:

$$u_{wave}(z,t) = p_{wave}(z,t) \frac{\omega}{\rho g} \frac{\cosh(kh)}{\sinh(kh)} = T(z,\omega) p_{wave}(z,t), \tag{3.6}$$

with T as the frequency-dependent transfer function.
Next the ADV-measured half-hour pressure record at location S1 is transformed with a Fast Fourier Transform (FFT) and multiplied with the frequency-dependent transfer function $T(\omega)$. Taking the inverse FFT then yields the pressure-derived velocity record. Comparing the cumulative velocity moments at S1 obtained with the measured horizontal velocity and the pressure derived velocities shows a good match with root mean square errors in the order of 10%. Supplementary Figure 3.10 shows the cumulative velocity moments calculated using the measured velocities (blue line) and the pressure-derived velocities (yellow line). Both lines show the same behaviour, but the magnitude of the pressure-derive velocity moments is slightly underestimated. Since this approach can only be used to estimate the wave orbital velocity, the measured mean velocity at the ADV is used to calculate the stirring for both the measured and pressure-derived velocity moments.



Supplementary Figure 3.10: Cumulative velocity moments calculated using the measured velocities (blue) and the pressure-derived velocities (yellow). **(a)** $\widetilde{\overline{u^3}}_{cum}$, short waves; **(b)** $3\widetilde{\overline{u}\widetilde{u}^2}_{cum}$, stirring; **(c)** $3\widetilde{\overline{u_{ig}u^2}}_{cum}$, infragravity waves.

Chapter 4

Drivers of cross-shore chenier dynamics off a drowning coastal plain

Abstract

A chenier is a beach ridge, consisting of sand and/or shells, overlying a muddy substrate. In this chapter, we explore the cross-shore dynamics of cheniers in their 'active' phase, i.e. the phase between their formation and their landing on the shore and can no longer be reached by daily wave and tidal influences. While cheniers described in literature are known to only migrate onshore until they reach a stable position with their crest level above tidal influences, observations in Demak suggest the existence of an alternative stable state, highly dynamic in the short term, but stable in the longer term. To explore this alternative stable state, we developed an idealised chenier model to investigate cross-shore chenier dynamics under daily wave and tidal influences. The model is able to predict both onshore and offshore migration; onshore migration is mainly driven by wave action, while offshore migration is induced by a tidal phase lag, or the effect of the storm season. For certain combinations of waves, tide (incl. phase lag) and a storm season effect, the model predicts a dynamically stable chenier. In absence of a phase lag and storm season effect, the model yields a 'classic' stable chenier that welds onto the shoreline by onshore migration

This chapter has been published as: Tas, S.A.J., van Maren, S.D., Helmi, M. & Reniers, A.J.H.M. (2022). Drivers of cross-shore chenier dynamics off a drowning coastal plain. *Marine Geology*, 445(106753). doi:10.1016/j.margeo.2022.106753.

4.1 Introduction

Cheniers are traditionally defined as ridges consisting of wave-reworked coarse-grained sediments, resting on top of muddy sediment, separated from the shoreline by a mudflat (Augustinus, 1989; Otvos and Price, 1979). While Otvos (2019) argues that the term 'chenier' may only be applied to ridges that are 'stranded', i.e. they are fixated between mudflats on both the landward and seaward side, and therefore are no longer influenced by daily wave and tidal processes, the term is also widely used for 'active cheniers', whose crest is still low enough to experience (occasional) overwash and can be considered dynamic. Some examples of active cheniers are the cheniers in the inter-bank phase along the coast of the Guianas (Anthony et al., 2010, 2013, 2019; Nardin and Fagherazzi, 2018; Augustinus, 1980; Brunier et al., 2019; Toorman et al., 2018), the cheniers that developed after the construction of a dike in Gomso Bay, Korea (Lee et al., 1994; Ryu et al., 2008), cheniers in the Firth of Thames, New Zealand (Woodroffe et al., 1983), and the cheniers forming the Saltés Island Chenier Plain in Spain (Morales et al., 2014). In this chapter we use this more generous interpretation of the term 'chenier' to include the active sandy ridges in a muddy intertidal zone.

Cheniers are usually found on mildly sloping coasts with a low to moderate wave-energy environment (Augustinus, 1989). Their formation depends on a specific balance between wave action and sediment availability and is generally episodic (Otvos and Price, 1979; Nardin and Fagherazzi, 2018; Anthony et al., 2019). Contrary to beach ridges found on sandy shores, which are built up from material similar in composition to the adjacent beach and shoreface (Taylor and Stone, 1996), the volume of a chenier is limited by the availability of coarser particles in the otherwise muddy shoreface (Anthony et al., 2019). As a result, when ridges are subjected to wave action, beach ridges may be able to build out both horizontally and vertically, but cheniers usually start migrating landward (and alongshore) instead of building up, due to the lack of additional sediment. Generally, cheniers continue to migrate landward by washover processes at a decelerating rate, until their crest is above spring tide or storm surge level (Augustinus, 1980, 1989; Morales et al., 2014; Rhodes, 1982; Woodroffe et al., 1983; Woodroffe and Grime, 1999). Only in the rare occasions when sufficient coarse sediment is available, cheniers are able to grow in volume and elevation, reducing sediment transport resulting from overwash processes and the resulting landward migration rate (Neal et al., 2002). For situations with sufficient sediment availability, the cheniers may then prograde seaward and/or alongshore (Neal et al., 2002; Augustinus, 1980). The landward migration may also end when a new chenier develops seaward of the active chenier (Woodroffe et al., 1983) or in the event of renewed coastal progradation (Augustinus, 1989). Often, relict cheniers can be observed as a series of coast-parallel ridges in the landscape, separated by muddy soil and/or peat, defined as a chenier plain (Russell and Howe, 1935; Otvos and Price, 1979).

Cheniers are also found along the coastline of Demak, a region on the north coast

of Central Java (see Figure 4.1a, indicated by the red circle) (Winterwerp et al., 2020; Marfai et al., 2016; Tas et al., 2020; van Bijsterveldt et al., in prep.b). Relict cheniers do not exist in the coastal plain, so this single band of cheniers along the coast is not part of a chenier plain. Even in landscapes that have undergone extreme (antropogenic) changes, relict cheniers are easily distinguishable because of their higher elevation and different composition, generating a sharp contrast to their surroundings. As a result, they are often used for roads, dikes and settlements (Russell and Howe, 1935; Anthony et al., 2011). The existence of a chenier plain can also be seen in deflections in drainage patterns (Otvos and Price, 1979). In the coastal area of Demak, however, all roads, dikes and villages are on lines perpendicular to the coastline, following the embankments of rivers and canals (see Figures 4.1b-c).

The mangrove-mud coast of Demak has experienced extreme coastal erosion over the last decades (Ervita and Marfai, 2017); at some locations the coastline has retreated with more than a kilometre (compare Figure 4.1b and Figure 4.1c). The mangrove forest that used to cover the entire coastal area (Lang, 1869) has been nearly completely converted to aquaculture ponds or cleared for the expansion of the nearby city of Semarang. Furthermore, ground water extraction has caused subsidence up to 20 cm/year in Semarang (Abidin et al., 2013; Kuehn et al., 2010), but also in rural areas subsidence is large enough to drown coastal villages, the vegetated foreshore and mudflats (van Bijsterveldt et al., in prep.a). As a result, a large part of the coastal plain is now flooded by tides on a daily basis.

Demak features a tropical monsoon climate, alternating a dry, southeasterly monsoon, usually between April and November, with a wet, northwesterly monsoon. Thanks to the orientation of the coastline in Demak, the southeasterly wind is directed offshore, and results in very calm conditions nearshore. The highest waves occur in the afternoon, when an onshore sea breeze develops locally (Fitrianti et al., 2018). Waves are generally higher during the onshore-directed NW monsoon, but during this period also storms occasionally occur. The tide can be characterised as micro-tidal with a maximum tidal range of around 1 m and it is mixed, mainly diurnal (based on water level time series measured between May 2016 and December 2018 in Semarang (Flanders Marine Institute (VLIZ) and Intergovernmental Oceanographic Commission (IOC), 2021)).

The cheniers in Demak are not only unique in their absence of a chenier plain, but also for their cross-shore dynamics. In other locations around the world, the cross-shore migration of cheniers is largely in the landward direction (Augustinus, 1989; Otvos, 2019; Quaresma et al., 2007) with migration rates usually decreasing over time because as the chenier moves higher, overwash becomes less frequent. For example, both in Saemangum, Korea and Mont-Saint-Michel Bay, France initially an onshore migration speed of 50 m/y was reported, which later reduced to 5 m/y in Korea (Kim et al., 2020) and 1-2 m/y in France (Weill et al., 2012). The highest onshore migration rates were reported on the Saltés Island chenier plain in Spain, up to 675 m in 3 years, averaging 225 m/y (Morales et al., 2014). Woodroffe et al. (1983) recorded onshore migration of 10 m within a week, due to

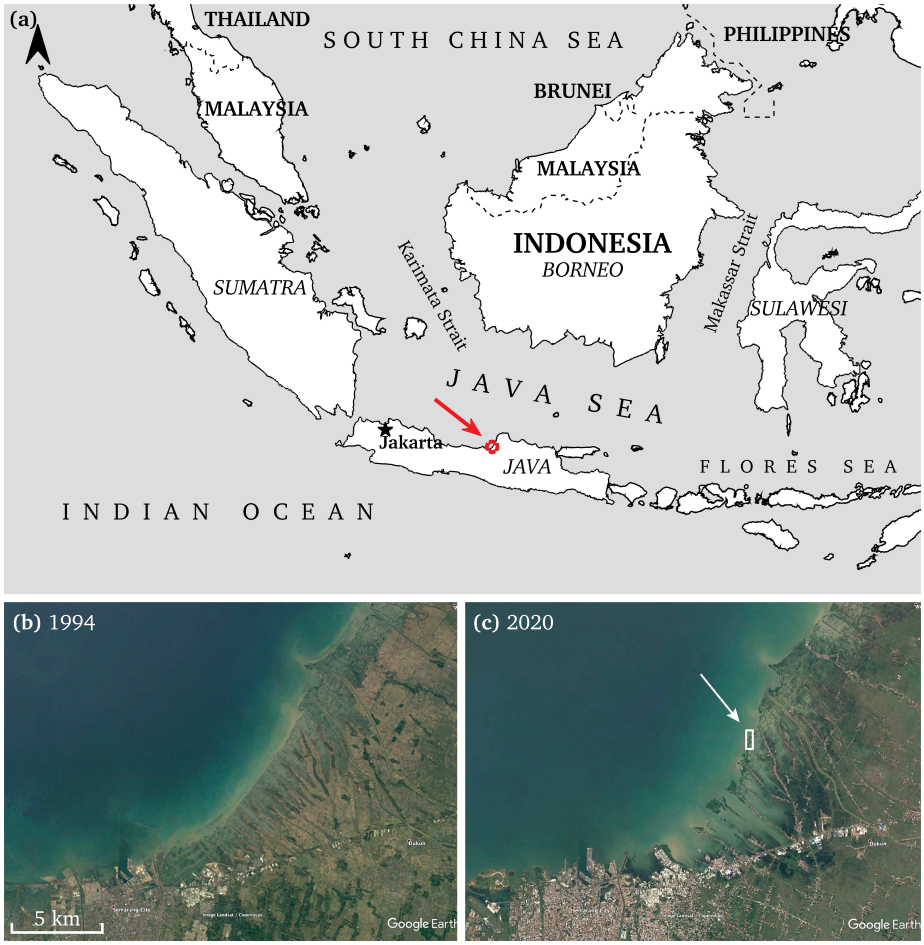


Figure 4.1: **(a)** Map of the Java Sea and surroundings. The red dot on the north coast of Central Java indicates the location of the two inset photos shown in **(b)** and **(c)**, which are satellite images of the coastline of Demak in 1994 and 2020 respectively (Google Earth, 2021). They highlight the extreme coastal erosion and coastline retreat in this area, as well as the rapid development of Semarang in the south. The white rectangle in (c) indicates the location of the zoomed satellite images in Figures 4.2a-d.

a storm event. Brunier et al. (2019) measured onshore migration rates of cheniers over coastlines that were rapidly retreating as a result of mangrove removal and fragmentation due to urbanisation and farming (very similar to the situation in Demak), and these rates were much higher than in areas with a healthy mangrove coastline (up to 70 m in 6 months). However, satellite images of Demak between 2009 and 2018 (see Figures 4.2a-d) reveal that the chenier remained more or less at the same location over a period of 10 years. However, on shorter timescales the

chenier is very dynamic, moving landward up to 8 m/day (see Figure 4.2e and Chapter 3).

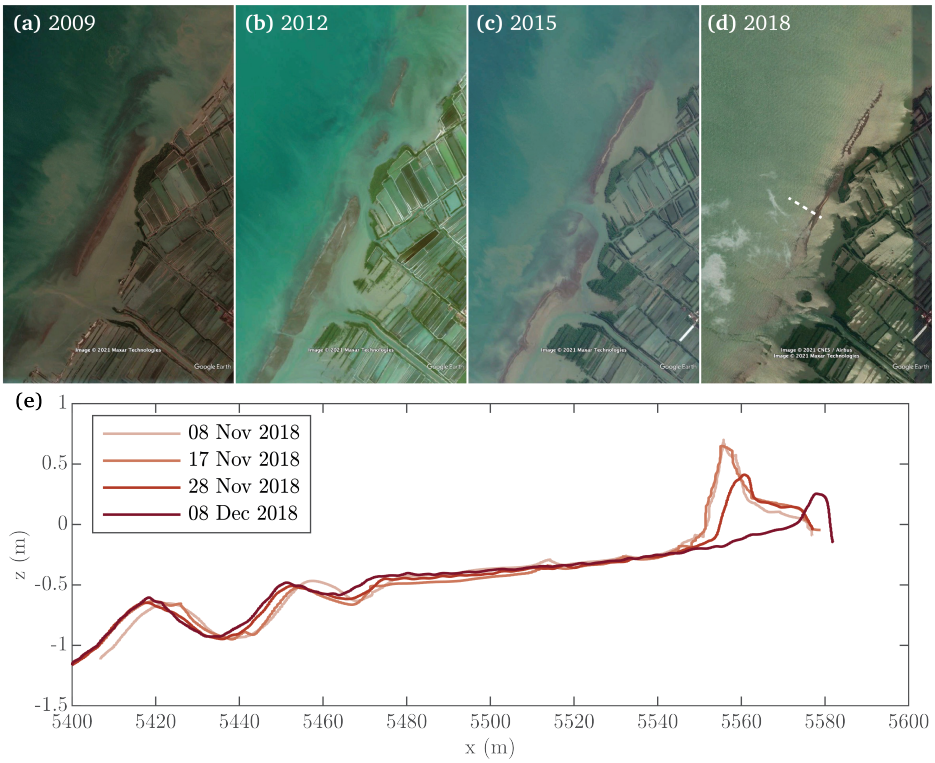


Figure 4.2: Google Earth images (Google Earth, 2021) showing the position of a chenier in **(a)** 2009, **(b)** 2012, **(c)** 2015 and **(d)** 2018 (see the white rectangle in Figure 4.1c for the location of this chenier along the coast of Demak). The profiles in **(e)** were measured with a Differential Global Positioning System (DGPS) between 8 November 2018 (light red line) and 8 December 2018 (dark red line). The white dashed line in (d) indicates the transect along which the profiles in (e) were measured.

The aim of this chapter is to understand the drivers of cross-shore chenier dynamics during their 'active phase', i.e. the phase between their formation and the moment the chenier is stranded on the shoreline and no longer mobile in response to daily wave and tidal influences. Whereas cheniers described in literature have one primary migration mode (landward migration until stranded), observations of the chenier in Demak suggest that there may be an alternative stable state where a chenier is very dynamic in the short term, but still maintains an equilibrium position (not attached to the coastline) over longer timescales. This implies that there is also a mechanism that transports the chenier offshore. To better understand the short-term and long-term dynamics and underlying transport mechanisms, we have constructed an idealised morphodynamic chenier model. The set-up of this model is described in Section 4.2. In Section 4.3, we calibrate the model results

with (short term) field measurements, and then address the chenier response to various boundary conditions. In Section 4.4 we compare the model results to observed chenier dynamics in literature, assess the specific dynamics in Demak, draw an analogy between breaker bars and cheniers, and discuss how cheniers could be part of a negative feedback loop induced by the erosion of a drowning coastal plain.

4.2 Methods

A wide range of morphological models exists in literature, ranging from high complexity numerical models to a simple set of empirical equations. High complexity models often account for most of the relevant transport processes, but they also have several disadvantages. Computational times are often long, it is not straightforward to differentiate underlying processes, and imperfect descriptions of the physics may lead to unrealistic model behaviour (such as the predictions of nearshore sandbar dynamics; see Cohn et al. (2019); Dubarbier et al. (2015); Spaans (2019)). Idealised models are specifically designed to focus on processes that are considered essential to describe a particular phenomenon. Idealised models are fast and suitable to investigate certain processes, but lack the complex physics of numerical models. When selecting a modelling approach, the most appropriate scales (temporal and spatial) of the system need to be determined. Observations of the chenier system in Demak (see Figure 4.2) have shown that a large range of timescales is required: from the short-term dynamics, to the long-term (average) stability. Besides resolving the appropriate scales, the selected modelling approach should be computationally feasible, have a sound physical basis and demonstrate useful predictive skill (French et al., 2016).
In this section we will present a hybrid model, which is essentially an idealised model coupled to a complex numerical model. The numerical model provides the sound physical basis on short time scales (role of waves and tides in sediment transport and morphology), which is synthesised in a look-up table. The idealised model is inspired by the elegant barrier model of Lorenzo-Trueba and Ashton (2014), and computes long-term chenier morphodynamics for a range of scenarios using the look-up table generated by the numerical model. This hybrid approach allows for a very low computational effort. The model is applied in exploratory mode (Murray, 2003), i.e. to investigate the role of specific processes, so not to reproduce a specific development in great detail.

4.2.1 Chenier geometry

We approximate the cross-sectional dynamics of the chenier with an idealised geometry, similar to idealised geometries of deltas and barrier islands (Parker and Muto, 2003; Lorenzo-Trueba and Ashton, 2014), see Figure 4.3a. The model consists of two components: the muddy subsurface, and the sandy chenier. We assume the muddy substrate to be static; it has a constant slope of β and there is

no sediment exchange between the two components. The chenier body is defined by four parameters: the chenier toe (indicated with subscript T), the beachface toe (subscript S), the toe of the back-barrier face (subscript B) and the height of the chenier crest (H, defined as the vertical distance between the beachface toe and the crest of the chenier). The model assumes conservation of sand volume, so the surface area defined by these four parameters in the cross-section remains constant. The surface area/volume of the chenier is represented by one single point in the computations: the chenier center (subscript C). This point is defined horizontally as the middle between the beachface and the back-barrier face, $x_C = x_S + (x_B - x_S)/2$, and vertically as the highest point of the chenier, $z_C = z_S + H$. The chenier toe has a slope α, which is steeper than the offshore shoreface slope β. The slope of the beach and back-barrier is several orders of magnitude steeper (Heward, 1981) and are approximated as vertical.

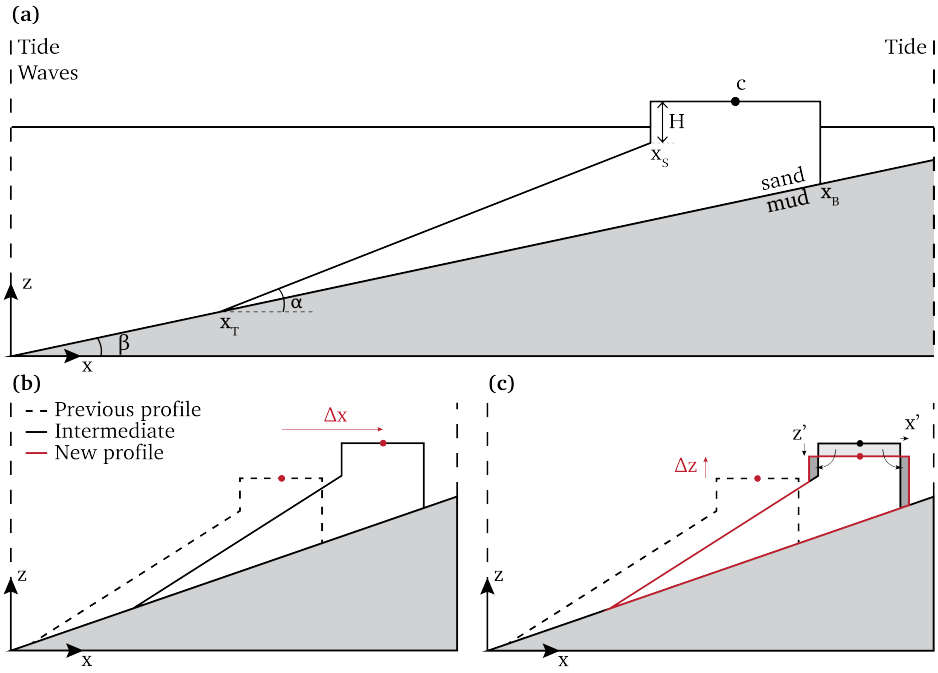


Figure 4.3: **(a)** Idealised chenier geometry, defined by the chenier toe (x_T), the beachface toe (x_S), the toe of the back-barrier face (x_B) and the chenier crest height (H). The chenier center (C) is indicated with a dot. The chenier body is composed of sand (white) and lies on top of a muddy substrate (gray). The muddy shoreface has a slope of β, and the chenier slope has a steeper slope of α. The chenier evolution is explained in two steps: **(b)** first the entire chenier unit is moved horizontally with Δx along the muddy substrate; **(c)** then the vertical change is corrected with z' such that the total vertical change equals Δz. This vertical correction yields a change in width with x' on both sides in order to conserve the volume/surface area of the chenier.

4.2.2 Chenier dynamics

The idealised chenier evolves over time by prescribing hourly displacement rates, computed with a process-based model (Delft3D), which will be specified in more detail in the section hereafter. Every hour, the chenier center moves horizontally with Δx and vertically with Δz (derived from Delft3D for the specific boundary conditions at that time step), and the shape of the chenier (height and width) changes such that the total volume of sand remains constant. This procedure is explained in two steps and is illustrated in Figures 4.3b-c: first, the entire chenier migrates upslope (or downslope if $\Delta x < 0$), without changing the shape of the chenier (see Figure 4.3b). Since the muddy substrate has a slope β, this horizontal migration with Δx automatically yields a vertical change as well, equal to $\beta \Delta x$. However, this vertical change is not necessarily equal to the total vertical change of the chenier center, Δz. Therefore, the vertical change needs to be corrected with z' such that the total vertical change of the chenier center equals $\Delta z = \beta \Delta x - z'$ (see Figure 4.3c). In case $\Delta z < \beta \Delta x$, sediment is removed from the crest of the chenier, and equally distributed on both sides in terms of lateral expansion x' (so that the horizontal position of the chenier center is maintained). In case $\Delta z > \beta \Delta x$, the crest of the chenier is heightened with sediment from both sides of the chenier crest, reducing the width of the chenier with $2x'$ and increasing the height of the chenier H with z'. The new coordinates of the four chenier parameters (subscript 1) can be expressed in function of Δx, Δz, and the coordinates at the previous time step (subscript 0):

$$x_{T,1} = x_{T,0} + \Delta x\,, \tag{4.1}$$
$$z_{T,1} = z_{T,0} + \beta \Delta x\,, \tag{4.2}$$
$$x_{S,1} = x_{S,0} + \Delta x - x'\,, \tag{4.3}$$
$$z_{S,1} = z_{S,0} + \beta \Delta x - \alpha x'\,, \tag{4.4}$$
$$x_{B,1} = x_{B,0} + \Delta x + x'\,, \tag{4.5}$$
$$z_{B,1} = z_{B,0} + \beta \Delta x + \beta x'\,, \tag{4.6}$$
$$H_1 = H_0 - \beta \Delta x + \Delta z\,; \tag{4.7}$$

where

$$x' = \frac{(x_{B,0} - x_{S,0})(\beta \Delta x - \Delta z)}{2H_0 + 2\Delta z + z_{S,0} - z_{B,0} - \beta \Delta x}\,. \tag{4.8}$$

For all steps in the model described above, sediment mass is conserved (i.e. the total body of sand in the chenier does not change in time). The horizontal and vertical displacements, Δx and Δz are a function of (1) the offshore wave height, $H_{s,\infty}$; (2) the water depth on top of the chenier crest, h_{top} (see Figure 4.4c); (3) the phase of the tide (ebb or flood); and (4) a phase lag, θ (see Figure 4.4c). We use a process-based model to determine the relationship between Δx and Δz on one hand, and the tidal and wave conditions on the other hand, through a large

number of model realisations. Before introducing this process-based model, we first elaborate on the the phase lag θ.

4.2.3 Boundary conditions

The chenier only becomes mobile when it is fully submerged[1], i.e. when the water level η exceeds the chenier crest level $\eta > z_S + H$. Field observations (Chapter 3) showed that both tide and waves are responsible for sediment transport on the cheniers of Demak. Waves transport sediment directly, through skewness, and indirectly, through stirring, where waves stir up the sediment which is then transported by tidal currents. Tidal currents are only sufficiently strong to resuspend sediments when the water depth above the chenier is very small. Most sediment transport occurs when high tide (i.e. inundated chenier) coincides with high wave events. Weill et al. (2012), for instance, showed that most chenier migration took place when the 4.4-year and/or 18.6-year tidal cycles caused higher water levels in the Mont-Saint-Michel Bay, while we linked chenier migration to the interaction between the diurnal component of the tide and the sea breeze-induced waves which occurred in the afternoon (Chapter 3).

Due to coastal erosion and subsidence, large parts of the coastal plain in Demak flood during each tide. This drowning of the coastal plain induces a phase lag in tidal flow over the chenier. Due to the strong antropogenic influence in this area, this phase lag is even more pronounced than in undisturbed systems, for the following reasons. The drowned coastal plain is characterised by a few channels (either remnants of man-made channels, or naturally formed creeks) with relatively low hydraulic drag (Bayliss-Smith et al., 1979; Friedrichs, 2010), while the rest of the basin is covered by obstacles (such as mangrove vegetation, aquaculture pond bunds, houses etc.) which generate high friction (Temmerman et al., 2005; Horstman et al., 2013, 2021). The rising tide can enter the tidal basin through the channels, eventually flooding the entire area; during ebb the water flows back first over the high-friction shallow areas, before reaching the channels and creeks (Friedrichs and Madsen, 1992; Mazda et al., 1995; Horstman et al., 2021). Due to the high resistance, this ebb flow is slowed down, and a tidal phase lag develops between the tidal basin and the open sea. Lower friction in the straight, man-made channels and higher friction on the tidal flats due to remnants of constructions creates an even larger phase lag. This phase lag generates a cross-shore water level gradient near the mouth of the channels and creeks. When a (sufficiently long) chenier is present in front of a channel mouth, this water level gradient occurs over the chenier crest, resulting in a residual seaward-directed flow. The magnitude of this flow (and the resulting sediment transport) is related to the tidal range and inversely related to the water depth above the chenier crest. This results in three boundary conditions for the idealised chenier model: an offshore wave height, applied at the seaward boundary, and two water levels, one

[1] In reality this is less straightforward: while the mean water level may be below the chenier crest level, higher waves could roll over the crest and transport sediment. To account for this transport, the water level in the model is increased with 10% of the significant wave height.

applied at the seaward boundary and one at the landward boundary. During flood, these water levels are in phase, while during ebb a phase lag may be prescribed at the landward boundary, see Figure 4.4.

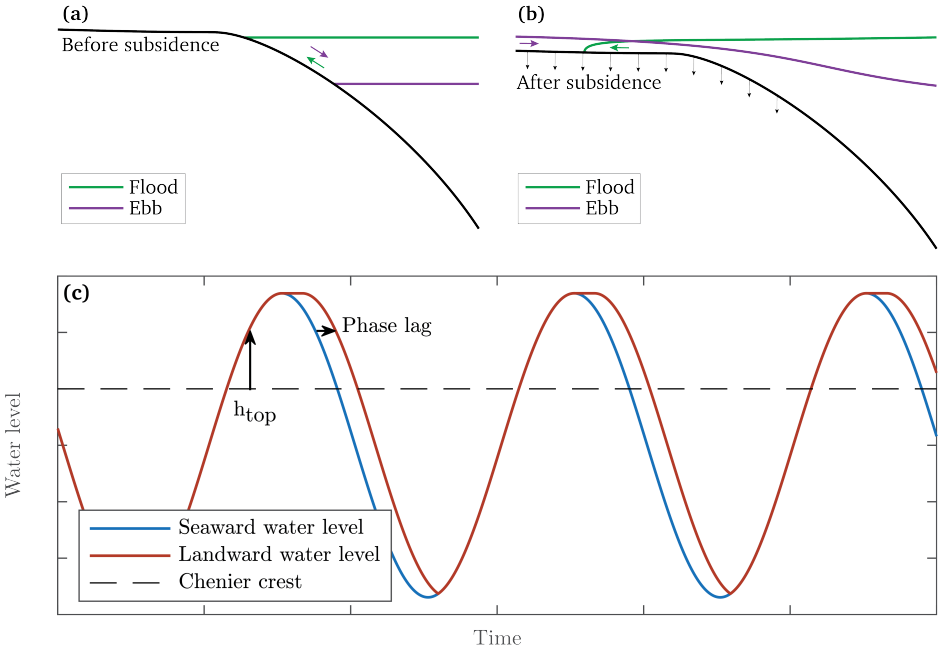


Figure 4.4: **(a)** Situation without a drowned hinterland due to subsidence: no phase lag. **(b)** Situation where subsidence has caused the hinterland to flood with each high tide (green line), which causes a phase lag to develop during ebb (purple line); water levels are vertically exaggerated for illustrative purposes. **(c)** Water level time series applied to the seaward model boundary (blue line) and landward model boundary (red line). During flood both water levels are in phase, during ebb the landward water level lags behind.

4.2.4 Process-based model

The values of Δx and Δz used in the idealised model are computed using a morphodynamic model set-up in Delft3D. Delft3D is a process-based modelling suite that is capable of simulating hydrodynamics (flow and waves), sediment transport and morphology (Lesser et al., 2004). This Delft3D model set-up uses an alongshore uniform, generalised profile representative for a chenier (dashed line in Figure 4.5a). Similar to the idealised geometry, the chenier center of this generalised profile in D3D is defined as the part of the chenier above the lowest low water line. The chenier center of the generalised profile used in Delft3D has the same coordinates as the center of the idealised geometry used in the idealised model (solid line in Figure 4.5a).
At the seaward boundary of the Delft3D domain, a time-varying water level and wave height is prescribed. The wave height is the wave height at deep water,

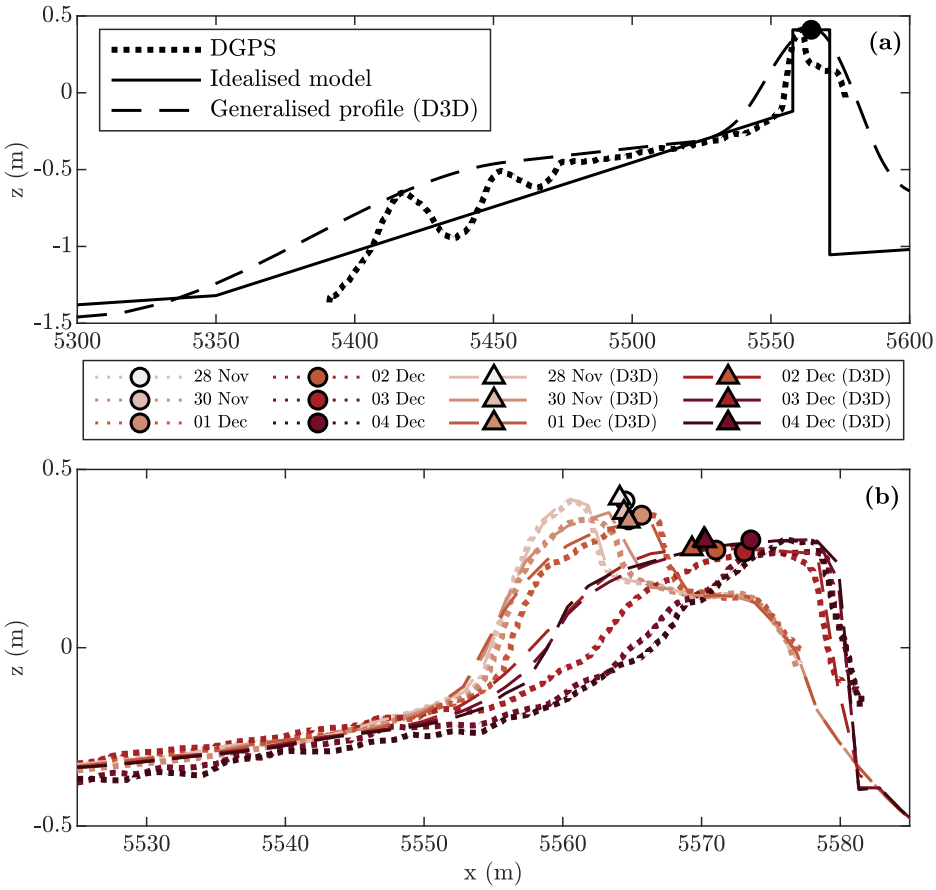


Figure 4.5: **(a)** Bathymetric profile measured with a DGPS in Demak, Indonesia (dotted line), with its representative idealised geometry (solid line) and a generalised chenier profile for the Delft3D simulations (dashed line). The chenier center of all three profiles coincides and is indicated with a dot. **(b)** Comparison of the validation run with Delft3D (dashed lines) to the measured profiles (dotted lines). The colours represent the days between 28 November 2018 and 4 December 2018. The chenier center of the measured profiles is indicated with a dot, and a triangle for the Delft3D profiles.

corrected for shoaling to the water depth at the model domain boundary. The landward end of the domain is also an open boundary, where only a water level time series is prescribed (to which the phase lag θ applies).

The Delft3D model is run for a representative range of calm to moderate conditions, representative for the SE monsoon season: (1) $H_{s,\infty} = 0 - 2$ m; (2) $h_{top} = 0 - 2$ m; (3) ebb or flood; and (4) $\theta = 0 - 20$ min. Since measurements were collected during the SE monsoon season, the model can only be validated for calm to moderate conditions (see Section 4.2.5), and therefore storm conditions are not considered here. For each possible combination of boundary conditions, the model is run for 6 hours, and the bed level change between the second and

sixth hour of the model simulation is used to determine the average change per hour (so total change divided by 4 hours). These values are stored in a hourly displacement matrix (see Figure 4.6). For each time step in the idealised chenier model, the values of Δx and Δz are interpolated for the current values of $H_{s,\infty}$, h_{top}, ebb/flood, and θ from the displacement matrix.

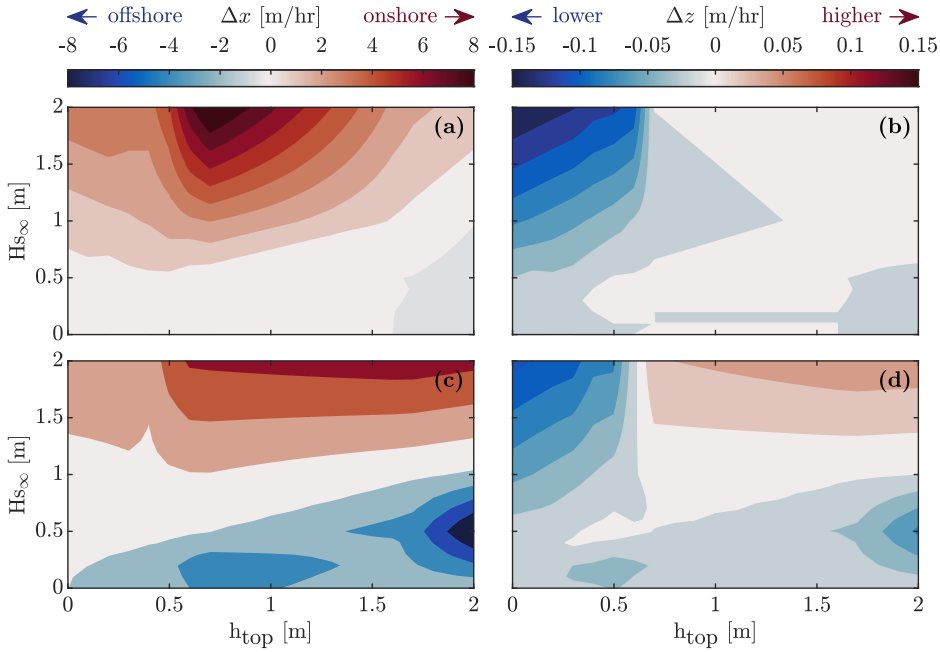


Figure 4.6: Hourly horizontal and vertical displacement based on the Delft3D model for some of the scenarios. The left column (**(a)** and **(c)**) shows the values of Δx and the right column (**(b)** and **(d)**) Δz; while the upper row (a and b) shows the displacements for a situation during ebb without a phase lag ($\theta = 0$ min) and the lower row (c and d) a situation during ebb with a phase lag of $\theta = 10$ min. Within the contour plot, the horizontal axis shows the water depth on top of the chenier h_{top} and the vertical axis the deep water wave height $H_{s,\infty}$. The red colour represents an onshore or upward shift for Δx and Δz respectively, blue means offshore-directed (Δx) or lowering (Δz).

Figure 4.6 visualises the different hourly displacements for a range of water depths above the chenier (horizontal axis) and offshore wave heights (vertical axis). The left panels (a and c) show the hourly horizontal displacement Δx in m, where blue colours represent offshore migration and red colours onshore migration; the right panels (b and d) show the hourly vertical displacement Δz in m, where blue colours represent lowering of the chenier crest and red colours heightening. The first row (a and b) shows a scenario during ebb when there is no phase lag; the second row (c and d) shows a scenario during ebb with a phase lag $\theta = 10$ min. From Figure 4.6a we can derive that higher waves lead to more onshore transport, and combined with Figure 4.6b, higher waves also lead to a lowering of the chenier crest for small water depths. The absence of blue shades in Figure 4.6a reveals

that under these circumstances, the chenier only migrates onshore. Only when introducing a phase lag during ebb (Figures 4.6c-d), the chenier also migrates in the offshore direction (for smaller wave heights in combination with larger water depths).

4.2.5 Validation Delft3D model

The Delft3D model was validated with 6 days of data collected at a chenier off the mangrove-mud coast in Demak, Indonesia between 28 November 2018 and 4 December 2018. The measured initial profile (dotted line in Figure 4.5a) is used as initial profile for this validation run. For the validation run, offshore waves were measured with a WaveDroid directional wave buoy and water levels were measured with two OSSI-010-003C-01 Wave Loggers, one which was deployed seaward of the chenier and one landward. The profiles computed with Delft3D (dashed lines, triangle for chenier center) are shown in Figure 4.5b and compared to the measured profiles (dotted lines, dot for chenier center). While the exact shape of the profiles diverges slightly over time, the migration of the chenier center of both the measured and modelled profiles remain very similar.

4.3 Results

4.3.1 Calibration idealised chenier model

The first set of model results with the idealised model (not shown here) predicted a gradual lowering of the chenier crest. This lowering results from the tendency that morphodynamic models such as Delft3D tend to flatten bars (van Duin et al., 2004). We mitigate this shortcoming through a vertical correction z_{corr}, so that the Δz applied in Equations 4.3-4.7 becomes $\Delta z = \Delta z_{D3D} + z_{corr}$. The value of z_{corr} was calibrated using the measured profiles. Various distributions were tested, but in the end the most optimal results were obtained for a constant value of $z_{corr} = 0.0015$ m/hr. The resulting profiles computed with the idealised model simulation are shown in Figure 4.7 (solid lines) and compared to the measured profiles (dotted lines).
While the modelled profiles may not perfectly follow the measured profiles, the trends are very similar: small changes the first days, followed by a larger landward migration and lowering, and on the last days small horizontal migration accompanied by some heightening of the crest.

4.3.2 Idealised boundary conditions

As a next step, the model is run for a much longer time span of 10 years. These longer model simulations are first executed with a schematic, idealised set of boundary conditions. A water level time series is constructed with the two main tidal constituents in Demak: K1 and M2. Based on the typical sea-breeze

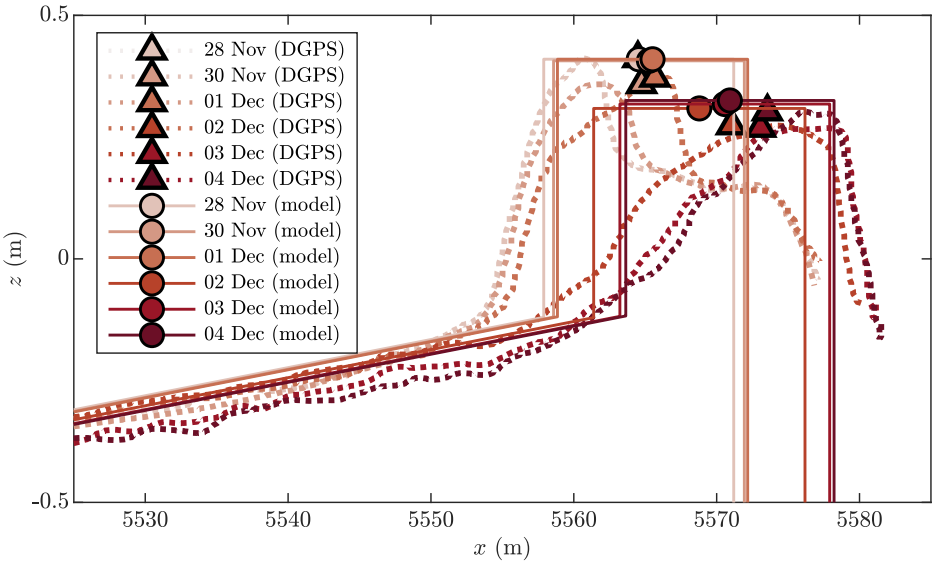


Figure 4.7: Comparison of the idealised model (solid lines) with measured profile changes (dotted lines). The chenier center in the idealised model profiles is indicated with a dot and in the computed model profiles with a triangle.

induced waves, a schematic wave time series is constructed, with waves during the afternoon and evening only (between 14h00 and 22h00), while the rest of the day no waves occur (since the SE monsoon wind is directed offshore, resulting in very calm conditions nearshore). During the sea breeze, the wave height is constant, $H_{s,\infty} = 0.23$ m, representative for the waves measured with a WaveDroid at deep water during sea breeze events. Figure 4.8 shows the resulting profiles after 10 years as a result of these schematic boundary conditions, both without a phase lag ($\theta = 0$, Figure 4.8a), and with a phase lag ($\theta = 3.5$ minutes; Figure 4.8b).
For the scenario without phase lag (Figure 4.8a), the chenier migrates onshore. Interestingly, this migration rate is not constant throughout the year. For a couple of months, the chenier migrates rather rapidly onshore, generally accompanied by a small lowering of the crest level. This onshore migration is halted rather abruptly, and replaced by a strong vertical growth, until the chenier has reached a height close to high water level. It remains stable for a while, until at some point the maximum water levels are high enough to submerge the chenier. The chenier crest then lowers rapidly and the chenier again migrates rapidly onshore starting a new cycle that is repetitive over multiple years. This cyclic pattern is a result of the timing between the sea breeze-induced waves and the tide. The sea breeze always occurs at exactly the same time (during the afternoon, between 14h00 and 22h00), but the time of the (diurnal) high tide shifts a day in a year (see Figure 3.9).
The persistent wave-driven onshore migration in Figure 4.8a result in onshore welding of the chenier, and not in a dynamically stable chenier as observed in

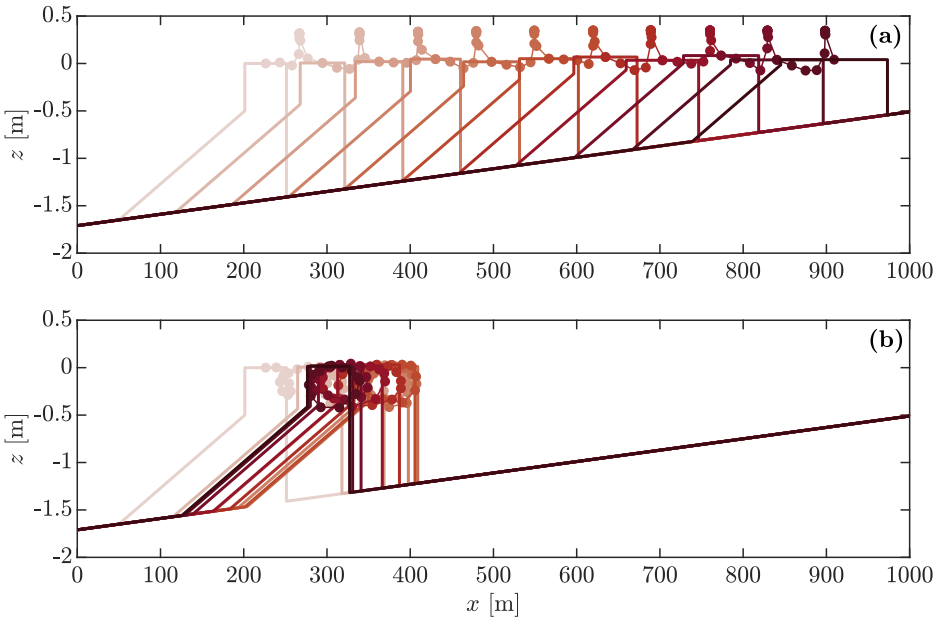


Figure 4.8: Chenier evolution under idealised boundary conditions, for a situation **(a)** without phase lag, and **(b)** with a phase lag of $\theta = 3.5$ min. One profile per year is shown, with increasingly darker shades of red over time. The chenier center is indicated with a dot, and is shown for each month, giving an impression of the dynamics during the year.

Demak. This stability does result from a non-zero phase lag (Figure 4.8b). The phase lag (see section 4.2.3) creates a water level gradient over the chenier, with higher water levels on the landward side. This induces flow over the chenier in the offshore direction, driving offshore sediment transport. For values of θ close to $\theta = 3.5$ min (and a sea breeze-induced wave height of $H_{s,\infty} = 0.23$ m), the onshore migration by waves is balanced by the offshore migration during ebb induced by the phase lag. As the timing between the sea breeze-induced waves and the tide shifts, one process becomes dominant over the other, resulting in a circular pattern over the year. This balance only occurs for a very small range of combinations of wave height and phase lag; for all other combinations the chenier either migrates onshore or offshore.

4.3.3 Stochastic boundary conditions

In the previous section, the boundary conditions were reduced to a set of idealised conditions to identify the role of moderate wave conditions and θ. In reality, the boundary conditions are much more variable. The tide consists of a wide range of constituents, and while the pattern of the sea breeze is fairly regular, its magnitude and presence may vary. To account for these variations, the model is forced with water levels computed with a full set of tidal constituents, and a stochastic wave

climate based on measurements collected with a WaveDroid during August 2017, April 2018 and October-November 2018 (all during the SE monsoon season). The corresponding time series is constructed as follows.

Field observations show that a sea breeze occurred for 50% of time. The synthetic wave conditions time series is thus determined in two steps: first, the occurrence of a sea breeze (hence, whether there are waves in the afternoon) is determined randomly with a 50% probability of sea breeze. Then, if there is a sea breeze that day, a wave height is randomly picked from a database containing observed daily wave heights. For the first and last hour of the sea breeze event (14h00 and 22h00), the wave height is 50% of the representative wave height, the other six hours the wave height is 100% of the representative wave height to mimic the onset and waning of the sea breeze.

The random selection of wave input parameters allows for a stochastic evaluation of chenier dynamics by creating many realisations (500 in this case), generating a probability density function (pdf) of horizontal and vertical chenier displacement for various scenarios. The pdfs computed with four different values of θ (0, 2.5, 5 and 7 minutes; Figures 4.9a-b) reveal that for the situation without a phase lag (lightest shade blue, solid line), the horizontal and vertical migration is positive (i.e. the chenier migrates onshore and the crest level becomes higher).

For small phase lags, the chenier still migrates onshore (positive horizontal migration), but the crest level lowers (negative vertical migration). This vertical migration is accompanied by a widening of the crest, i.e. the chenier spreads out to become an increasingly thinner layer of sand on top of the muddy substrate. Moreover, the lowering of the crest is limited by the stable muddy substrate (which is a consequence of our assumption of a constant slope), so when the crest level reaches the muddy substrate, the chenier is assumed to have dissolved[2]. For $\theta = 2.5$ min, 95% of the model realisations reach this point within 10 years, with an average simulation time of 3.6 years. For $\theta = 5$ min, 98% of the model realisations reach this point within 10 years, with an average simulation time of 2.5 years. In other words, for small phase lags, the chenier dissolves as a wide, fine layer of sand on top of the muddy substrate. This layer of sand is located closer the shoreline for smaller phase lags.

For larger phase lags, such as $\theta = 7$ min (darkest blue, dotted line in Figures 4.9a-b), the chenier migrates in the offshore direction (with its crest just below MSL). As can be seen by the double peak in the pdfs, part of the simulations (around 25% of the model realisations) shows the same behaviour as for the smaller phase lags, with the chenier migrating onshore while lowering until the chenier sand spreads out over the muddy substrate and the chenier dissolves (although this fine layer of sand is further offshore compared to a situation with a smaller phase lag).

Similar to the idealised boundary conditions, the chenier remains stable horizontally for only a narrow range of phase lags θ. Smaller values lead to onshore

[2] The sand is still present in the system, so at a later point a new chenier may be formed, but that is beyond the scope of this model.

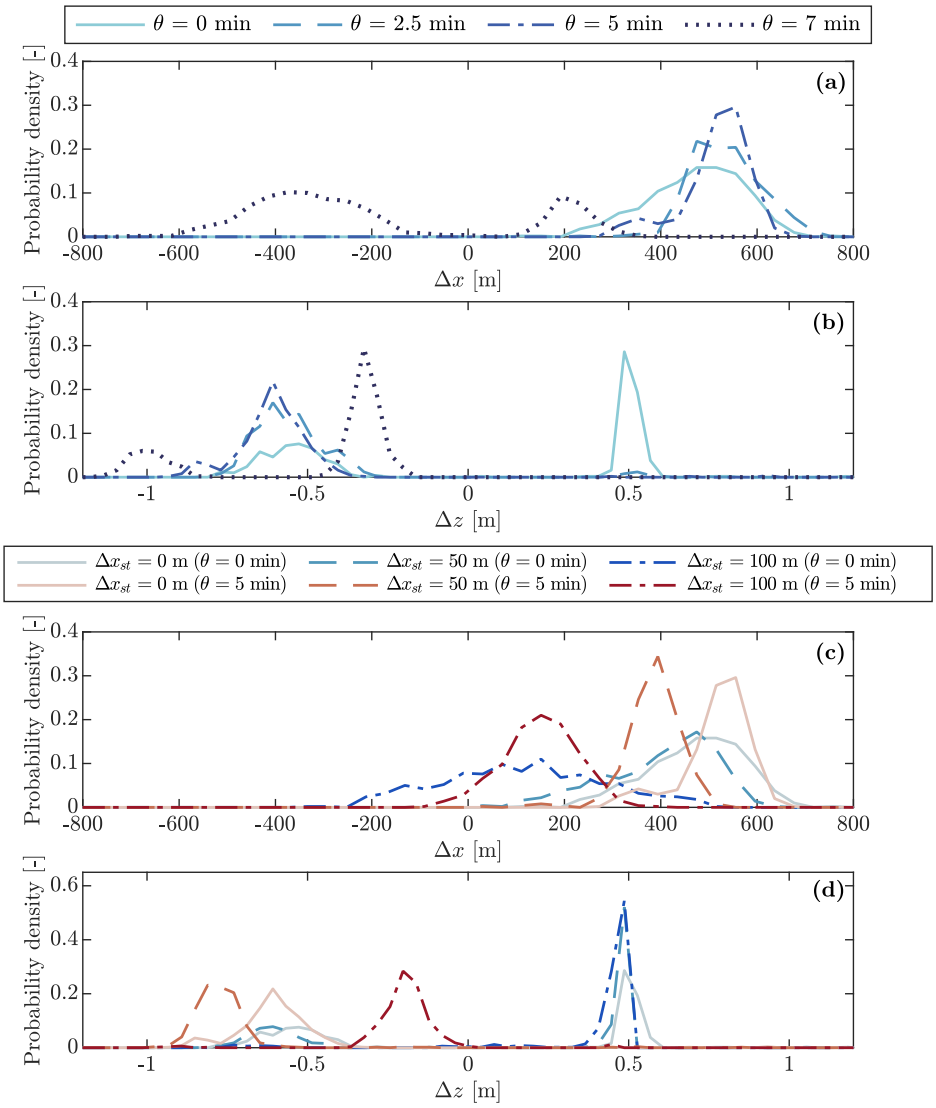


Figure 4.9: Probability density functions of the horizontal (**(a)** and **(c)**) and vertical (**(b)** and **(d)**) displacement (relative to the initial position) for different scenarios over a period of 10 years after 500 realisations. The effect of different phase lags is shown in **(a)** and **(b)**, with increasingly darker shades of blue (and going from solid via dashed, dash-dotted to dotted lines) for larger values of the phase lag, θ. The effect of a storm reset Δx_{st} is visualised in **(c)** and **(d)**, with increasingly darker shades for larger values of Δx_{st}. Blue lines represent a situation without a phase lag; red lines $\theta = 5$ min.

migration until either the crest reaches high tide, or the crest lowers until the chenier dissolves as a wide, thin layer of sand on the muddy substrate closer to the shoreline. Larger values lead to offshore migration, with the crest between

low tide and MSL.
While the phase lag mainly has a horizontal effect (onshore vs. offshore migration), it also has a small vertical effect (generally two orders of magnitude smaller than the horizontal displacement, see Figures 4.6 and 4.12). This vertical effect can cause an indirect horizontal effect, because by lowering the crest, the chenier is submerged longer, which in turn may lead to additional horizontal displacement. In some cases, it is therefore possible that a scenario with a phase lag may lead to more onshore migration than a scenario without a phase lag (compare the tails of the pdfs of $\theta = 0$ min and $\theta = 2.5$ min in Figure 4.9a).
The model realisations in Figures 4.9a-b assume a year-round dominance of sea-breeze conditions (as this was the period for which we had data available). However, these conditions are only representative for the SE monsoon season. Between December and March (the NW monsoon season) winds are constantly onshore, resulting in higher waves throughout the entire day, and with occasional storms. Due to the absence of measurements during the NW monsoon season, the idealised chenier model has not been tested and calibrated for such conditions. Moreover, there are no satellite images available during these months due to cloud cover. However, comparing the last satellite image before the NW monsoon season with the first image after, suggests that there is a net offshore migration over the NW monsoon season. To avoid using the model under storm conditions (for which we do not have field data to calibrate the model with, moreover during storm conditions other processes may govern the chenier dynamics) we simplify the net effect of the storm season as a net seaward displacement over a distance Δx_{st} at the last time step of the SE monsoon season. This new position is then the starting point for the calculations of the next SE monsoon season. The exact magnitude of such a storm reset is unknown; based on Google Earth images, it is estimated to be in the order of 50 m. However, cloud cover typical for the NW monsoon season prevent an accurate estimate for Δx_{st}. Therefore, $\Delta x_{st} = 50$ m and $\Delta x_{st} = 100$ m are both tested and compared to $\Delta x_{st} = 0$ m to assess the effect of this storm reset.
Figures 4.9c-d show the probability density functions of the horizontal and vertical displacements after 10 years, for different values of Δx_{st} (darker colours for larger storm resets) and with (red colours) and without (blue colours) phase lag. Without a phase lag, regardless of the magnitude of the storm reset Δx_{st}, the horizontal distribution is wide, but vertically very narrow. This indicates that all simulations converge to a crest around high tide, but there is quite some variation in the amount of horizontal migration. In the case of $\Delta x_{st} = 0$ m (lightest blue shade), the chenier shows the most onshore migration. For $\Delta x_{st} = 50$ m, the chenier still migrates onshore, but less; for $\Delta x_{st} = 100$ m the horizontal migration is smallest, and could be both in the onshore or offshore direction. For even larger values of Δx_{st} (not shown), all horizontal migration is offshore-directed.
In the scenarios with a moderate phase lag of $\theta = 5$ min, the chenier crest no longer reaches high tide (as described above). The simulations with a moderate storm reset ($\Delta x_{st} = 50$ m) follow the same behaviour as the scenario without

a storm reset, for most model realisations (97%) the chenier sand spreads out as a thin layer on top of the muddy substrate close to shore (average simulation time 5.1 years). However, due to the storm reset, this sand layer is located more seaward than the previous scenario without a storm reset. A larger storm reset ($\Delta x_{st} = 100$ m) does not follow this trend of onshore migration and diffusion over the muddy substrate; instead the chenier remains between MSL and low tide. The horizontal migration remains limited and could be either onshore or offshore. Without a phase lag, only 4% of the model realisations lead to chenier dissolution, and with a phase lag of $\theta = 5$ min, this is the case for less than 1%.
In summary, the storm reset's main effect is a seaward displacement. Due to this yearly seaward displacement (and consequent lowering), the chenier remains more dynamic, even if the crest reached a high enough elevation to prevent submergence by regular tides during the SE monsoon season. Throughout the year, the chenier's behaviour is still dominated by the interaction between the waves, tide and a possible phase lag.

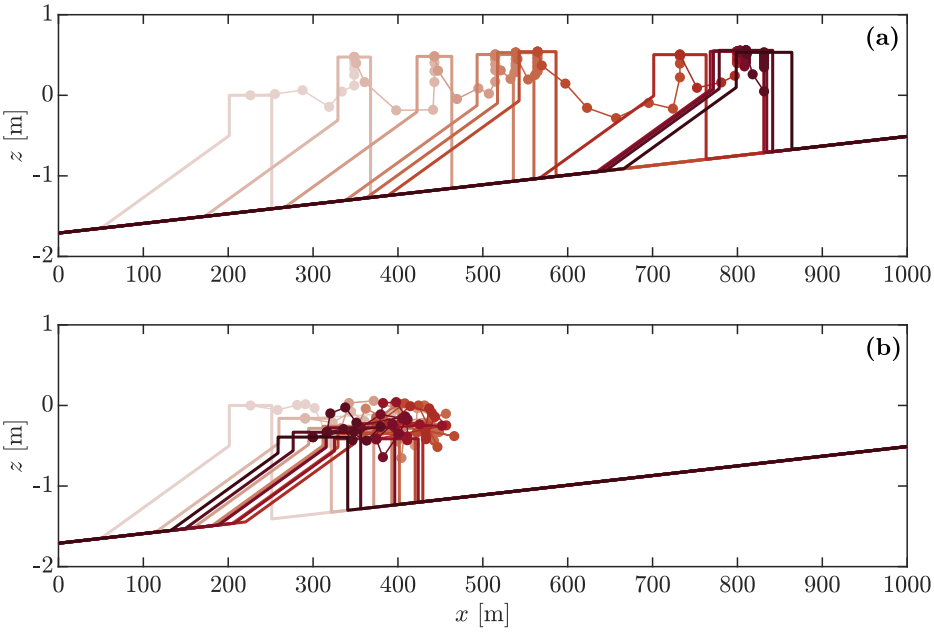


Figure 4.10: Chenier evolution over 10 years, under stochastic boundary conditions. One profile per year is pictured, in increasingly darker shades of red. The position of the chenier center is indicated with a dot for each month. Panel **(a)** shows a scenario without phase lag ($\theta = 0$ min) or storm reset ($\Delta x_{st} = 0$ m). Panel **(b)** shows a scenario with a phase lag of $\theta = 5$ min and a storm reset of $\Delta x_{st} = 100$ m.

As a final step, all the processes and short-term dynamics described above are combined to investigate the long-term dynamics (10 years), and possible stable chenier states. First, a 'classic' chenier is modelled, without phase lag or storm reset (see Figure 4.10a). The chenier migrates onshore, and the crest level

increases until it is close to the highest tidal levels. Once it reaches this high elevation, the onshore migration becomes more episodic, requiring very high tides to submerge the chenier before it can become mobile again. When the chenier is mobile, it follows the pattern of alternating strong onshore migration and local heightening. The chenier does not become as high as classically observed on coastal plains (Augustinus, 1989; Otvos, 2019; Quaresma et al., 2007; Morales et al., 2014; Woodroffe et al., 1983) because we do not account for storm surges in the boundary conditions.

When including a phase lag ($\theta = 5$ min) and yearly storm reset ($\Delta x_{st} = 100$ m), the net horizontal displacement of the chenier is much smaller (see Figure 4.10b). The onshore migration is counterbalanced by the gradual effect of the phase lag, and the yearly setback of the storm reset. Both also lower the chenier crest, and therefore increase the submergence time of the chenier, further increasing its dynamics. While initially the chenier migrates onshore, eventually a stable position is found, with the crest around MSL. At intra-annual scales (see dots for chenier location per month) the chenier is still very dynamic, both horizontally and vertically (in agreement with field observations of the chenier, see Figure 4.2e), but over annual to decadal scales its average position remains stable (consistent with satellite images, see Figures 4.2a-d). This dynamic behaviour is visualised in Figure 4.11, where Figure 4.11a shows a situation without subsidence (no tidal phase lag), and Figure 4.11b shows the behaviour on a drowning coastal plain (with a tidal phase lag).

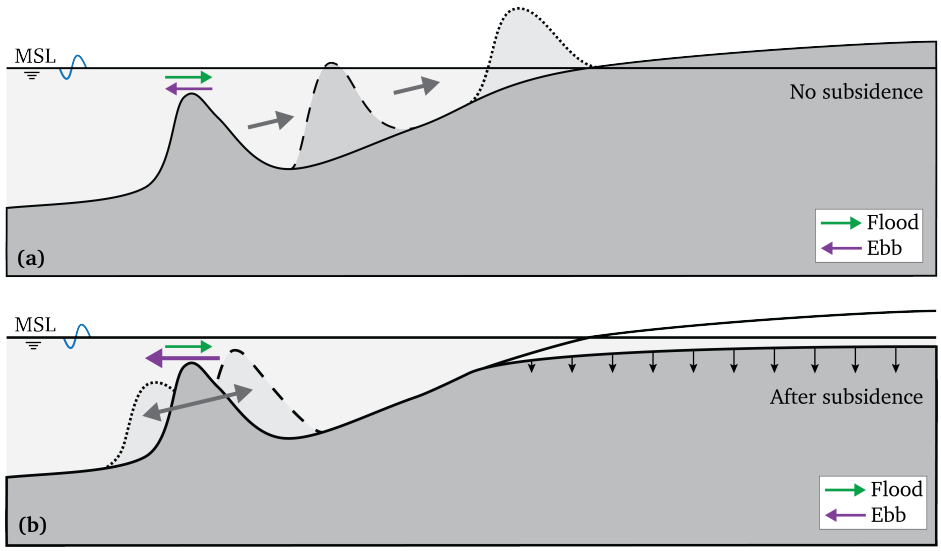


Figure 4.11: Conceptual figure summarising the findings of the idealised chenier model. **(a)** shows a coastline without phase lag, where the chenier only migrates onshore under wave action. **(b)** shows the situation off a drowning coastal plain, where a tidal phase lag generates offshore migration, balancing the wave-driven onshore migration, resulting in a dynamically stable chenier.

4.4 Discussion

As shown in Figure 4.10, the idealised chenier model is able to capture trends in chenier geometry under both onshore and offshore migration, mimicking trends we have observed in Demak and have been described in literature for cheniers at other locations around the world. Besides the trend, it is also interesting to compare the magnitude of the migration speeds. For the scenario without phase lag or storm reset the chenier moves on average 500 m landward over 10 years, or 50 m/y (see Figure 4.9a). This is the same order of magnitude as migration speeds observed in Korea (Kim et al., 2020) and France (Weill et al., 2012). Figure 4.10a shows that the migration speed varies over time, with monthly migration speeds varying strongly over the year. The largest onshore migration computed is around 40 m in one month. It is difficult to compare this value to values in literature, since most recordings cover much longer periods (over a year); the highest monthly migration speeds in literature (when averaging the recorded migration per month) are 17.5 m/month (351 m over 20 months in Saltés Island chenier plain, Spain, Morales et al. (2014)) and 13.6 m/month (95 m over 7 months in Firth of Thames, New Zealand, Woodroffe et al. (1983)). In Demak, the chenier moved 17 m in 10 days during a period of strong onshore migration (see Figure 4.2e), which would equal 51 m/month.

In this model set-up, two processes are capable of transporting the chenier offshore: the phase lag and the storm reset. While the phase lag has only a small effect over one tidal cycle, it takes place continuously, resulting in a large effect over longer time; the storm reset only occurs once a year, applying a large offshore displacement at once. We argue that both processes together are responsible for counterbalancing the onshore chenier migration in Demak. Scenarios with a storm reset ($\Delta x_{st} > 0$ m) but without phase lag ($\theta = 0$ min), see Figures 4.9c-d, show that, while it is possible to have a stable position over a long term for a large enough storm reset, the horizontal distribution is very broad. This means that such scenarios are relatively easily disturbed, and may not return to previous (equilibrium) positions. Scenarios with a phase lag ($\theta > 0$ min) but without storm reset ($\Delta x_{st} = 0$ m), see Figures 4.9a-b, reveal that only for a narrow range of θ an equilibrium is reached; while smaller values of θ invariably lead to onshore migration and lowering (until the chenier becomes a very wide, thin layer of sand on top of the muddy subsurface and dissolves), larger values result in transport of the chenier offshore. However, combining both a non-zero phase lag ($\theta > 0$ min) and a non-zero storm-reset ($\Delta x_{st} > 0$ m), yields a chenier which is very dynamic in the short term, but stable in the long term, and is able to recover from disturbances. Such a dynamic equilibrium can be obtained for different combinations of θ and Δx_{st}. We do not know the exact value of θ and Δx_{st}, and it is also highly probably that these vary over time (for example in response to the monsoon seasons, or due to continuing subsidence). However, on longer time scales the cheniers in Demak are stable, from which it may be concluded that both $\theta > 0$ min and $\Delta x_{st} > 0$ m. If not, only very specific combinations of boundary

conditions would yield long-term stability, and this would require the absence of any form of disturbance.

It is interesting to note the similarities and differences between cheniers and breaker bars. While they occur in different environments (cheniers occur on muddy coastlines, breaker bars are a feature of sandy coasts), they are both shore-parallel bodies of sand, reducing wave impact on the coastline. Classic cheniers are known to migrate onshore only, while breaker bars move slowly onshore under mild wave conditions and rapidly offshore under higher wave conditions (Wright and Short, 1984). Eventually, cheniers will become part of the coastline, as they migrate higher up the beachface until they reach above the highest water levels. Breaker bars, on the other hand, will migrate offshore until they reach the limit of the surf zone where they dissolve. Interestingly, the cheniers in Demak seem to posses properties of both 'classic' cheniers and breaker bars, showing both onshore and offshore migration. The model is able to capture all these dynamics, providing an explanation for the driving processes behind them.

A recommendation for future research would be to measure the chenier dynamics in Demak for a wider range of conditions (so also during the NW monsoon season), with special attention to the tidal phase lag, such that the values of θ and Δx_{st} are known for more situations. It may also be useful to repeat similar field observations at different locations around the world, since there is a lack of short-term, detailed observations of chenier dynamics during their 'active phase'.

Note that this model is developed for existing cheniers; their formation (and occasional dissolution) is not accounted for. For certain scenarios, many model realisations end early, when the chenier migrates onshore and the crest lowers, until it becomes a thin layer of sand on top of the muddy subsurface and the chenier dissolves. Therefore, another recommendation for future research is to investigate the development of cheniers; not only their initial formation, but also what would happen to such flattened cheniers, such that this behaviour can then also be integrated into the idealised chenier model.

The observed chenier in Demak, while very dynamic, maintains a relatively constant geometry, which allows our approach of using a look-up table based on a single, generic profile (see Figure 4.5a). However, if the chenier geometry varies strongly, feedback between the geometry and the displacements could be introduced by modelling different chenier geometries in Delft3D, creating multiple look-up tables. Furthermore, these extra model runs, as well as any additional field observations, could eventually be used to go from look-up tables to deterministic algorithms, which could be used to calculate the fluxes between the different chenier components (similar to the barrier island model of Lorenzo-Trueba and Ashton (2014), or the beach-dune model of Hallin et al. (2019)).

The tidal phase lag is found to be one of the important processes in stabilising the chenier in the nearshore zone. This phase lag is the result of strong coastal erosion and subsidence, which have caused breaches in the coastline and turned the coastal plain into a large tidal basin. The presence of a chenier in the nearshore creates a buffer against strong wave action, while still letting water and sediment

pass. By damping waves, the chenier protects the coastline against further erosion, and as such, the chenier actually generates a negative feedback on the erosion cycle. Moreover, the presence of a chenier could create a window of opportunity for the mangrove coast to restore and expand again, eventually naturally closing the breaches in the coastline. This would cancel the tidal phase lag, which may tip the chenier dynamics to a different stable state, where the chenier migrates onshore until it ends up in the shoreline. However, a small change to the phase lag, for example by closing off (part of) the hinterland by a dike, could disturb this chenier equilibrium. The dike would strongly reduce the tidal phase lag, which in turn reduces the seaward sediment transport, and the chenier would start migrating onshore. Attached to the shoreline, the chenier no longer creates a sheltered area for mangrove restoration, and there may be local deepening seaward of the chenier, which could eventually lead to aggravated coastal erosion. And finally, if the subsidence continues, the phase lag could even increase, until the seaward transport becomes dominant and the chenier migrates further offshore, leaving the shoreline unprotected.

4.5 Conclusions

Chenier dynamics on a day-to-day basis are driven by waves and tides. Most cheniers described in literature are known to migrate onshore only, until they stabilise high on the beachface, where they are no longer reached by even the highest tides. Observations in Demak suggest that there may also be an alternative stable state for cheniers, where they remain dynamic on the short-term, but hold a stable position at a certain distance from the shoreline in the longer term.

We have developed an idealised chenier model using output from a complex physics-based model to investigate the drivers of cross-shore chenier dynamics under daily wave and tidal influences. The model is able to capture trends in chenier geometry under both onshore and offshore migration. Onshore migration is mainly driven by wave action. Offshore migration occurs when a phase lag generated on the drowned coastal plain causes a water level gradient over the chenier.

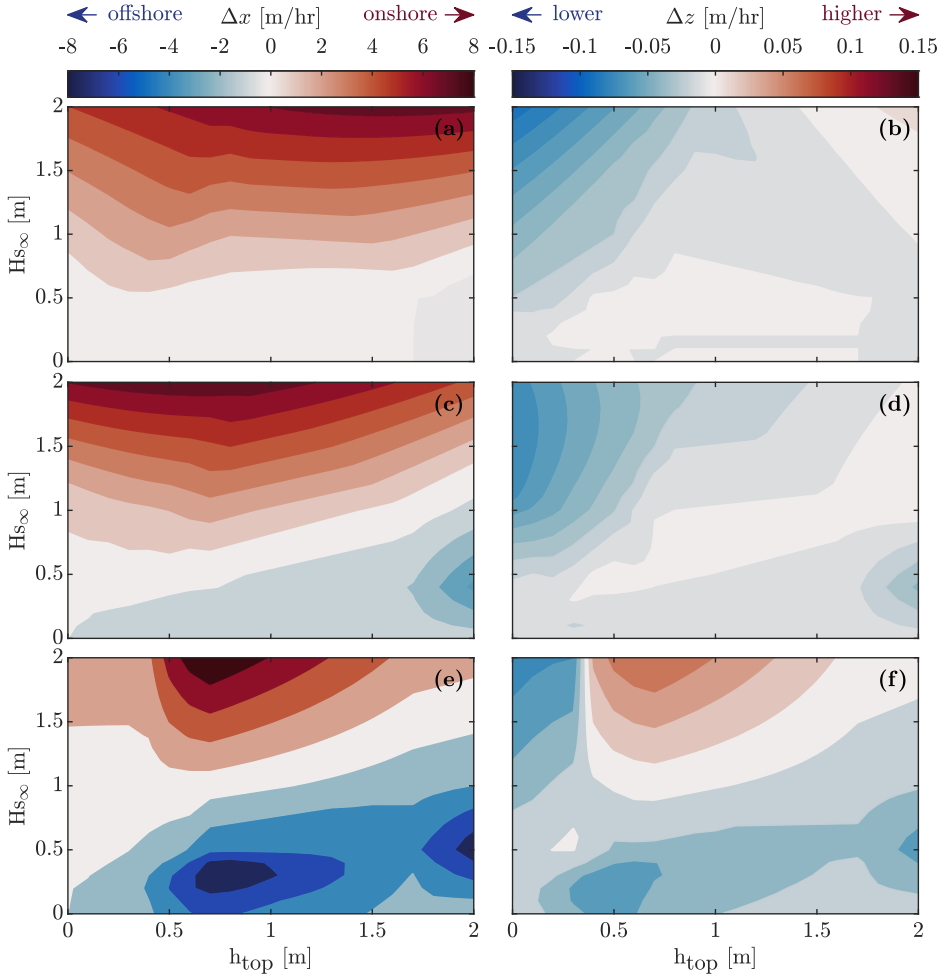
Both the tide and waves may vary over the year; waves due to seasonal effects, tide due to the interaction between the various tidal components. During the SE monsoon season in Demak, the wave climate is driven by a very regular sea breeze. Due to the mixed, mainly diurnal character of the tide, the timing of high water levels shifts over the day throughout the year. This leads to a yearly pattern in chenier dynamics, where based on the timing of the sea breeze vs. the high tide, a period of strong onshore migration is followed by a period of local vertical growth.

Without a tidal phase lag or storm reset, the model reproduces the typical chenier dynamics of strong onshore migration, until the chenier reaches a height that can no longer be reached by daily tidal influences: the ‘classic’ stable state. Introducing a phase lag (caused by subsidence of the coastal plain) and storm

reset (representing the net seaward displacement during the storm season) to the boundary conditions strongly impacts these chenier dynamics. Both introduce an offshore transport component, counterbalancing the onshore migration. While either process alone can produce a dynamically stable chenier, this stable position only occurs for a very narrow range of boundary conditions, and the equilibrium is easily disturbed. Both processes together, however, create a more robust equilibrium: very dynamic in the short term, due to the natural variation in boundary conditions, but stable in the long term: an alternative, dynamically stable state.

4.A Hourly horizontal and vertical displacements for all scenarios

The idealised chenier model is valid for calm to moderate conditions, representative for the SE monsoon season in Demak. Therefore, the hourly horizontal and vertical hourly displacements for a representative range of conditions have been determined with the Delft3D model: (1) $H_{s,\infty} = 0 - 2$ m; (2) $h_{top} = 0 - 2$ m; (3) ebb or flood; and (4) $\theta = 0 - 20$ min. In the main text, Figure 4.6, the hourly displacements for all wave heights and water depths of two sets of scenarios have been shown: ebb without a phase lag (Figures 4.6a-b); and ebb with a phase lag of $\theta = 10$ min (Figures 4.6c-d). Here, we include the remaining scenarios: flood (Supplementary Figures 4.12a-b); ebb with a phase lag of $\theta = 5$ min (Supplementary Figures 4.12c-d); and ebb with a phase lag of $\theta = 20$ min (Supplementary Figures 4.12e-f).



Supplementary Figure 4.12: Visualisation of the hourly displacement matrix for the scenarios not covered in the main article (see Figure 4.6). The first row (**(a)** and **(b)**) shows the displacements during flood; the second row (**(c)** and **(d)**) during ebb with a phase lag of $\theta = 5$ min; and the third row (**(e)** and **(f)**) during ebb with a phase lag of $\theta = 20$ min. The left column (a, c and e) gives the horizontal hourly displacement Δx in m/hr, where onshore migration is coloured red and offshore blue; the right column (b, d and f) gives the vertical hourly displacement Δz in m/hr, where red colours indicate that the chenier crest becomes higher, while for blue colours the crest lowers.

Chapter 5

Chenier formation through wave winnowing and tidal transport

Abstract

Cheniers are ridges consisting of coarse-grained sediments, resting on top of the fine sediment that forms the otherwise muddy coast. In this chapter, we use Delft3D to explore how cheniers are formed through wave winnowing. We identify three phases of chenier development: (1) a winnowing phase, during which mud is washed out of the seabed initially consisting of a mixture of sand and mud, (2) a sand transport phase, when the sand in the upper layer is transported onshore, and (3) a crest formation phase, during which a chenier crest rapidly develops at the landward limit of onshore sediment transport. The main mechanism driving onshore sand transport is wave asymmetry. During calm conditions, sand transport takes place within a narrow band limiting the volume of sand delivered nearshore, and therefore no chenier develops. In contrast, average storm conditions mobilise sufficient sand for a crest to develop. Our results thus reveal that chenier formation through wave winnowing does not require extreme storm conditions. Furthermore, our study showed that chenier formation through wave winnowing is a relatively slow process, with the largest time scales associated with the winnowing and sand transport. Once sufficient sand is available nearshore, the crest develops rapidly.

Parts of this chapter are submitted for publication in Journal of Geophysical Research: Earth Surface as: Tas, S.A.J., van Maren, S.D., & Reniers, A.J.H.M. Chenier formation through wave winnowing and tidal transport.

5.1 Introduction

Cheniers are ridges consisting of wave-reworked coarse-grained sediments, resting on top of muddy sediment (Augustinus, 1989; Otvos and Price, 1979). Cheniers may occur as a single ridge (e.g. in Demak, Indonesia) or they may be part of a chenier plain (e.g. in Louisiana, USA), where multiple clusters of cheniers, separated by mudflats, are observed. Chenier coastlines consist of mostly very fine sediments, with a small fraction of coarser grained particles, which can have a marine or fluvial origin. For example, the chenier sediment in Tourville Bay, Australia is of local, marine origin (Belperio et al., 1988) while sand in the cheniers in French Guiana originates from sand supplied by local rivers rather than from the mud banks migrating alongshore (Prost, 1989; Pujos et al., 2001; Anthony et al., 2010). Cheniers can be formed in two ways, which are related to the origin of the coarser (sandy) sediments (Augustinus, 1989). Sand can originate from winnowing, where mud is brought into suspension and the remaining sand is transported onshore through wave-driven sediment transport, accumulating in a sandy ridge. Alternatively, cheniers may develop from spits forming downdrift of river mouths. In this chapter, we will focus on the first mechanism: chenier formation through wave winnowing.

Winnowing requires sufficient wave energy, for example during a storm event (Woodroffe and Grime, 1999) or during a period of increased wave action (e.g. during inter-mudbank phases along the coast of the Guianas (Anthony et al., 2010)). Furthermore, sufficient coarser-grained particles need to be available in the nearshore zone where waves create sufficiently high bed shear stresses to suspend the fines and mobilise the coarser sediments. For example, in the Louisiana Chenier Plain, cheniers are formed near the mouths of rivers discharging high fluvial sediment loads (Rosen and Xu, 2011). When higher waves coincide with spring tides, both elements (wave energy and sediment availability) are reinforced, as the waves may now rework sediments that were not available during normal conditions, e.g. the chenier formation in the Firth of Thames (Woodroffe et al., 1983; Dougherty and Dickson, 2012).

The objective of this chapter is to understand how cheniers are formed through wave-induced winnowing. Despite the large amount of studies on cheniers (as in the references above), their formation is largely described in a qualitative sense, and a systematic study into chenier formation in response to wave and tidal processes is lacking. A first step towards a quantitative approach of chenier formation was made by Nardin and Fagherazzi (2018), who studied the development of entire chenier plains using Delft3D. In this chapter, we focus on the development of a single chenier, hence looking at much smaller spatial and temporal scales. We therefore deploy a process-based numerical model (Delft3D) to identify the responsible processes and mechanisms during the various phases of chenier genesis, and determine under which conditions a chenier develops. In Section 5.2.1 we provide an overview of the relevant sediment transport formulae and how they are implemented in Delft3D. Section 5.2.2 gives a brief overview of

the model set-up, which is based on the model developed in Chapter 4 through validation against field observations described in Chapter 3. We explore chenier development through a number of (idealised) scenarios described in Section 5.2.3. These scenarios reveal three phases of chenier formation which are presented in Section 5.3. The implications of our findings, as well as some limitations of our approach are discussed in Section 5.4 and the conclusions are presented in Section 5.5.

5.2 Methods

The formation of cheniers through wave-induced winnowing is explored using a Delft3D-FLOW morphodynamic model in combination with a SWAN wave model. Delft3D-FLOW solves the unsteady shallow water equations in two (depth-averaged) or three dimensions (Lesser et al., 2004) and SWAN is a third generation numerical wave model (Booij et al., 1999). Below we summarize the relevant sediment transport formulae that are used to calculate sediment transport in Delft3D, followed by a description of the model set-up.

5.2.1 Sediment transport in Delft3D

We consider two types of sediment: cohesive (mud) and non-cohesive (sand). Sand can be transported as bed load and as suspended load. Sediment transported as bed load is limited to a thin layer above the bed; sand particles higher in the water column are transported as suspended load. Mud is transported as suspended load or as fluid mud (for high concentrations the mud is transported as a viscous layer near the bed). Sediment transport (both sand and mud; both suspended and bed load) requires the exceedance of a critical bed shear stress to initiate movement of the sediment particles.
Bed load transport of sand is calculated using the empirical formula of van Rijn (1993). The suspended sediment transport of both mud and sand by currents is computed with an advection-diffusion equation. Additionally, there is also suspended sand transport due to wave asymmetry, as a result of asymmetric wave orbital velocities, which is approximated following van Rijn et al. (2001). In the next paragraphs, we will introduce the relevant sediment formulae.

Bed load transport

The bed load transport is calculated using the empirical formula of van Rijn (1993):

$$S_b = \begin{cases} 0.006\rho_s w_s D_{50} M^{0.5} M_e^{0.7} & \text{if } v_{\text{eff}} \geq v_{\text{cr}} \\ 0 & \text{if } v_{\text{eff}} < v_{\text{cr}} \end{cases}, \tag{5.1}$$

where S_b is the bed load transport (in kg/m/s), ρ_s is the sediment density (in kg/m^3), w_s is the settling velocity for the D_{50} of the sediment (in m/s), and

D_{50} is the median diameter of the sediment fraction (in m). M is the sediment mobility number due to waves and currents (see Equation 5.2) and M_e is the excess sediment mobility number (see Equation 5.3).
The sediment mobility number, M, is defined as:

$$M = \frac{v_{\text{eff}}^2}{(s-1)gD_{50}}, \tag{5.2}$$

and the excess sediment mobility number, M_e, is defined as:

$$M_e = \frac{(v_{\text{eff}} - v_{\text{cr}})^2}{(s-1)gD_{50}}, \tag{5.3}$$

where v_{eff} is the effective velocity due to waves and currents (see Equation 5.4, in m/s), v_{cr} is the critical velocity for the initiation of motion (see Equation 5.6, in m/s), s is the relative density (see Equation 5.5) and g is the gravitational acceleration (in m/s^2).

The effective velocity due to waves and currents, v_{eff}, is:

$$v_{\text{eff}} = \sqrt{v_{\text{R}}^2 + U_{\text{on}}^2}, \tag{5.4}$$

where v_{R} is the magnitude of the depth-averaged current velocity (in m/s) and U_{on} is the onshore-directed, high frequency near-bed orbital velocity (in m/s), calculated using a modification of the method of Isobe and Horikawa (1982) by Grasmeijer and van Rijn (1998).
The relative density s is defined as:

$$s = \frac{\rho_s}{\rho_w}. \tag{5.5}$$

The critical velocity for the initiation of motion is determined based on a parametrisation of the Shields curve (van Rijn, 1993; Soulsby, 1997):

$$v_{\text{cr}} = \begin{cases} 0.19{D_{50}}^{0.1}\log_{10}\left(\frac{4h}{D_{90}}\right) & \text{if } D_{50} \leq 0.5 \text{ mm} \\ 8.5{D_{50}}^{0.6}\log_{10}\left(\frac{4h}{D_{90}}\right) & \text{if } 0.5 \text{ mm} < D_{50} \leq 2 \text{ mm} \end{cases}, \tag{5.6}$$

where h is the water depth (in m) and D_{90} is the sediment diameter (in m) for which 90% of the sediment has a smaller diameter, and is based on the composition of the local sediment mixture. In this case, $D_{90} = 1.5D_{50}$.
The bed load transport S_b consists of a current-driven component, $S_{b,c}$, and a wave-driven component, $S_{b,w}$:

$$S_b = \sqrt{{S_{b,c}}^2 + {S_{b,w}}^2 + 2|S_{b,c}||S_{b,w}|\cos(\varphi)}, \tag{5.7}$$

with φ the angle between the current and wave direction. From this equation it follows that the current-driven and wave-driven components, $S_{b,c}$ and $S_{b,w}$

respectively, can be calculated as:

$$S_{b,c} = \begin{cases} \frac{S_b}{\sqrt{1+r^2+2|r|\cos(\varphi)}} & \text{if } r \leq 100 \\ 0 & \text{if } r > 100 \end{cases}, \tag{5.8}$$

$$|S_{b,w}| = \begin{cases} r|S_{b,c}| & \text{if } r \geq 0.01 \\ 0 & \text{if } r < 0.01 \end{cases}, \tag{5.9}$$

with:

$$r = \left(\frac{|U_{\text{on}}| - v_{\text{cr}}}{|v_{\text{R}}| - v_{\text{cr}}} \right)^3. \tag{5.10}$$

Suspended transport

Suspended transport is described by an advection-diffusion equation. In depth-averaged mode ($\partial/\partial z = 0$) and assuming longshore uniformity ($\partial/\partial y = 0$) this equation reads:

$$\frac{\partial ch}{\partial t} + \frac{\partial Uch}{\partial x} - h\frac{\partial}{\partial x}\left(\epsilon_{s,x} \frac{\partial c}{\partial x} \right) = E - D \tag{5.11}$$

where c is the concentration (in kg/m^3), h is the water depth (in m), U is the depth-averaged velocity in x-direction (in m/s), w_s is the settling velocity (in m/s), $\epsilon_{s,x}$ is the horizontal eddy diffusivity (in m^2/s), E is the erosion flux (in kg/m^2/s) and D is the deposition flux (in kg/m^2/s). In Equation 5.11, the second term gives the advective transport, the third term the diffusive transport and the right hand side represents the source and sink terms (to and from the bed). For cohesive sediment, the erosion and depositional fluxes are calculated with the Partheniades erosion formulation (Partheniades, 1965) and a permanent deposition flux (Winterwerp, 2007):

$$E = M_{\text{ero}} S(\tau_{\text{cw,max}}, \tau_{\text{cr,e}}), \tag{5.12}$$

and

$$D = w_s c_b, \tag{5.13}$$

where M_{ero} is an erosion parameter (in kg/m^2/s), $S(\tau_{\text{cw,max}}, \tau_{\text{cr,e}})$ is an erosion function (see Equation 5.14) and c_b is the average sediment concentration near the bed (in kg/m^3).
The erosion function is defined as:

$$S(\tau_{\text{cw,max}}, \tau_{\text{cr,e}}) = \begin{cases} \left(\frac{\tau_{\text{cw,max}}}{\tau_{\text{cr,e}}} - 1 \right) & \text{if } \tau_{\text{cw,max}} > \tau_{\text{cr,e}} \\ 0 & \text{if } \tau_{\text{cw,max}} \leq \tau_{\text{cr,e}} \end{cases}, \tag{5.14}$$

Here, $\tau_{\text{cr,e}}$ is the critical bed shear stress for erosion (in N/m^2) and $\tau_{\text{cw,max}}$ is the maximum bed shear stress due to current and waves (in N/m^2). This maximum bed shear stress is computed with the parametrisation of Soulsby et al. (1993):

$$|\tau_{\text{cw,max}}| = Z(|\tau_c| + |\tau_w|), \tag{5.15}$$

where τ_c is the bed shear stress due to currents (in N/m^2), τ_w is the bed shear stress due to waves (in N/m^2), and Z is a dimensionless parameter.
The bed shear stress due to currents, τ_c, is defined as

$$\tau_c = \frac{g\rho_w U|U|}{C^2}, \tag{5.16}$$

where U is the depth-averaged velocity (in m/s) and C is the Chézy coefficient (in m$^{1/2}$/s).
The magnitude of the bed shear stress due to waves alone is defined as:

$$\tau_w = 0.5\rho_w f_w {u_{\text{orb}}}^2, \tag{5.17}$$

where f_w is the wave friction factor (defined in Equation 5.19) and u_{orb} is the peak orbital velocity (in m/s) and can be calculated using linear wave theory:

$$u_{\text{orb}} = \frac{\sqrt{\pi}}{4}\frac{H_{\text{rms}}\omega}{\sinh(kh)}. \tag{5.18}$$

Here H_{rms} is the root-mean-square wave height (in m), $\omega = 2\pi/T$ is the wave angular frequency (in s^{-1}) and $k = 2\pi/L$ is the wave number (in m^{-1}) which can be derived from the linear wave dispersion relationship.
The wave friction factor under pure oscillatory flow is calculated following Swart (1974):

$$f_w = \begin{cases} 0.00251\exp\left[5.21\left(\frac{A}{k_s}\right)^{-0.19}\right] & \text{if } \frac{A}{k_s} > \frac{\pi}{2} \\ 0.3 & \text{if } \frac{A}{k_s} \leq \frac{\pi}{2} \end{cases}, \tag{5.19}$$

where k_s is the Nikuradse roughness height (in m) (which can be derived from the Chézy coefficient, see Equation 5.21) and A, the orbital excursion length, equals:

$$A = \frac{u_{\text{orb}}}{\omega}. \tag{5.20}$$

The Nikuradse roughness height is derived from the Chézy coefficient using the formulation of White-Colebrook:

$$k_s = 12h10^{-C/18} \tag{5.21}$$

The dimensionless parameter Z from Equation 5.15 is defined as:

$$Z = 1 + aX^m(1-X)^n, \tag{5.22}$$

with:

$$X = \frac{|\tau_c|}{|\tau_c| + |\tau_w|}. \tag{5.23}$$

The value of the parameters a, m and n can be determined through the following expression:

$$\chi = \left(\chi_1 + \chi_2 |\cos\varphi|^J\right) + \left(\chi_3 + \chi_4 |\cos\varphi|^J\right) \log_{10}\left(\frac{f_w}{C}\right) \tag{5.24}$$

where φ is the angle between the current direction and the direction of wave propagation and χ represents a, m or n. The fitting coefficients based on Fredsøe (1984) are used, see Table 5.1.

Table 5.1: Fitting coefficients for wave-current boundary layer model, using FR84 (Fredsøe, 1984)

FR84	χ_1	χ_2	χ_3	χ_4
a	-0.06	1.70	-0.29	0.29
m	0.67	-0.29	0.09	0.42
n	0.75	-0.27	0.11	-0.02
J	0.80			

In addition to the suspended transport via advection and diffusion (which in this case is mostly mud transport), there is also suspended sand transport due to wave asymmetry. This component represents the effect of asymmetric wave orbital velocities on suspended sediment transport within about 0.5 m of the bed and can be approximated following van Rijn et al. (2001):

$$S_{s,w} = f_{\text{SUSW}} \gamma U_A S_S, \tag{5.25}$$

where f_{SUSW} is a user-defined tuning parameter, γ is the phase lag coefficient ($\gamma = 0.2$), U_A is the velocity asymmetry value (in m/s, see Equation 5.26) and S_S is the suspended sediment load (in kg/m/s, see Equation 5.27).
The velocity asymmetry value, U_A, is defined as:

$$U_A = \frac{{U_{\text{on}}}^4 - {U_{\text{off}}}^4}{{U_{\text{on}}}^3 + {U_{\text{off}}}^3}, \tag{5.26}$$

and the suspended sediment load, S_S, as:

$$S_S = 0.007 \rho_s D_{50} M_e. \tag{5.27}$$

In Delft3D, this transport component is included in the bed load vector, because it does not exhibit the relaxation effects of an advection-diffusion relation (Deltares, 2021).

5.2.2 Model set-up

Most model settings are adopted from the model set-up in Chapter 4, which was validated against field observations (see also Chapter 3). We follow a quasi 1D approach: the model is set up in depth-averaged mode and is alongshore uniform. In order to avoid shadow effects, the WAVE-domain is much wider than the FLOW domain. The grid cell size Δx reduces from 25 m at deep water to 1.5 m nearshore. The bed has a constant slope of 1:500 and consists initially of a homogeneous mixture of 2 fractions: mostly mud and a small sand fraction ($D_{50} = 235\mu$m). The mud in Demak is very soft (with a strength of the mud layer being much too low to carry a human). Little is known about the erosion properties of such thick mud bed properties. The most similar conditions for which erosion properties of such thick fluid mud beds have been described in literature are those of van Maren et al. (2015b), using a critical bed shear stress $\tau_{\text{cr,e}} = 0.5$ N/m^2. Settling velocities in similar environments generally range from 0.2 to 5 mm/s (Soulsby et al., 2013; Manning and Dyer, 2007; van Maren et al., 2015a; van Leussen and Cornelisse, 1993). Measurements in Demak suggested a small settling velocity on the lower end of this range (Deltares and BioManCO, 2019), hence we set $w_s = 0.5$ mm/s. The dry bed density is typically around $\rho_{\text{dry}} = 300$ kg/m^3. With all other parameters largely based on observations or earlier work, the last remaining parameter (the erodibility parameter M_{ero}) was calibrated such that the bed was dynamic but still attained dynamic equilibrium, $M_{\text{ero}} = 1.10^{-4}$ kg/m^2/s.

The bed composition is modelled using a layered bed stratigraphy: the bed is composed of multiple layers in order to account for winnowing of mud from the mixed bed. The active upper layer is 2 mm thick and always fully mixed. Upon deposition, sediments settle in the upper layer, leading to migration of sediments from the upper layer to the first bed stratigraphy layer. Only the upper layer is available for erosion, and upon erosion sediment from the first stratigraphy layer migrates to the active layer. The stratigraphy layers have a maximum thickness of 10 cm, except the lowest layer when the maximum of 10 layers is reached (this layer is limited by a non-erodible boundary 1 m below the initial bed level).

At the offshore boundary, a (time-varying) water level and wave height is prescribed (see Section 5.2.3 hereafter). A delayed transfer of wave energy in the landward direction is computed with a roller model (Svendsen, 1984; Nairn et al., 1991; Reniers et al., 2004). This introduces a time lag (and therefore spatial lag) between the moment of wave breaking and the moment of energy dissipation, which is necessary for realistic modelling of cross-shore profile development of barred beaches (Reniers et al., 2004).

The computational time was reduced by introducing a morphological acceleration factor MorFac (multiplying the bed level change every timestep with MorFac). We have scaled the MorFac with the wave height, using a smaller factor for larger wave heights (hence larger/faster bed level changes) and verified our choice by comparing the model results with a smaller MorFac.

5.2.3 Model scenarios

Boundary conditions representing the conditions in Demak, Indonesia are defined in multiple model scenarios, see Table 5.2. Three wave scenarios are defined: (1) sea breeze-induced waves, representing the energetic conditions during the SE monsoon season; (2) average storm conditions, which occur multiple times per NW monsoon season; and (3) extreme storm conditions, representing a storm with a return period of 10 years. The extreme storm conditions are estimated based on the peak-over-threshold analysis of Alferink (2022) performed on Wave Watch III data, which were validated against field observations. A simple sinusoidal tide is prescribed at the offshore boundary, composed of the largest constituent in Demak, K1 (see Section 2.4.2), with three varying amplitudes representing no tide ($a_{K1} = 0$ m), neap tide ($a_{K1} = 0.25$ m) and spring tide ($a_{K1} = 0.5$ m). The sand fraction in the initial sediment mixture is varied between 5, 10 and 20%. Each wave scenario is combined with any of the tidal amplitudes and sand fractions (27 scenarios). These idealised scenarios are supplemented with one more realistic scenario, applying realistic time series for water levels and wave conditions at the offshore boundary (see Section 5.3.6).

Table 5.2: Wave conditions for the three wave scenarios

Wave conditions	H_s [m]	T_p [s]	MorFac
Sea breeze	0.6	3.5	100
Average storm	1.3	5.6	25
Extreme storm	2.47	7.7	7.5

5.3 Results

Figure 5.1 shows the formation of a chenier under constant wave conditions representing average storm conditions ($H_s = 1.3$ m and $T_p = 5.6$ s, see Table 5.2), in the absence of tide (constant water level), starting from a fully mixed bed with 10% sand. The chenier develops in three phases: (1) winnowing, during which mud is washed out and the upper layer of the bed becomes increasingly sandy; (2) the sand in the upper layer is transported landward; and (3) crest formation, essentially the abrupt heightening of the chenier crest when sufficient sediment is available. During phase 1 and 2, when a thin sand layer is formed and transported landward, bed level changes are small; most morphodynamic changes take place during phase 3 when the chenier crest develops. The chenier exemplified in Figure 5.1 reaches its full height after 120 days, after which the speed of bed level changes slow down.
Chenier development is subsequently explored for other wave conditions as well: lower waves (representing an energetic sea breeze-day during the SE monsoon season) and higher waves (representing an extreme storm). The resulting evolution of the sand fraction in the upper layer of the bed (left column, panels 5.2a,

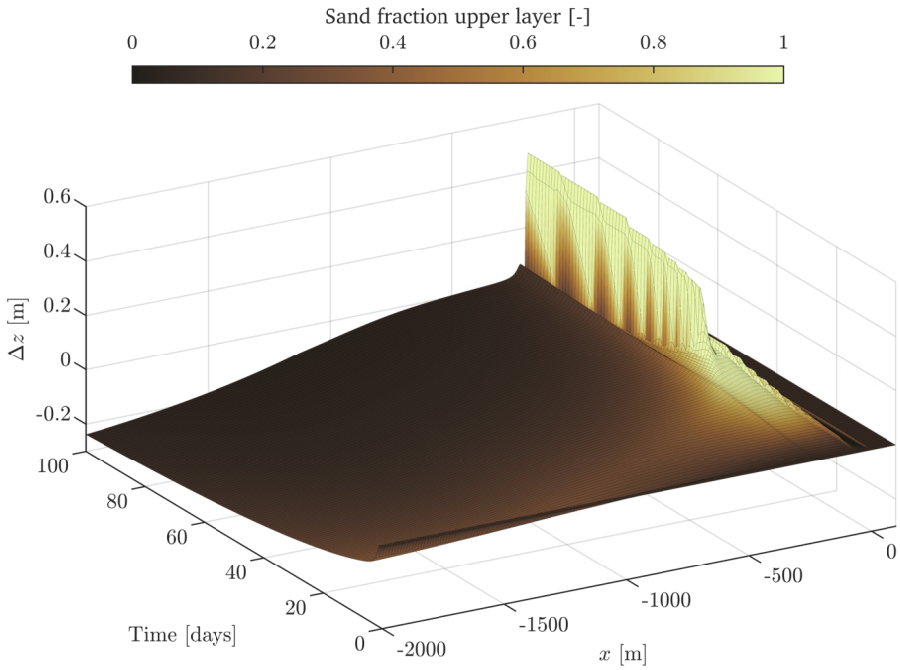


Figure 5.1: Changes in bed elevation and composition over time. The horizontal axes represent the time and x-coordinate (with the origin of the x-axis corresponding to the shoreline at MSL). The vertical axis represents the elevation change relative to the initial profile, and the colours represent the sand fraction of the upper layer (with 0 only mud and 1 only sand; the sand fraction of the initial mixture was equal to 0.1). The boundary conditions are constant over time, representing average storm conditions ($H_s = 1.3$ m and $T_p = 5.6$ s) and a constant water level.

5.2d and 5.2g), bed level changes (middle column, panels 5.2b, 5.2e and 5.2h) and sand transport (right column, panels 5.2c, 5.2f and 5.2i) are given in Figure 5.2, for extreme storm conditions (upper row), average storm conditions (middle row) and energetic sea breeze conditions (lower row) respectively.
For all wave scenarios, mud is winnowed from the bed and sand is subsequently transported landward, but only for the higher wave scenarios a chenier crest develops (Figures 5.2b and 5.2e). The sediment sorting (left column) and sand transport (right column) exhibit similar trends, which suggests that onshore sand transport depends on sand availability, which is a direct result of winnowing. This landward transported sand culminates close to the shoreline and, for the higher wave conditions, develops into a chenier crest.

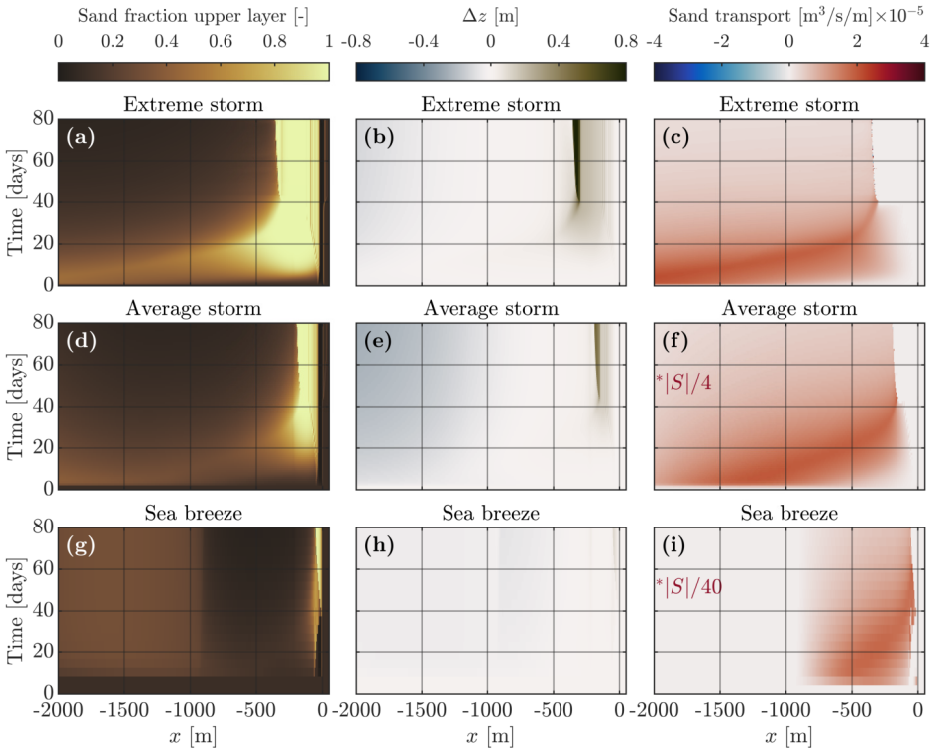


Figure 5.2: Evolution of the sand fraction in the upper layer (left column, **(a,d,g)**), the bed level change (middle column, **(b,e,h)**) and the sand transport (right column, **(c,f,i)**) for three wave scenarios (extreme storm, average storm, and sea breeze). *In order to visualize the sand transport trends for all scenarios, the colour scale is corrected with a factor $1/4$ and $1/40$ in panels (f) and (i), respectively (i.e. the darkest red represents a a transport of 4.10^{-5} m^3/s/m in (c), 1.10^{-5} m^3/s/m in (f) and 1.10^{-6} m^3/s/m in (i)).

5.3.1 Phase 1: Winnowing

For all wave scenarios, mud is eroded over almost the entire domain (see Figure 5.3, left y-axis, when $|\tau_{cw,max}| - \tau_{cr,e} > 0$). However, the onset of sand transport requires higher flow velocities (when $|v_{eff}| - v_{cr} > 0$, right y-axis in Figure 5.3). This difference is especially relevant for the sea breeze scenario (Figure 5.3c), where mud is eroded over a much wider area, while sand is only eroded landward of $x = -900$ m. This means that seaward of $x = -900$ m, mud is being eroded from the upper bed layer, but the sand particles remain immobile, which results in a higher sand fraction in the upper bed layer (visible in Figure 5.2g). Landward of $x = -900$ m, both sediment fractions are mobilised. For higher waves (see Figures 5.3a-b), the erosion thresholds for both sediment fractions are exceeded at increasingly deeper water, resulting in erosion of both mud and sand over almost the entire domain.

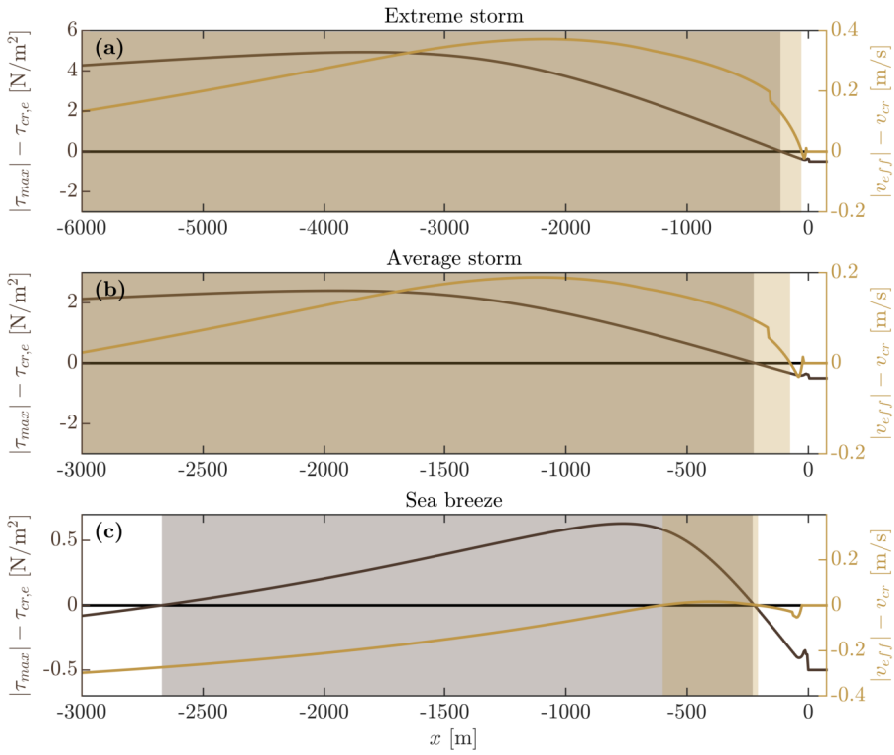


Figure 5.3: Visualisation of the area where the threshold for the initiation of motion is exceeded for three wave scenarios: **(a)** extreme storm, **(b)** average storm and **(c)** sea breeze. Mud (dark brown, left y-axis) is eroded when $|\tau_{cw,max}| - \tau_{cr,e} > 0$ and sand (light brown, right y-axis) is eroded when $|v_{eff}| - v_{cr} > 0$.

5.3.2 Phase 2: Sand transport

Sand transport (right column in Figure 5.2) is directly linked to the availability of sand in the upper layer (left column Figure 5.2). Sand transport is therefore supply-limited, i.e. not only governed by the transport capacity, but also by the sand availability (and thus winnowing). During phase 2, the main mechanism for onshore sand transport is wave asymmetry, as demonstrated with a simple sensitivity analysis. The modelled onshore sand transport by wave asymmetry can be modified with a user-defined parameter f_{SUSW} (calibrated to 0.5 using field observations, see Section 4.2.5). Applying a much lower value ($f_{SUSW} = 0.05$) results in a much lower onshore sand transport (compare panels 5.4a-c with panels 5.4d-f), revealing that onshore transport indeed results predominantly from wave asymmetry.

Although there is still some onshore sand transport for the scenario with a ten times smaller value for f_{SUSW} (Figure 5.4f), leading to a sandy region near the shoreline (Figure 5.4d), the total volume of onshore sand transport and resulting

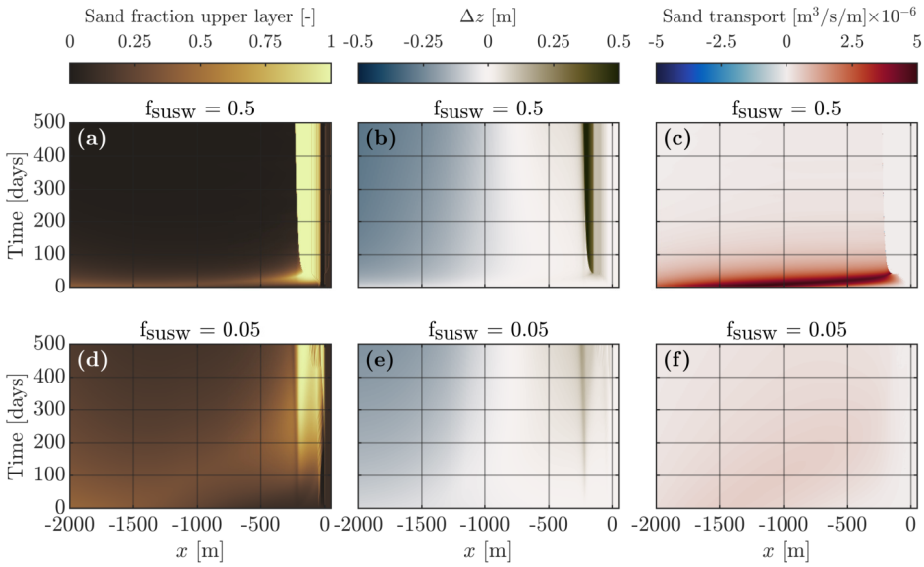


Figure 5.4: Sand fraction in the upper layer (left column, **(a,d)**), bed level change (middle column, **(b,e)**) and total sand transport (right column, **(c,f)**) for values of $f_{\text{SUSW}} = 0.5$ (upper row) and $f_{\text{SUSW}} = 0.05$ (lower row).

bathymetric change (Figure 5.4e) is small.

5.3.3 Phase 3: Crest formation

The last phase of chenier formation is rapid sand accumulation at one location, thereby shaping a chenier crest. This process is very fast and abrupt: once a certain threshold is exceeded, the crest height rapidly increases.
Sedimentation (and erosion) can be directly linked to sediment transport gradients. A negative transport gradient is defined as a landward decrease in sediment transport, resulting in sediment deposition. Figure 5.5 shows the bed level change (left column), the sand transport (middle column) and the sand transport gradient (right column) for a scenario during average storm conditions. The three rows show a different initial sand content, in this section we focus on the middle row (sand content of 10%), the other rows (5% and 20% sand) will be discussed in Section 5.3.4.
Initially, sediment transport is maximal in deeper water ($x = 1000 - 1500$ m at $t = 0$ in Figure 5.5e). Sand is eroded seaward of this sand transport peak (positive transport gradient in Figure 5.5f) and deposited landward (negative transport gradient). The winnowed sand body migrates landward, driven by wave asymmetry and a gradual depletion of sand in the sand-mud mixture. The moment the peak sand transport rate is close to the shore ($x = 200$ m at $t = 40$ days in Figure 5.5e), the decrease in transport in the landward direction is concentrated

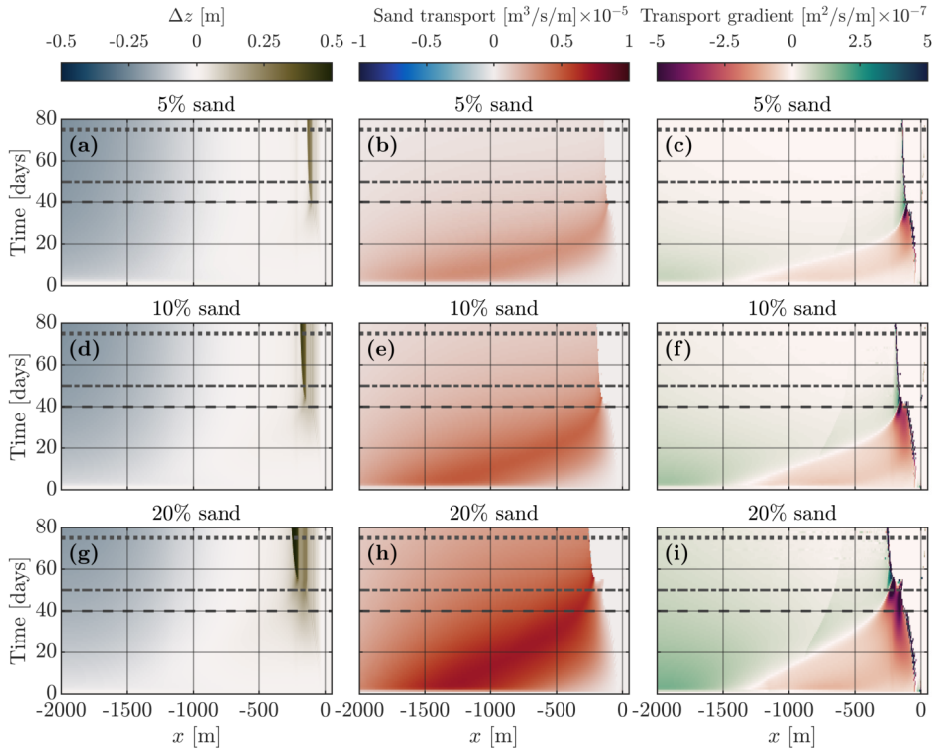


Figure 5.5: Bed level change (left column, **(a,d,g)**), sand transport (middle column, **(b,e,h)**) and sand transport gradient (right column, **(c,f,i)**) for three different initial sand fractions: 5% (upper row), 10% (middle row) and 20% (lower row). The horizontal dashed lines correspond to the different panels in Figure 5.6 (dashed line: 40 days, panel 5.6a; dash-dotted line: 50 days, panel 5.6b; and dotted line: 75 days, panel 5.6c).

over such a narrow zone that a chenier crest emerges (Figure 5.5d).

5.3.4 Effect of the initial sand fraction

The size of the developed cheniers, but also the time required to develop a chenier, depends not only on the waves (as evaluated above) but also on the sand fraction in the sand-mud mixture. Figure 5.6 shows the chenier formation process for three different initial sand fractions (different shades of brown) at three points in time (panels a-c, corresponding to the time markers in Figure 5.5).
Interestingly, the lowest initial sand fraction (darkest line in Figure 5.6) leads to the fastest emerging chenier. This initially counter-intuitive observation can be explained by winnowing. Because of the lower sand content in the bed, the upper bed layers are more quickly depleted of sand, the maximum transport peak converges more rapidly with the shoreline, and as a result crest formation (phase 3) starts earlier. The onset of crest formation for the scenario with 10% sand is

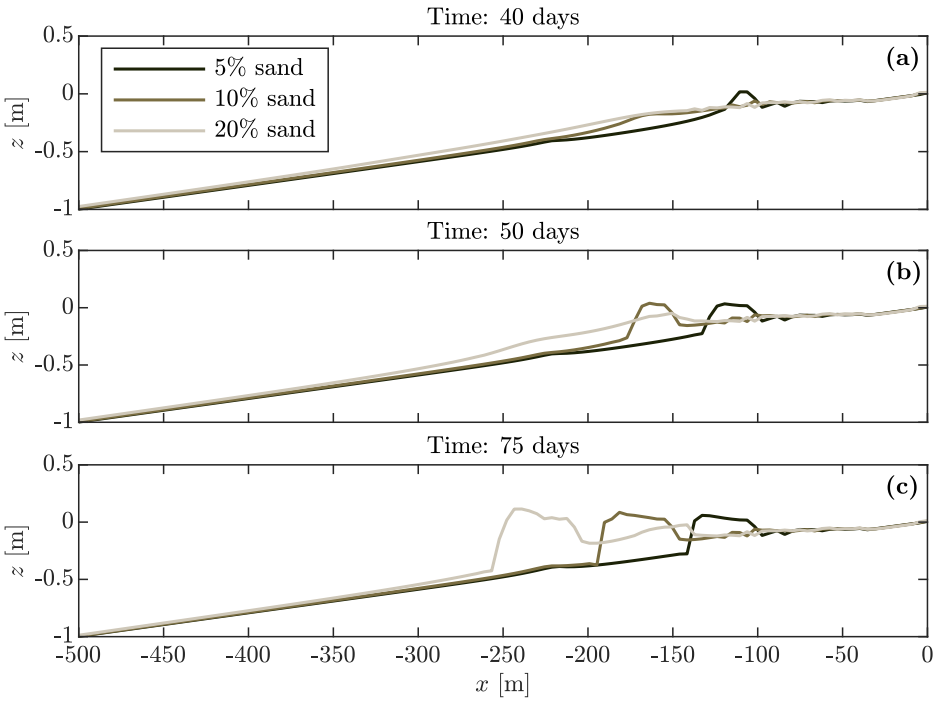


Figure 5.6: Bed level evolution at three moments in time (panel **(a)** after 40 days, panel **(b)** after 50 days, and panel **(c)** after 75 days) for three different initial sand fractions: 5% (darkest shade brown), 10% (medium shade brown) and 20% (lightest shade brown). The three sand fraction scenarios are the same as in Figure 5.5.

visible around $x = -170$ m (Figure 5.6a) and for the scenario with 20% sand around $x = -230$ m (Figure 5.6b). The chenier crest is located where the fine sand layer (which slowly built out from the water line) converges with the steepest transport gradients (see Figures 5.5c, 5.5f and 5.5i).

5.3.5 Effect of tides

The model scenarios evaluated up to now assume a constant water level. In the following scenario a single tidal component (K1, the dominant constituent) is prescribed as boundary condition with an amplitude of 0.5 m (the amplitude of spring tide in Demak). Chenier formation under average storm conditions and the simplified tide is visualized in Figure 5.7.
The effect of tides on chenier formation can be inferred from Figure 5.7 (with tides) and Figure 5.1 (same wave conditions, but constant water level). With tidal forcing, the chenier develops more slowly compared to a simulation without tides (crest formation after 90 days versus 43 days), and the crest is located more landward (around $x = -70$ m versus $x = -155$ m) and higher (around $z = 0.55$ m above MSL versus $z = 0.10$ m above MSL).

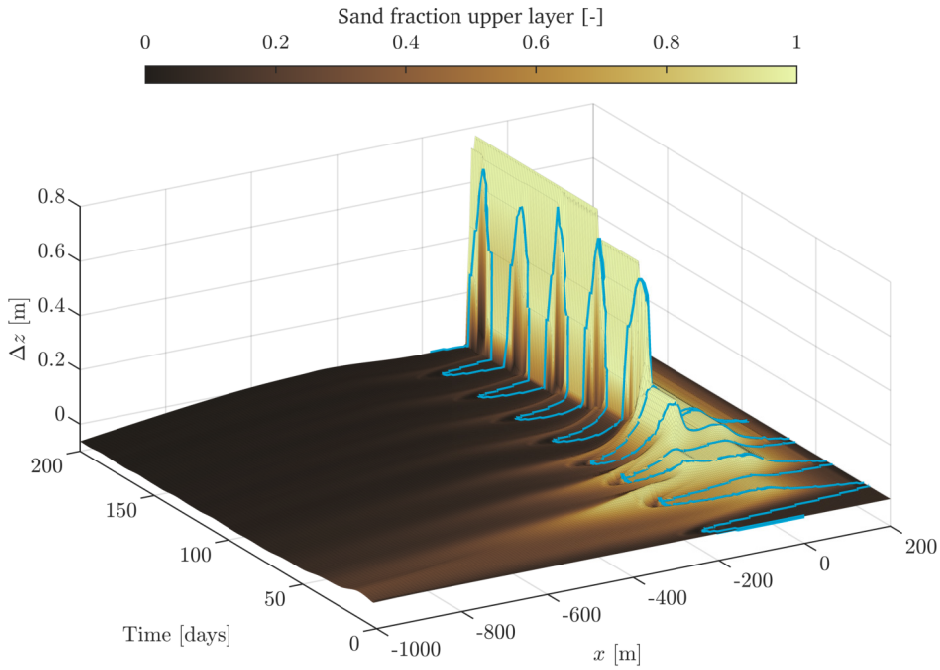


Figure 5.7: Changes in bed elevation and composition over time. The horizontal axes represent the time and x-coordinate, and the vertical axis the elevation change relative to the initial profile. The colors show the sand fraction of the upper bed layer. At the offshore boundary, a constant wave condition is applied (average storm; $H_s = 1.3$ m and $T_p = 5.6$ s), a simple tidal signal ($a_{K1} = 0.5$ m) and starting from a fully mixed bed with a sand content of 10%. The blue line shows the water line at each time step.

This difference is related to the time and spatially varying water depths and bed shear stresses. In the intertidal zone, sand is only transported when the bed is submerged (the migrating water line is indicated with the blue line in Figure 5.7), and therefore the chenier cannot develop during periods of emergence. This explains the slower development of the chenier under tidal conditions. The height of the chenier crest is limited by two factors: the water surface and the available volume of sand. The maximum water surface is higher for tidal conditions, leading to a higher crest height. But in addition to this, the waves propagate further landward during high tide, thus enlarging the bed surface from which sand can be winnowed (i.e., more sand is available under tidal conditions, favouring a higher chenier).

5.3.6 Realistic boundary conditions

As a final step, chenier formation under realistic time series for the wave conditions and water levels is evaluated. Wave conditions were derived from the

Wave Watch III hindcast data (The WAVEWATCH III Development Group, 2019) for the NW monsoon season between 1 December 2016 and 1 March 2017. The water levels were calculated using all tidal constituents derived from the water level data measured at Semarang (see Section 2.4.2). A morphological factor of 5 was applied to realise bed level changes within acceptable computational periods (Figure 5.8).

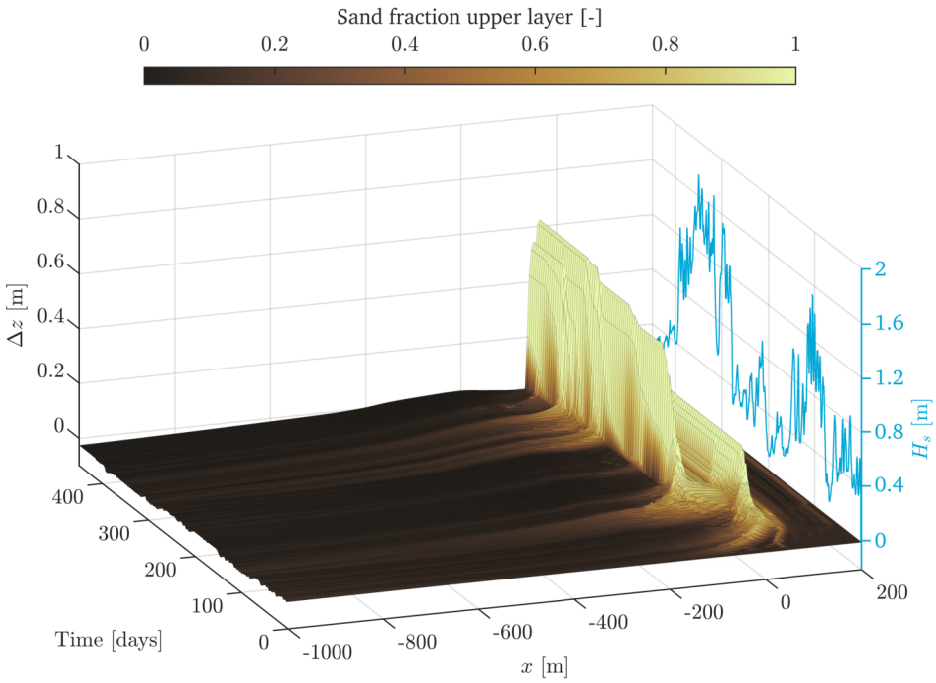


Figure 5.8: Changes in bed elevation and composition over time. The horizontal axes represent the time and x-coordinate, and the vertical axis the elevation change relative to the initial profile. On a secondary z-axis (blue axis) the significant wave height at the offshore boundary is given. The colors show the sand fraction of the upper bed layer. At the offshore boundary, a time series for the wave conditions and water levels representative for the NW monsoon season were applied.

During the first weeks, the wave height is low (rarely exceeding 0.8 m). As a result, sand is only winnowed from a narrow nearshore zone and transported to the coastline (phase 1 and 2), but the amount of sand is insufficient to develop into a crest (phase 3). A fine sand layer develops relatively high in the profile, above MSL.

Winnowing and sand transport occur over a much wider zone during the first storm ($t = 100$ days), and more sand is transported landward. This leads to sufficient nearshore sand availability for the formation of a chenier crest. The crest is formed at the seaward edge of the sand layer, which is relatively far landward.

After a brief period with calmer conditions (during which the chenier remains

static although sand is transported landward to form a fine sand sheet seaward of the chenier), a new storm initiates a second phase of substantial onshore sand transport and the formation of a second chenier crest. This crest is again located at the seaward edge of the sand layer, and is thus located more seaward than the first chenier crest. This crest quickly grows in height and shelters the older chenier crest from wave action, until it stabilises with its crest around the highest tidal levels. Later storm periods transport new volumes of sand nearshore, leading to a slight widening of the chenier crest in the seaward direction.
A notable difference between this model scenario with varying boundary conditions and the previous scenarios with constant boundary conditions, is the role of the calmer periods between storms. The wave energy during these calm periods is too weak to transport sufficient sand nearshore to develop into a chenier crest. However, there is still onshore sand transport. This sand supplied during calm conditions provides the material for rapid chenier formation during stormy periods. Therefore cheniers may more rapidly emerge during storms following a period of relatively calm conditions.

5.4 Discussion

We have numerically investigated chenier formation for a range of hydrodynamic boundary conditions representing the environmental conditions near Demak, Indonesia (see Table 5.2). A chenier developed for 18 of the 27 scenarios: the only conditions for which no chenier crest developed were for smaller, sea breeze-induced waves. These various hydrodynamic conditions influence the location where the chenier emerges (x_{crest}) and the time it takes for the chenier to develop (t_{crest}). Figure 5.9 summarises x_{crest} and t_{crest} for all scenarios with chenier development. Here, the moment of crest formation was defined as the moment the chenier crest reaches 50% of its final crest height, which coincides with the moment of rapid crest heightening (when the highest transport gradients reach the shoreline - see also Figure 5.5).
The chenier crest develops further offshore for scenarios with higher waves (filled markers) and/or higher initial sand content (yellow markers). Both contribute to a larger sand volume in the nearshore, which allows the initial nearshore sand layer to build out further offshore. A larger tidal range slows down the speed of chenier formation (high t_{crest}), as the varying water levels lead to a larger range in water depths and bed shear stresses. The diagram also provides more details on the role of the initial sediment substrate. The results in section 5.3.4 suggested that a chenier develops slower for higher sand content but closer inspection of Figure 5.9 reveals that this is only true for for high wave conditions or in the absence of tide. For moderate wave (H_s = 1.3 m) and tide (a_{K1} = 0.25–0.5 m) conditions (open triangles and squares) the duration of crest formation is independent of the initial sand content.
Chenier formation has always been associated with extreme storms (e.g. Woodroffe and Grime (1999); Dougherty and Dickson (2012)), but our model results suggest

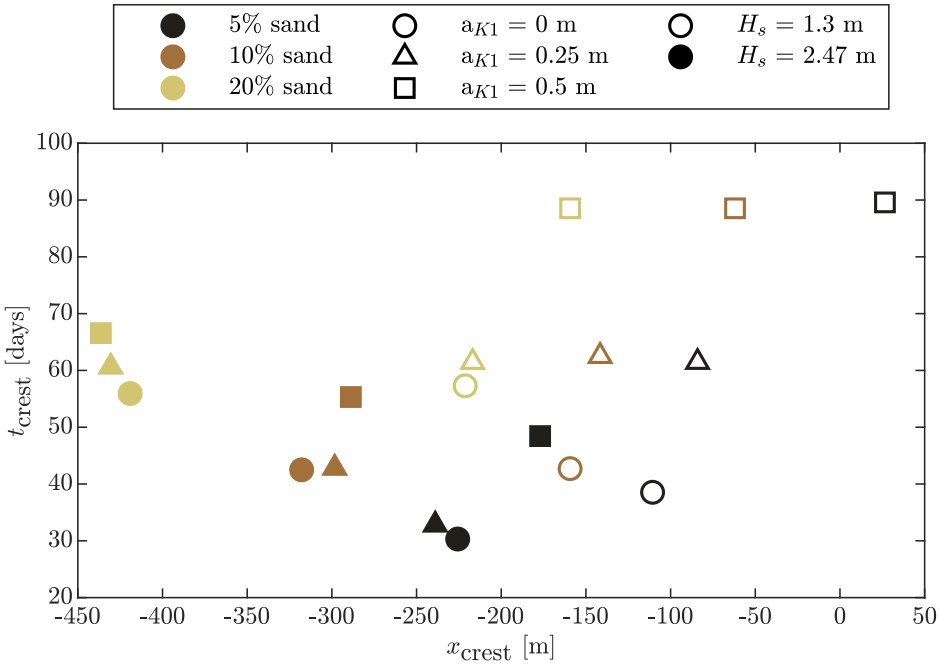


Figure 5.9: Location of the chenier crest (horizontal axis) and duration until crest development (vertical axis) for all scenarios that resulted in a chenier (18 out of 27 scenarios described in Table 5.2, excluding the sea breeze wave conditions). The shape of the data points relate to the tidal range (circle: no tide, triangle: neap tide, square: spring tide), the colours represent the sand content of the bed (lighter for higher sand content) and the two wave conditions are distinguished by the fill (no fill: average storm conditions, filled: extreme storm conditions).

that also milder storm conditions are important for chenier formation. This can be explained with the three phases which drive the formation of cheniers: winnowing, onshore transport, and crest formation. Milder storms regularly occurring during the NW monsoon season are already energetic enough to activate all three phases of chenier formation. Furthermore, small amounts of sand are still transported nearshore during calmer periods in-between. While the winnowing phase has been described qualitatively in previous work (Augustinus, 1980; Rhodes, 1982; Woodroffe and Grime, 1999; Nardin and Fagherazzi, 2018; Anthony et al., 2019), our findings provide the first quantitative investigation on this winnowing process in relation to the development of individual cheniers.

Our model results further suggest that the largest timescales are associated with phase 1 (winnowing) and 2 (onshore transport). The actual crest formation, however, is very fast (see also Section 5.3.3). In our model approach the timescales of winnowing are dependent on the state of the initial sediment bed (fully mixed), and therefore it takes a long time for the chenier to develop. It is also not realistic that storm conditions occur uninterrupted for 50 days (as in our moderate and

high storm conditions simulations). However, a sequence of storms (and calmer periods and seasons in between) may eventually set up a sufficiently pre-sorted situation, which could allow a regular, short storm to form a chenier.
The scenario with a realistic time series for the wave conditions and water levels reveal the development of a second chenier crest, seaward of the first crest. This may seem similar to bar systems which often have multiple shore-parallel bars occurring simultaneously (Short, 1991; Ruessink et al., 2003; Walstra et al., 2012). However, in contrast to submerged bars, chenier crests quickly develop to a height around or above MSL, thus emerging during (part of) each tidal cycle. As a result, the most seaward chenier crest cuts off the more landward crest from tidal and wave influences, blocking any further sand supply and effectively stopping its dynamics. This is in agreement with observations by Woodroffe et al. (1983) on the chenier plain in the Firth of Thames, New Zealand.
By using the stratigraphy schematisation in Delft3D to model separate bed layers, we modelled the winnowing process in detail. We showed that even for very low sand content (5%), a chenier can be formed. This agrees with the findings of Nardin and Fagherazzi (2018) that sand availability usually is not the limiting factor in chenier formation (except for extremely low sand contents). This finding explains the presence of cheniers in areas without a nearby source of coarser sediments, e.g. in Demak, Indonesia.
Possibly the largest limitation of our modelling approach is the absence of sand-mud interactions. In our model set-up, a cohesive (mud) and a non-cohesive (sand) fraction were considered independently: the sand fraction is mainly transported as suspended load due to wave asymmetry once a critical bed shear stress based on the Shields curve is exceeded; the mud fraction is transported as a suspended load, once the critical bed shear stress for erosion is exceeded. However, a sand-mud mixture will behave as a cohesive mixture when the mud content is higher than 30% (van Ledden et al., 2004). Such a mixture will typically have a higher critical bed shear stress for erosion (van Rijn, 2020). Furthermore, we assumed a relatively low settling velocity and critical bed shear stress for the mud fraction. Altogether, this means that our model results may overestimate the speed (and extent) at which winnowing takes place.

5.5 Conclusions

A numerical model (Delft3D) is used to analyse how cheniers develop through wave-induced winnowing and transport. We identify three phases in chenier genesis: (1) winnowing, when the mud is washed out and the upper layer of the sediment becomes increasingly sandy; (2) sand transport, when the sand in the upper layer is transported landward; and (3) crest formation, when the sand culminates at one point, resulting in a rapid heightening of the chenier crest. Winnowing takes place when mud is eroded from the bed and brought into suspension (when $\tau_{cw,max} > \tau_{cr,e}$), leaving behind a fine layer of sand. Sand transport takes places when the threshold for the initiation of motion is exceeded

(when $v_{\text{eff}} > v_{\text{cr}}$). The onshore sand transport is mainly driven by wave asymmetry, and is supply-limited (directly depending on the winnowing). Crest formation occurs when the peak of the sand transport rate converges at the shoreline, locally generating steep negative transport gradients resulting in rapid sedimentation.
The model study suggests that chenier formation does not require extreme storm conditions. Winnowing and onshore sand transport (phases 1 and 2) already take place under calm conditions, but crest formation (phase 3) requires sufficient sand to be transported nearshore. Under sea breeze conditions, the area where sand transport takes place is too small to supply sufficient sand to develop into a crest, only creating a thin nearshore layer of sand. However, average storm conditions which are exceeded several times per year, do generate sand transport over a sufficiently large spatial scale for a chenier to develop. Calm conditions therefore do not directly lead to chenier development but do result in landward transport of sand (as long as the upper layer of the bed is not depleted) which speeds up the formation of a crest during more energetic periods following that period of calm conditions.
Starting from a well-mixed bed, chenier formation is a slow process (requiring at least 8-10 weeks of uninterrupted storm conditions). Especially the time period associated with winnowing and sand transport (phases 1 and 2) is long, followed by a rapid crest formation (phase 3). The model study reveals that cheniers generally develop quicker for a lower sand content in the bed because the upper bed layers are more quickly depleted of sand. Therefore, the maximum sand transport converges more rapidly with the shoreline (onset of crest formation, phase 3). On the other hand, larger tidal amplitudes slow down chenier formation, due to temporal and spatial variability of bed shear stresses and periods of emergence in the region of chenier development.

Chapter 6

The role of cheniers in stabilising mangrove-mud coasts

The aim of this dissertation is to improve understanding of chenier dynamics within the context of eroding mangrove-mud coasts, with a focus on cross-shore dynamics at the scale of waves and tides. This research objective is translated into three research questions (see Chapter 1), which were addressed in the previous chapters (Chapters 3-5). This chapter revisits these research questions and brings their answers into a wider context of eroding mangrove-mud coasts, and provides recommendations for further research.

6.1 New insights

Which processes control the cross-shore dynamics of a chenier during calm conditions?

In order to better understand the processes controlling the short-term dynamics of a chenier, we carried out field observations in Demak, Indonesia (see Chapter 3). Despite relatively calm hydrodynamics (the measurements took place during the SE monsoon season), the chenier migrated surprisingly fast in the landward direction. Using velocity moments as a proxy for the sediment transport, we demonstrate the role of waves and tides in driving this landward migration. Waves only generate substantial sediment transport when a chenier is submerged during periods with higher waves. Waves transport sediment directly, via wave skewness (generating higher orbital flow velocities in the landward than in the seaward direction) and indirectly, via wave orbital motion stirring up sediment (which may subsequently be transported by tidal currents). The tides generate a landward-directed sediment transport when the water over the chenier crest is shallow (high crest level relative to mean sea level). Finally, we show that the cross-shore chenier dynamics are especially sensitive to the timing of waves and tide: most transport takes place when high water levels coincided with relatively high waves.

Which processes are responsible for the dynamic equilibrium of cheniers on a drowning coastal plain?

Our field observations, as well as descriptions of other cheniers in literature, only describe landward migration of cheniers. Herein cheniers continue their landward migration until they reach a stable position with their crest level above tidal influences. However, satellite photos of the chenier in Demak suggest the existence of an alternative stable state in the intertidal zone, with a chenier which is highly dynamic in the short term, but stable in the longer term. To explore this alternative stable state, we developed an idealised chenier model to investigate cross-shore chenier dynamics under daily wave and tidal influences. With the model, we were able to predict both onshore and offshore migration. Onshore migration is mainly driven by wave action, while offshore migration is induced by a tidal phase lag, or the effect of the storm season. The phase lag is induced by the the large tidal volumes inundating the drowning coastal plain. For certain combinations of waves, tides (incl. phase lag) and storm season effects, the model study predicted a dynamically stable chenier, similar to the cheniers observed in Demak. Without a phase lag and/or storm season effect, the model yields a classic stable chenier that welds onto the shoreline by onshore migration, as described in literature for other cheniers. The dependence on the phase lag suggests that stable cheniers may be observed more frequently along drowning mangrove-mud coasts.

How are cheniers formed through wave winnowing and tidal transport?

A processed-based model (Delft3D) was deployed to unravel mechanisms responsible for chenier formation from a mud-dominated substrate. We identified three phases of chenier development: (1) a winnowing phase, during which mud is washed out of the seabed initially consisting of a mixture of sand and mud, (2) a sand transport phase, when the sand in the upper layer is transported onshore, and (3) a crest formation phase, during which a chenier crest rapidly develops at the landward limit of onshore sediment transport. The main mechanism driving onshore sand transport is wave asymmetry. During calm conditions, sand transport takes place within a narrow zone, limiting the volume of sand delivered nearshore, and therefore no chenier develops. In contrast, average storm conditions mobilise sufficient sand for a crest to develop. Our results thus revealed that chenier formation through wave winnowing does not require extreme storm conditions. Furthermore, we showed that chenier formation through wave winnowing is a relatively slow process. The largest time scales are associated with winnowing and sand transport, in contrast to the rapid crest development.

6.2 Implications for mangrove-mud coasts

Demak: An analogue for accelerated sea level rise?

Globally, sea level is rising at a rate of 3.3 $\pm$ 0.4 mm/y (Cazenave et al., 2014), as a result of global warming (thermal expansion of sea water and melting of ice caps (Cazenave et al., 2008)). Subsidence may locally add to this eustatic sea level rise, jointly referred to as relative sea level rise. While sea level rise may seem a relatively slow process, in Semarang, the subsidence is typically an order of magnitude larger than the eustatic sea level rise (Chaussard et al., 2013; Marfai and King, 2007; Abidin et al., 2013). In other words, the rate of relative sea level rise currently experienced in Demak may be globally more common in one or two centuries.

Cheniers are often associated with erosive episodes, since they are formed when waves rework the sediment. Once formed, they tend to migrate landward until they weld onto the shoreline, above the highest tidal levels. In Demak, a counterbalancing mechanism caused by a tidal phase lag leads to a more offshore positioned chenier, providing wave sheltering for the otherwise exposed coastline (see Chapter 4). This tidal phase lag is an indirect result of the drowning of the coastal plain (explained in Figure 4.4).

The cheniers in Demak therefore act as a natural defense mechanism of an eroding and subsiding mangrove-mud coast. 'Classic' cheniers weld onto the shoreline, where they not only protect the shore against wave attack, but also cut off the mangroves from sediment supply during calm and regular conditions (which is required to keep up with relative sea level rise). At a drowning coastal plain like Demak, the chenier's position is maintained in the intertidal zone. At this location, the chenier is still highly efficient at damping incoming waves. However, it also allows sediment transport into the mangrove fringe, and even promotes the development of a mudflat bordering the mangrove fringe (van Bijsterveldt et al., in prep.b). Hence, the chenier optimises the conditions for mangroves to keep up with relative sea level rise.

Sedimentation experiments of van Bijsterveldt et al. (in prep.a) show that mangrove trees can survive a sedimentation event of up to 20 cm, which is much higher than the sedimentation required to keep up with relative sea level rise. However, in rapidly subsiding areas such as Demak, such rapid sedimentation requires very high sediment concentrations (see also the estimations of Gijón Mancheño et al. (in prep.)). At lower sediment concentrations, the mangroves cannot keep up with relative sea level rise, and coastline retreat and erosion will follow. This may further increase the tidal phase lag, which may eventually disturb the dynamically stable state of the chenier. In that case, the chenier may end up at deeper water, where it is less efficient at damping incoming wave energy, or it may dissolve into a fine sand layer, completely exposing the mangrove fringe and leading to accelerated erosion and mangrove decay. Alternatively, the chenier may breach (see Figures 6.1 and 6.2c), reducing the water level gradients over

the chenier and the offshore-directed sediment transport. In this case, the chenier may migrate onshore, either until it reaches a new dynamic equilibrium, or until it welds onto the shoreline, leading to suffocation of the mangrove fringe.

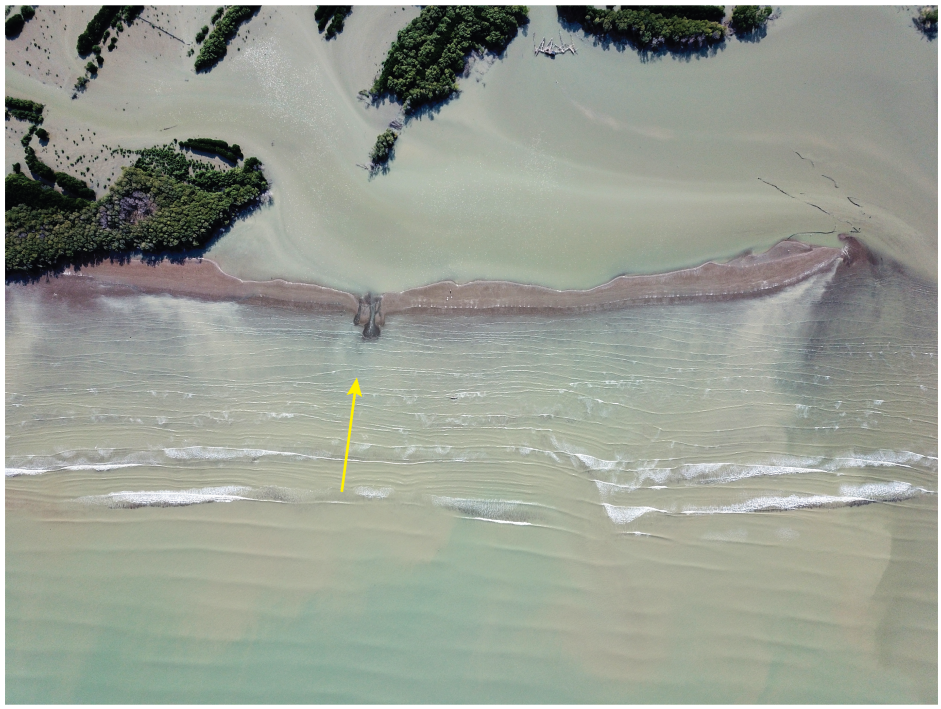


Figure 6.1: Chenier breach (yellow arrow) after spring tide (photo by S.A.J. Tas).

Nourishment potential

Along sandy shores, nourishing is a common strategy to protect and stabilise vulnerable coastlines against sea level rise and erosion (Stronkhorst et al., 2018; de Schipper et al., 2021). Along muddy shores, nourishing is much more complex, as the settling and consolidation times of fine sediment are much longer than of sand, allowing waves and tides to carry the nourished sediments away from the intended area (Baptist et al., 2019; Schulz et al., 2021). However, cheniers demonstrate that even a small fraction of sand may contribute substantially to protecting vulnerable muddy coasts. Our findings in Chapter 5 suggest that chenier formation may be accelerated by a local source of coarse sediments in the nearshore (such as local rivers or the erosion of old cheniers).

We see two options for chenier-style nourishments on muddy coasts: (1) direct chenier nourishment, either by adding sand to an existing chenier, or by constructing a sandy ridge at the intended location of the artificial chenier (similar to beachface nourishments on sandy coasts (Dean, 2002; Hanson et al., 2002)), or

(2) indirect sand supply, by adding sand to the foreshore and letting the natural dynamics transport the sand nearshore and develop into a chenier (similar to shoreface nourishments). While the first option could yield immediate protection by the chenier, nourishing in the intertidal zone of muddy coasts is logistically challenging and therefore expensive (the mild foreshore slopes requiring long pumping distances from the dredging vessel to the chenier location). Supplying sand at slightly deeper water and employing natural dynamics to transport the sediment onshore, could potentially yield a more stable chenier, but will take longer to develop. It also requires the right environmental conditions to generate onshore transport. However, both options require the availability of sand. Even though the required volume is relatively small, sand is often not readily available along muddy coastlines, making this an expensive operation and therefore possibly not cost-effective.

While a chenier in the intertidal zone can be very efficient in protecting a vulnerable mangrove-mud coast, there is also the risk of the chenier migrating landward and welding with the shoreline, potentially suffocating the mangroves at the seaward fringe. If relative sea level rise continues, such a chenier will continue to migrate landward and suffocate more and more mangroves. Therefore, we only see potential for nourishment in areas where all processes for dynamically stable cheniers are present (e.g. a drowning coastal plain generating a tidal volume that provides a landward transport component balancing onshore transport by wave asymmetry).

Toll road Semarang-Demak

A new segment of the Trans-Java Toll Road is planned between Semarang and Demak (see Figure 6.2e). The first part of this trajectory (closest to Semarang) will also serve as a sea dike. Such a sea dike is very expensive, and building on the soft soils of muddy coasts is challenging (Kempfert and Raithel, 2002). Such structures are vulnerable to local scour seaward of the dike due to wave reflection (Winterwerp et al., 2013; Anthony and Gratiot, 2012).

Besides these technical difficulties, a dike may also have unintended negative impact on the surrounding mangrove-mud coast. A healthy mangrove greenbelt requires a certain minimum width to be sustainable (Duke et al., 2007; Xie et al., 2020). This width is determined by requirements regarding both physical factors (wave attenuation and sediment retention) as well as biological factors (allowing biodiversity and natural zonation). Constructing the dike too close to sea will lead to mangrove squeeze and eventually the degradation of the remaining mangrove greenbelt (Phan et al., 2015).

The findings presented within this thesis reveal another potential impact of such an interruption of the coastal zone. Depending on its exact location and the geometry of the coastal plain, the dike may strongly reduce the tidal prism. This may then introduce a tidal phase lag, which strongly influences the cross-shore chenier dynamics (Chapter 4). If a dike is constructed landward of the chenier,

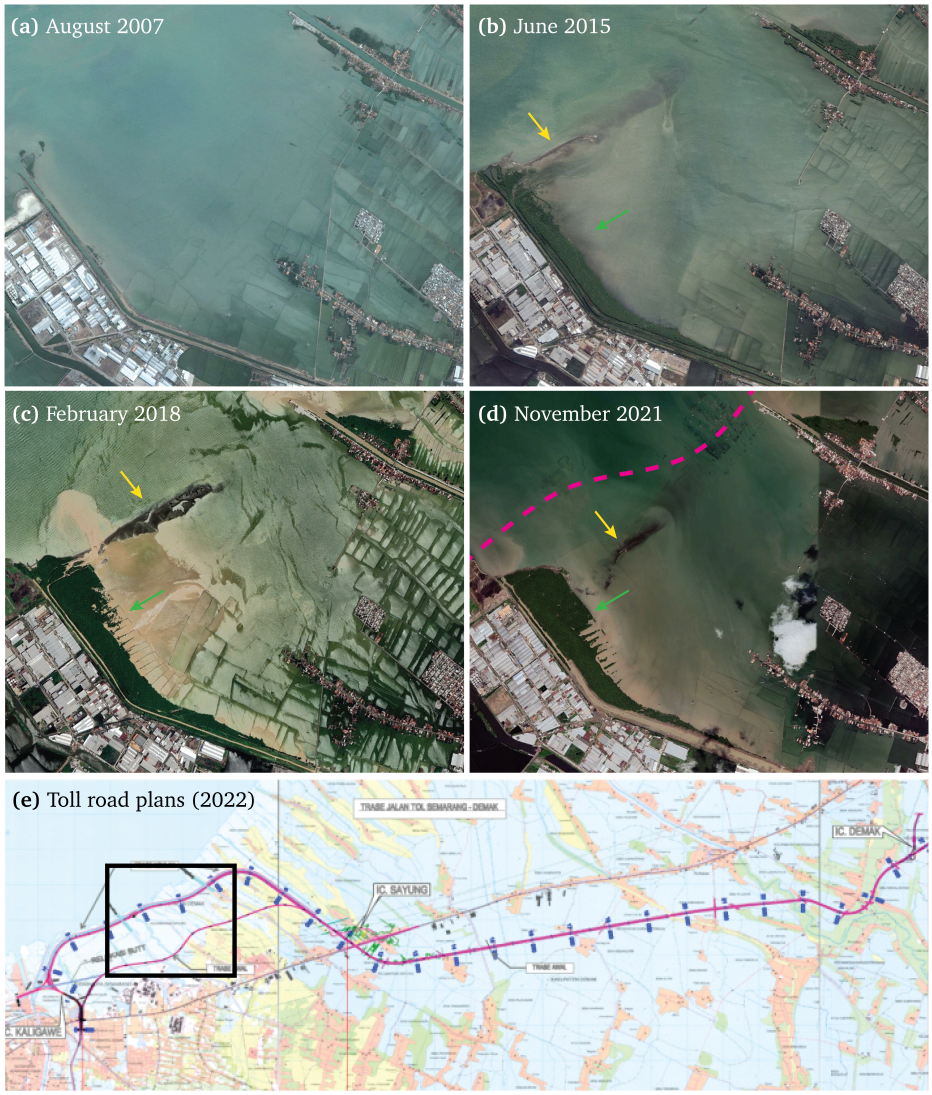


Figure 6.2: Satellite images (Google Earth, 2022) showing the evolution of the coastline just north of Semarang harbour in **(a)** August 2007, **(b)** June 2015, **(c)** February 2018, and **(d)** November 2021. The yellow arrow indicates a chenier, the green arrow a recovering mangrove forest. **(e)** Trajectory of the planned toll road and sea dike between Semarang and Demak (Biro Infrastruktur dan Sumber Daya Alam Setda Provinsi Jawa Tengah, 2018). The black rectangle indicates the location of the satellite images. The planned trajectory is also added to panel (d) (pink dashed line).

this may lead to accelerated onshore migration of the chenier, possibly suffocating any remaining mangrove stands in front of the dike.
The trajectory of the Semarang-Demak toll road is planned seaward of the current

coastline. This area suffered from severe subsidence, resulting in coastline retreat of more than 2 km. In 2007, all mangrove cover was gone (either replaced by aquaculture or eroded), see Figure 6.2a. By 2015, a chenier (indicated with the yellow arrow in Figure 6.2b) is observed at the tip of the headland, and a narrow mangrove fringe (green arrow in Figure 6.2b) has established at its lee side. Over the years this chenier is relatively dynamic, sometimes connected to the headland (2015), and sometimes disconnected (2018) as a result of breaching. Meanwhile, the mangroves continued to expand.
Figure 6.2d shows the most recent satellite photo, with the projected trajectory of the toll road/dike (construction to start in 2022) indicated by the pink dashed line. At this location, the dike will block all waves and currents and therefore sediment transport. Not only will this prevent further mangrove expansion, it will also prevent the existing mangrove area landward of the road (both the bed and the mangroves themselves) to grow vertically and compensate for land subsidence (which is up to 20 cm/y here (Marfai and King, 2007; Abidin et al., 2013), see Section 2.2), which will eventually lead to their drowning.

6.3 Recommendations for future research

From 1D to 3D

Throughout this thesis, we assumed longshore uniformity and simplified our approach to the cross-shore dimension only. However, many chenier coastlines are non-uniform in the alongshore direction (e.g., the Demak coastline) or are subject to longshore currents resulting from prevailing winds, ocean currents, or obliquely incident waves (e.g., the Guianas coastline). In a longshore uniform approach, a chenier is an infinitely long ridge parallel to the shore, while in Demak, multiple short cheniers occur at a similar distance from the shoreline. On the other hand, relict cheniers of tens of kilometres long can be observed in other locations, e.g. in China (Cangzi and Walker, 1989) and Louisiana (Russell and Howe, 1935).
The length of the chenier directly determines the influence of the coastal plain on the cross-shore chenier dynamics, through the tidal phase lag (the longer the chenier, the larger the water level gradient due to the tidal phase lag can become over the chenier). If this water level gradient becomes too large, the chenier may breach (see Figure 6.1). This immediately reduces the tidal phase lag, which in turn impacts the cross-shore chenier dynamics (see Chapter 4). Extending the current 1D approach to a 2DH approach would allow to include these effects.
In this study, we adopted a depth-averaged approach. However, especially during storm conditions, depth-varying processes play an important role in sediment transport. Undertow, which is an offshore-directed current near the bed compensating the wave-driven onshore-directed surface current, has an important effect on sediment transport, as the sediment concentration is higher near the bed. However, when the chenier is not fully emerged, the mass flux is not entirely compensated by undertow, as part of the water can flow away via the back of the

chenier (similar to shallow areas on ebb-tidal deltas, (Bertin et al., 2009)). To fully account for these effects, the 2DH approach could be further extended to a 3D approach.

Chenier dynamics during storm conditions

Our observations during the SE monsoon season showed cheniers to be surprisingly dynamic during calm conditions (Chapter 3). Unfortunately, we did not measure chenier dynamics during the NW monsoon season. Moreover, satellite images taken during this season are mostly not useful due to the dense cloud cover. Based on satellite images in the SE monsoon season (see Figure 3.3), we know that cheniers migrate offshore during the NW monsoon season. This is consistent with observations of breaker bar behaviour along open sandy coasts, which move offshore during storm conditions (e.g., Walstra et al. (2012)). In our idealised chenier model (Chapter 4), we accounted for this by introducing an estimated 'storm reset', a net offshore displacement. However, we know that during the NW monsoon season of 2017-2018, a very high storm completely reorganised the cheniers nearshore (C.E.J. van Bijsterveldt, personal communication, December 2017). Therefore, observations of chenier dynamics during NW monsoon conditions would help to understand chenier response under energetic conditions, as well as identify possible thresholds for chenier stability.

Dynamically stable cheniers in other locations

As far as we know, the cheniers in Demak are the only examples of dynamically stable cheniers. However, most chenier research has focused on longer term dynamics at the larger scales of the chenier plain. Therefore, it could be that dynamically stable cheniers shaped such chenier plains, but have not yet been observed and reported due to the temporal and spatial scales of previous studies. Furthermore, as relative sea level rise continues and accelerates, more coastal plains worldwide will drown, potentially creating conditions for dynamically stable cheniers to develop. But also if the active cheniers are not in a dynamically stable state, more detailed observations of their dynamics at smaller spatial and temporal scales will increase the understanding of chenier migration rates and development.

Bio-morphodynamic modelling

This chenier study was motivated by the role they can play in stabilising (eroding) mangrove-mud coasts. Especially in the intertidal zone, cheniers can create windows of opportunity for mangrove establishment. Vice versa, our work also showed that the coastal plain strongly influences the chenier stability. To further study the role of cheniers on mangrove-mud coasts, we suggest to include cheniers in a bio-morphodynamic model. While morphodynamic models in-

clude the physical effects vegetation can have on hydro- and morphodynamics, bio-morphodynamic models also include how the physics affect vegetation, for example through vegetation growth and species distribution. Such models couple a hydro-morphodynamic model (e.g. Delft3D) to a dynamic vegetation model (e.g. Temmerman et al. (2005); Balke et al. (2011); Xie et al. (2020, 2022)). The approach we followed to develop the idealised chenier model (see Chapter 4) could be used to develop an additional module to include chenier dynamics in a bio-morphodynamic model.

Bibliography

Abidin, H. Z., Andreas, H., Gumilar, I., Sidiq, T. P., Fukuda, Y., Andreas, H., Gumilar, I., Sidiq, T. P., and Land, Y. F.: Land subsidence in coastal city of Semarang (Indonesia): characteristics, impacts and causes, Geomatics, Natural Hazards and Risk, 4, 226–240, doi:10.1080/19475705.2012.692336, 2013.

Alferink, M.: Wave transmission through permeable structures in Demak Indonesia, Msc thesis, Faculty of Civil Engineering and Geosciences, Delft University of Technology, URL http://resolver.tudelft.nl/uuid:23dc0cc4-9658-44ab-a067-5800a0731853, 2022.

Alongi, D. M.: Mangrove forests: Resilience, protection from tsunamis, and responses to global climate change, Estuarine, Coastal and Shelf Science, 76, 1–13, doi:10.1016/j.ecss.2007.08.024, 2008.

Alongi, D. M.: The Energetics of Mangrove Forests, Springer, doi:10.1007/978-1-4020-4271-3, 2009.

Anderson, J. B., Wallace, D. J., Simms, A. R., Rodriguez, A. B., and Milliken, K. T.: Variable response of coastal environments of the northwestern Gulf of Mexico to sea-level rise and climate change: Implications for future change, Marine Geology, 352, 348–366, doi:10.1016/j.margeo.2013.12.008, 2014.

Anthony, E. J.: Chenier plain development in northern Sierra Leone, West Africa, Marine Geology, 90, 297–309, doi:10.1016/0025-3227(89)90132-1, 1989.

Anthony, E. J.: Beach-ridge development and sediment supply: examples from West Africa, Marine Geology, 129, 175–186, doi:10.1016/0025-3227(95)00111-5, 1995.

Anthony, E. J. and Gratiot, N.: Coastal engineering and large-scale mangrove destruction in Guyana, South America: Averting an environmental catastrophe in the making, Ecological Engineering, 47, 268–273, doi:10.1016/j.ecoleng.2012.07.005, 2012.

Anthony, E. J., Gardel, A., Gratiot, N., Proisy, C., Allison, M. A., Dolique, F., and Fromard, F.: The Amazon-influenced muddy coast of South America: A review of mud-bank-shoreline interactions, Earth-Science Reviews, 103, 99–121, doi:10.1016/j.earscirev.2010.09.008, 2010.

Anthony, E. J., Gardel, A., Dolique, F., and Marin, D.: The Amazon-influenced mud-bank coast of South America: an overview of short- to long-term morphodynamics of 'inter-bank' areas and chenier development, Journal of Coastal Research, ICS 2011, 25–29, URL https://www.jstor.org/stable/26482126, 2011.

Anthony, E. J., Gardel, A., and Gratiot, N.: Fluvial sediment supply, mud banks,

cheniers and the morphodynamics of the coast of South America between the Amazon and Orinoco river mouths, in: Geological Society, London, Special Publications, edited by Martini, I. P. and Wanless, H. R., vol. 388, pp. 533–560, The Geological Society of London, doi:10.1144/SP388.8, 2013.

Anthony, E. J., Brunier, G., Gardel, A., and Hiwat, M.: Chenier Morphodynamics on the Amazon-Influenced Coast of Suriname, South America: Implications for Beach Ecosystem Services, Frontiers in Earth Science, 7, 1–20, doi:10.3389/feart.2019.00035, 2019.

Augustinus, P. G. E. F.: Actual development of the chenier coast of Suriname (South America), Sedimentary Geology, 26, 91–113, doi:10.1016/0037-0738(80)90007-X, 1980.

Augustinus, P. G. E. F.: Cheniers and chenier plains: A general introduction, Marine Geology, 90, 219–229, doi:10.1016/0025-3227(89)90126-6, 1989.

Badan Meteorologi Klimatologi dan Geofisika: Automatic Weather Station - Maritim Semarang, retrieved from http://202.90.199.132/aws-new/monitoring/3000000014, January 2019, 2020.

Bailard, J. A. and Inman, D. L.: An Energetics Bedload Model for a Plane Sloping Beach: Local Transport, Journal of Geophysical Research, 86, 2035–2043, doi:10.1029/JC086iC03p02035, 1981.

Balke, T., Bouma, T. J., Horstman, E. M., Webb, E. L., Erftemeijer, P. L. A., and Herman, P. M. J.: Windows of opportunity: Thresholds to mangrove seedling establishment on tidal flats, Marine Ecology Progress Series, 440, 1–9, doi:10.3354/meps09364, 2011.

Bao, T. Q.: Effect of mangrove forest structures on wave attenuation in coastal Vietnam, Oceanologia, 53, 807–818, doi:10.5697/oc.53-3.807, 2011.

Baptist, M. J., Gerkema, T., van Prooijen, B. C., van Maren, D. S., van Regteren, M., Schulz, K., Colosimo, I., Vroom, J., van Kessel, T., Grasmeijer, B. T., Willemsen, P., Elschot, K., de Groot, A. V., Cleveringa, J., van Eekelen, E. M. M., Schuurman, F., de Lange, H. J., and van Puijenbroek, M. E. B.: Beneficial use of dredged sediment to enhance salt marsh development by applying a 'Mud Motor', Ecological Engineering, 127, 312–323, doi:10.1016/j.ecoleng.2018.11.019, 2019.

Bayliss-Smith, T. P., Healey, R., Lailey, R., Spencer, T., and Stoddart, D. R.: Tidal Flows in Salt Marsh Creeks, Estuarine and Coastal Marine Science, 9, 235–255, doi:10.1016/0302-3524(79)90038-0, 1979.

Beijerinck, W. and von Schierbrand, W. C.: Topographische kaart der Residentie Semarang, URL http://hdl.handle.net/1887.1/item:2013206, 1871.

Belperio, A. P., Gostin, V. A., Cann, J. H., and Murray-Wallace, C. V.: Sediment-organism zonation and the evolution of Holocene tidal sequences in Southern Australia, in: Tide-influenced sedimentary environments and facies, edited by de Boer, P. L., van Gelder, A., and Nio, S. D., pp. 475–497, D. Reidel Publlishing Company, Dordrecht, the Netherlands, 1988.

Bertin, X., Fortunato, A. B., and Oliveira, A.: A modeling-based analysis of processes driving wave-dominated inlets, Continental Shelf Research, 29, 819–

834, doi:10.1016/j.csr.2008.12.019, 2009.

Biro Infrastruktur dan Sumber Daya Alam Setda Provinsi Jawa Tengah: Trase jalan tol Semarang-Demak dan tanggul laut kota Semarang (The route of the Semarang-Demak toll road and the Semarang city sea wall), retrieved from http://biroinfrasda.jatengprov.go.id/programkegiatan/trase-jalan-tol-semarang-demak-dan-tanggul-laut-kota-semarang/, 25 March 2022, 2018.

Blasco, F., Saenger, P., and Janodet, E.: Mangroves as indicators of coastal change, Catena, 27, 167–178, doi:10.1016/0341-8162(96)00013-6, 1996.

Booij, N., Ris, R. C., and Holthuijsen, L. H.: A third-generation wave model for coastal regions: 1. Model description and validation, Journal of Geophysical Research, 104, 7649–7666, doi:10.1029/98JC02622, 1999.

Bowen, A. J.: Simple models of nearshore sedimentation: Beach profiles and longshore bars, The coastline of Canada, 1980.

Brunier, G., Anthony, E. J., Gratiot, N., and Gardel, A.: Exceptional rates and mechanisms of muddy shoreline retreat following mangrove removal, Earth Surface Processes and Landforms, 44, 1559–1571, doi:10.1002/esp.4593, 2019.

Bunting, P., Rosenqvist, A., Lucas, R. M., Rebelo, L. M., Hilarides, L., Thomas, N., Hardy, A., Itoh, T., Shimada, M., and Finlayson, C. M.: The global mangrove watch - A new 2010 global baseline of mangrove extent, Remote Sensing, 10, doi:10.3390/rs10101669, 2018.

Cangzi, L. and Walker, H. J.: Sedimentary Characteristics of Cheniers and the Formation of the Chenier Plains of East China, Journal of Coastal Research, 5, 353–368, URL https://www.jstor.org/stable/4297538, 1989.

Carugati, L., Gatto, B., Rastelli, E., Lo Martire, M., Coral, C., Greco, S., and Danovaro, R.: Impact of mangrove forests degradation on biodiversity and ecosystem functioning, Scientific Reports, 8, doi:10.1038/s41598-018-31683-0, 2018.

Cazenave, A., Lombard, A., and Llovel, W.: Present-day sea level rise: A synthesis, Comptes Rendus - Geoscience, 340, 761–770, doi:10.1016/j.crte.2008.07.008, 2008.

Cazenave, A., Dieng, H. B., Meyssignac, B., Von Schuckmann, K., Decharme, B., and Berthier, E.: The rate of sea-level rise, Nature Climate Change, 4, 358–361, doi:10.1038/nclimate2159, 2014.

Chappell, J. M. A.: Contrasting Holocene sedimentary geologies of lower Daly River, northern Australia, and lower Sepik-Ramu, Papua New Guinea, Sedimentary Geology, 83, 339–358, doi:10.1016/0037-0738(93)90020-6, 1993.

Chaussard, E., Amelung, F., Abidin, H., and Hong, S. H.: Sinking cities in Indonesia: ALOS PALSAR detects rapid subsidence due to groundwater and gas extraction, Remote Sensing of Environment, 128, 150–161, doi:10.1016/j.rse.2012.10.015, 2013.

Codiga, D. L.: Unified tidal analysis and prediction using the UTide Matlab functions, Technical report 01, Graduate School of Oceanography, Univer-

sity of Rhode Island, Narragansett, RI, URL ftp://www.po.gso.uri.edu/pub/downloads/codiga/utide/UTideCurrentVersion.zip, 2011.

Cohn, N. and Ruggiero, P.: The influence of seasonal to interannual nearshore profile variability on extreme water levels: Modeling wave runup on dissipative beaches, Coastal Engineering, 115, 79–92, doi:j.coastaleng.2016.01.006, 2016.

Cohn, N., Hoonhout, B. M., Goldstein, E. B., de Vries, S., Moore, L. J., Durán Vinent, O., and Ruggiero, P.: Exploring Marine and Aeolian Controls on Coastal Foredune Growth Using a Coupled Numerical Model, Journal of Marine Science and Engineering, 7, doi:10.3390/jmse7010013, 2019.

Cook, P. J. and Polach, H. A.: A chenier sequence at Broad Sound, Queensland, and evidence against a Holocene high sea level, Marine Geology, 14, 253–268, doi:0025-3227(73)90004-2, 1973.

Daniel, J. R. K.: The chenier plain coastal system of Guyana, Marine Geology, 90, 283–287, doi:10.1016/0025-3227(89)90130-8, 1989.

de Schipper, M. A., Ludka, B. C., Raubenheimer, B., Luijendijk, A. P., and Schlacher, T. A.: Beach nourishment has complex implications for the future of sandy shores, Nature Reviews Earth and Environment, 2, 70–84, doi:10.1038/s43017-020-00109-9, 2021.

de Wit, F., Tissier, M., and Reniers, A. J. H. M.: Characterizing Wave Shape Evolution on an Ebb-Tidal Shoal, Journal of Marine Science and Engineering, 7, 367, doi:10.3390/jmse7100367, 2019.

Dean, R. G.: Beach nourishment: Theory and practice, World Scientific, River Edge, NJ, doi:10.1142/2160, 2002.

Deltares: Delft3D-FLOW. Simulation of multi-dimensional hydrodynamic flows and transport phenomena, including sediments. User Manual, Tech. rep., Deltares, Delft, URL https://content.oss.deltares.nl/delft3d/manuals/Delft3D-FLOW_User_Manual.pdf, 2021.

Deltares and BioManCO: Sediment analysis of Demak, Tech. rep., Deltares, 2019.

Donato, D. C., Kauffman, J. B., Murdiyarso, D., Kurnianto, S., and Stidham, M.: Mangroves among the most carbon-rich forests in the tropics, Nature Geoscience, 4, 293–297, doi:10.1038/ngeo1123, 2011.

Dougherty, A. J. and Dickson, M. E.: Sea level and storm control on the evolution of a chenier plain, Firth of Thames, New Zealand, Marine Geology, 307-310, 58–72, doi:10.1016/j.margeo.2012.03.003, 2012.

Draut, A. E., Kineke, G. C., Velasco, D. W., Allison, M. A., and Prime, R. J.: Influence of the Atchafalaya River on recent evolution of the chenier-plain inner continental shelf, northern Gulf of Mexico, Continental Shelf Research, 25, 91–112, doi:10.1016/j.csr.2004.09.002, 2005.

Dubarbier, B., Castelle, B., Marieu, V., and Ruessink, G.: Process-based modeling of cross-shore sandbar behavior, Coastal Engineering, 95, 35–50, doi:10.1016/j.coastaleng.2014.09.004, 2015.

Duke, N. C.: Mangrove floristics and biogeography, in: Tropical Mangrove Ecosystems, edited by Robertson, A. I. and Alongi, D. M., chap. 4, pp. 63–100, Ameri-

can Geophysical Union, Washington, DC, USA, doi:10.1029/CE041, 1992.

Duke, N. C.: Oil spill impacts on mangroves: Recommendations for operational planning and action based on a global review, Marine Pollution Bulletin, 109, 700–715, doi:10.1016/j.marpolbul.2016.06.082, 2016.

Duke, N. C., Meynecke, J. O., Dittman, S., Ellison, A. A., Anger, K., Berger, U., Cannicci, S., Diele, K., Ewel, K. C., Field, C. D., Koedam, N., Lee, S. Y., Marchand, C., Nordhaus, I., and Dahdouh-Guebas, F.: A World Without Mangroves?, Science, 317, 41–42, doi:10.1126/science.317.5834.41b, 2007.

Dyhr-Nielsen, M. and Sorensen, T.: Some sand transport phenomena on coasts with bars, Coastal Engineering, pp. 855–865, doi:10.1061/9780872620285.054, 1970.

Ervita, K. and Marfai, M. A.: Shoreline Change Analysis in Demak, Indonesia, Journal of Environmental Protection, 08, 940–955, doi:10.4236/jep.2017.88059, 2017.

Fitrianti, N., Harryanto, Y. D., Simamora, E. V. S., Bintari, H. F. A., Hartoko, A., Anggoro, S., and Zainuri, M.: Analysis of daily wind circulation toward sea level rise in Semarang, in: IOP Conference Series: 1st International Conference on Maritime Sciences and Advanced Technology "Ocean Science and Technology Toward a Global Maritime Axis", vol. 162, pp. 1–11, IOP, doi:10.1088/1755-1315/162/1/012018, 2018.

Flanders Marine Institute (VLIZ) and Intergovernmental Oceanographic Commission (IOC): Sea level monitoring facility, doi:10.14284/482, http://www.ioc-sealevelmonitoring.org. Accessed on 2021-07-20, 2021.

Foreman, M. G. G. and Henry, R. F.: The harmonic analysis of tidal model time series, Advances in Water Resources, 12, 109–120, doi:10.1016/0309-1708(89)90017-1, 1989.

Fredsøe, J.: Turbulent boundary layer in wave-current motion, Journal of Hydraulic Engineering, 110, 1103–1120, doi:https://doi.org/10.1061/(ASCE)0733-9429(1984)110:8(1103), 1984.

French, J., Payo, A., Murray, B., Orford, J., Eliot, M., and Cowell, P.: Appropriate complexity for the prediction of coastal and estuarine geomorphic behaviour at decadal to centennial scales, Geomorphology, 256, 3–16, doi:10.1016/j.geomorph.2015.10.005, 2016.

Friedrichs, C. T.: Barotropic tides in channelized estuaries, in: Contemporary Issues in Estuarine Physics, edited by Valle-Levinson, A., pp. 27–61, Cambridge University Press, Cambridge, UK, doi:10.1017/CBO9780511676567.004, 2010.

Friedrichs, C. T. and Madsen, O. S.: Nonlinear Diffusion of the Tidal Signal in Frictionally Dominated Embayments, Journal of Geophysical Research, 97, 5637–5650, doi:10.1029/92JC00354, 1992.

Friess, D. A.: Ecosystem Services and Disservices of Mangrove Forests: Insights from Historical Colonial Observations, Forests, 7, doi:10.3390/f7090183, 2016.

Gallagher, E. L., Elgar, S., and Guza, R. T.: Observations of sand bar evolution on a natural beach, Journal of Geophysical Research, 103, 3203–3215,

doi:10.1029/97JC02765, 1998.

Gijón Mancheño, A.: Restoring mangroves with structures, Phd thesis, Department of Hydraulic Engineering, Faculty of Civil Engineering and Geosciences, Delft University of Technology, in prep.

Gijón Mancheño, A., Herman, P. M. J., Jonkman, S. N., Kazi, S., and Urrutia, I.: Mapping Mangrove Opportunities with Open Access Data : A Case Study for Bangladesh, Sustainability, 13, doi:10.3390/su13158212, 2021a.

Gijón Mancheño, A., Jansen, W., Uijttewaal, W. S. J., Reniers, A. J. H. M., van Rooijen, A. A., Suzuki, T., Etminan, V., and Winterwerp, J. C.: Wave transmission and drag coefficients through dense cylinder arrays: Implications for designing structures for mangrove restoration, Ecological Engineering, 165, 106 231, doi:10.1016/j.ecoleng.2021.106231, 2021b.

Gijón Mancheño, A., Jansen, W., Winterwerp, J. C., and Uijttewaal, W. S. J.: Predictive model of bulk drag coefficient for a nature-based structure exposed to currents, Scientific Reports, 11, 1–13, doi:10.1038/s41598-021-83035-0, 2021c.

Gijón Mancheño, A., Reniers, A. J. H. M., van Wesenbeeck, B. K., van Bijsterveldt, C. E. J., Tas, S. A. J., Wilms, T., Muskanonfola, M., and Winterwerp, J. C.: Restoring eroding mangrove coastlines using nature-based structures, in prep.

Giri, C., Ochieng, E., Tieszen, L. L., Zhu, Z., Singh, A., Loveland, T., Masek, J., and Duke, N.: Status and distribution of mangrove forests of the world using earth, Global Ecology and Biogeography, 20, 154–159, doi:10.1111/j.1466-8238.2010.00584.x, 2011.

Google Earth: Satellite images of Demak, Indonesia between 2015 and 2018, https://earth.google.com/web/. Accessed 2020-10-14., 2020.

Google Earth: Satellite images of Demak, Indonesia between 1994 and 2020, https://earth.google.com/web/. Accessed 2021-06-05., 2021.

Google Earth: Satellite images of Demak, Indonesia between 2007 and 2021, https://earth.google.com/web/. Accessed 2022-03-25., 2022.

Grasmeijer, B. T. and van Rijn, L. C.: Breaker Bar Formation and Migration, in: 26th International Conference on Coastal Engineering, pp. 2750–2758, doi:10.1061/9780784404119.208, 1998.

Greensmith, J. T. and Tucker, E. V.: The origin of Holocene shell deposits in the chenier plain facies of Essex (Great Britain), Marine Geology, 7, 403–425, URL http://repositorio.unan.edu.ni/2986/1/5624.pdf, 1969.

Hallin, C., Larson, M., and Hanson, H.: Simulating beach and dune evolution at decadal to centennial scale under rising sea levels, PLoS ONE, 14, doi:10.1371/journal. pone.0215651, 2019.

Hanson, H., Brampton, A., Capobianco, M., Dette, H. H., Hamm, L., Laustrup, C., Lechuga, A., and Spanhoff, R.: Beach nourishment projects, practices, and objectives - A European overview, Coastal Engineering, 47, 81–111, doi:10.1016/S0378-3839(02)00122-9, 2002.

Haurwitz, B.: Comments on the sea-breeze circulation, Journal of Meteorology, 4,

1–8, doi:10.1175/1520-0469(1947)004<0001:COTSBC>2.0.CO;2, 1947.

Henderson, S. M., Allen, J. S., and Newberger, P. A.: Nearshore sandbar migration predicted by an eddy-diffusive boundary layer model, Journal of Geophysical Research, 109, doi:10.1029/2003JC002137, 2004.

Heward, A. P.: A Review of Wave-Dominated Clastic Shoreline Deposits, Earth-Science Reviews, 17, 223–276, doi:10.1016/0012-8252(81)90022-2, 1981.

Hijma, M. P., Shen, Z., Törnqvist, T. E., and Mauz, B.: Late Holocene evolution of a coupled, mud-dominated delta plain–chenier plain system, coastal Louisiana, USA, Earth Surface Dynamics, 5, 689–710, doi:10.5194/esurf-5-689-2017, 2017.

Hoefel, F. and Elgar, S.: Wave-induced sediment transport and onshore sandbar migration, Science, 299, 1885–1887, doi:10.1126/science.1081448, 2003.

Hogarth, P. J.: The Biology of Mangroves and Seagrasses, Oxford University Press, third edition edn., doi:10.1093/acprof:oso/9780198568704.001.0001, 2015.

Holland, K. T. and Elmore, P. A.: A review of heterogeneous sediments in coastal environments, Earth-Science Reviews, 89, 116–134, doi:10.1016/j.earscirev.2008.03.003, 2008.

Horne, D., O'Neill, B., and Lees, B.: Process implications of chenier dates in Australia, Marine Geology, 353, 163–168, doi:10.1016/j.margeo.2014.04.008, 2014.

Horne, D., Lees, B., Cupper, M., and Fitzsimmons, K.: The development of the Princess Charlotte Bay chenier plain: New results and insights, Marine Geology, 364, 12–20, doi:10.1016/j.margeo.2015.03.004, 2015.

Horstman, E. M., Dohmen-Janssen, C. M., and Hulscher, S. J. M. H.: Flow routing in mangrove forests: A field study in Trang province, Thailand, Continental Shelf Research, 71, 52–67, doi:10.1016/j.csr.2013.10.002, 2013.

Horstman, E. M., Bryan, K. R., and Mullarney, J. C.: Drag variations, tidal asymmetry and tidal range changes in a mangrove creek system, Earth Surface Processes and Landforms, pp. 1–19, doi:10.1002/esp.5124, 2021.

Huh, O. K., Walker, N. D., and Moeller, C.: Sedimentation along the Eastern Chenier Plain Coast: Down Drift Impact of a Delta Complex Shift, Journal of Coastal Research, 17, 72–81, URL https://www.jstor.org/stable/4300150, 2001.

Intergovernmental Panel on Climate Change: IPCC Special Report on the Ocean and Cryosphere in a Changing Climate, URL https://www.ipcc.ch/srocc/, 2019.

Isla, F. I., Vilas, F. E., Bujalesky, G. G., Ferrero, M., Gonzalez Bonorino, G., and Arche Miralles, A.: Gravel drift and wind effects on the macrotidal San Sebastian Bay, Tierra del Fuego, Argentina, Marine Geology, 97, 211–224, doi:10.1016/0025-3227(91)90027-2, 1991.

Isobe, M. and Horikawa, K.: Study on water particle velocities of shoaling and breaking waves, Coastal Engineering in Japan, 23, 109–123, doi:10.1080/05785634.1982.11924340, 1982.

Jolivet, M., Gardel, A., and Anthony, E. J.: Multi-decadal Changes on the Mud-

dominated Coast of Western French Guiana: Implications for Mesoscale Shoreline Mobility, River-mouth Deflection, and Sediment Sorting, Journal of Coastal Research, pp. 185–194, doi:10.2112/SI88-014.1, 2019.

Kathiresan, K. and Bingham, B. L.: Biology of mangroves and mangrove ecosystems, Advances in Marine Biology, 40, 81–251, doi:10.1016/S0065-2881(01)40003-4, 2001.

Kempfert, H. and Raithel, M.: Experiences on Dike Foundations and Land Fills on Very Soft Soils, in: Proceedings of the International Workshop of the International Society for Soil Mechanics and Geotechnical Engineering, 36, pp. 176–181, URL https://www.kup-geotechnik.com/media/2002_kempfert_mexiko.pdf, 2002.

Kim, D., Jo, J., Kim, B., Ryu, J., and Choi, K.: Influence of dike-induced morphologic and sedimentologic changes on the benthic ecosystem in the sheltered tidal flats, Saemangeum area, west coast of Korea, Environmental Pollution, 257, 113 507, doi:10.1016/j.envpol.2019.113507, 2020.

Kuehn, F., Albiol, D., Cooksley, G., Duro, J., Granda, J., Haas, S., Hoffmann-Rothe, A., and Murdohardono, D.: Detection of land subsidence in Semarang, Indonesia, using stable points network (SPN) technique, Environmental Earth Sciences, 60, 909–921, doi:10.1007/s12665-009-0227-x, 2010.

Lang, C.: Kaart van den spoorweg van Samarang naar de Vorstenlanden, http://hdl.handle.net/1887.1/item:811882. Accessed 2020-10-14, 1869.

Lee, H.-J., Chun, S.-S., Chang, J. H., and Han, S. J.: Landward Migration of Isolated Shelly Sand Ridge (Chenier) on the Macrotidal Flat of Gomso Bay, West Coast of Korea: Controls of Storms and Typhoon, Journal of Sedimentary Research, A64, 886–893, doi:10.1306/D4267EF6-2B26-11D7-8648000102C1865D, 1994.

Lesser, G. R., Roelvink, J. A., van Kester, J. A. T. M., and Stelling, G. S.: Development and validation of a three-dimensional morphological model, Coastal Engineering, 51, 883–915, doi:10.1016/j.coastaleng.2004.07.014, 2004.

Lewis, R. R.: Ecological engineering for successful management and restoration of mangrove forests, Ecological Engineering, 24, 403–418, doi:10.1016/j.ecoleng.2004.10.003, 2005.

Lohmann, U., Sausen, R., Bengtsson, L., Cubasch, U., Perlwitz, J., and Roeckner, E.: The Köppen climate classification as a diagnostic tool for general circulation models, Climate Research, 3, 177–193, URL https://www.jstor.org/stable/24863394, 1993.

López-Angarita, J., Roberts, C. M., Tilley, A., Hawkins, J. P., and Cooke, R. G.: Mangroves and people: Lessons from a history of use and abuse in four Latin American countries, Forest Ecology and Management, 368, 151–162, doi:10.1016/j.foreco.2016.03.020, 2016.

Lorenzo-Trueba, J. and Ashton, A. D.: Rollover, drowning, and discontinuous retreat: Distinct modes of barrier response to sea-level rise arising from a simple morphodynamic model, Journal of Geophysical Research: Earth Surface, 119,

779–801, doi:10.1002/2013JF002941, 2014.

Manning, A. J. and Dyer, K. R.: Mass settling flux of fine sediments in Northern European estuaries: Measurements and predictions, Marine Geology, 245, 107–122, doi:10.1016/j.margeo.2007.07.005, 2007.

Marfai, M. A. and King, L.: Monitoring land subsidence in Semarang, Indonesia, Environmental Geology, 53, 651–659, doi:10.1007/s00254-007-0680-3, 2007.

Marfai, M. A., Tyas, D. W., and Nugraha, I.: The morphodynamics of Wulan Delta and its impacts on the coastal community in Wedung subdistrict, Demak regency, Indonesia, Journal of Environmental Protection, 7, 60–71, doi:10.4236/jep.2016.71006, 2016.

Mazda, Y., Kanazawa, N., and Wolanski, E.: Tidal asymmetry in mangrove creeks, Hydrobiologia, 295, 51–58, doi:10.1007/BF00029110, 1995.

Mcbride, R. A., Taylor, M. J., and Byrnes, M. R.: Coastal morphodynamics and Chenier-Plain evolution in southwestern Louisiana, USA: A geomorphic model, Geomorphology, 88, 367–422, doi:10.1016/j.geomorph.2006.11.013, 2007.

Meldahl, K. H.: Pleistocene shoreline ridges from tide-dominated and wave-dominated coasts: northern Gulf of California and western Baja California, Mexico, Marine Geology, pp. 61–72, doi:10.1016/0025-3227(95)80004-U, 1995.

Miller, S. T. K., Keim, B. D., Talbot, R. W., and Mao, H.: Sea breeze: Structure, forecasting, and impacts, Reviews of Geophysics, 41, doi:10.1029/2003RG000124, 2003.

Miththapala, S.: Coastal Ecosystems Series Volume 2: Mangroves, Tech. rep., Ecosystems and Livelihoods Group Asia, IUCN, Colombo, Sri Lanka, 2008.

Morales, J. A., Borrego, J., and Ballesta, M.: Influence of harbour constructions on morphosedimentary changes in the Tinto-Odiel estuary mouth (south-west Spain), Environmental Geology, 46, 151–164, doi:10.1007/s00254-004-1014-3, 2004.

Morales, J. A., Borrego, J., and Davis, R. A.: A new mechanism for chenier development and a facies model of the Saltés Island chenier plain (SW Spain), Geomorphology, 204, 265–276, doi:10.1016/j.geomorph.2013.08.011, 2014.

Murray, A. B.: Contrasting the Goals, Strategies, and Predictions Associated With Simplified Numerical Models and Detailed Simulations, in: Prediction in Geomorphology, edited by Wilcock, P. R. and Iverson, R. M., pp. 151–165, American Geophysical Union (AGU), doi:10.1029/135GM11, 2003.

Nairn, R. B., Roelvink, J. A., and Southgate, H. N.: Transition Zone Width and Implications for Modelling Surfzone Hydrodynamics, in: 22nd International Conference on Coastal Engineering 1990, edited by Edge, B. L., pp. 68–81, American Society of Civil Engineers, doi:10.1061/9780872627765.007, 1991.

Nam, V. N., Sasmito, S. D., Murdiyarso, D., Purbopuspito, J., and MacKenzie, R. A.: Carbon stocks in artificially and naturally regenerated mangrove ecosystems in the Mekong Delta, Wetlands Ecology and Management, 24, 231–244, doi:10.1007/s11273-015-9479-2, 2016.

Nanson, R. A., Vakarelov, B. K., Ainsworth, R. B., Williams, F. M., and Price,

D. M.: Evolution of a Holocene, mixed-process, forced regressive shoreline: The Mitchell River delta, Queensland, Australia, Marine Geology, 339, 22–43, doi:10.1016/j.margeo.2013.04.004, 2013.

Nardin, W. and Fagherazzi, S.: The Role of Waves, Shelf Slope, and Sediment Characteristics on the Development of Erosional Chenier Plains, Geophysical Research Letters, 45, 8435–8444, doi:10.1029/2018GL078694, 2018.

Neal, A., Richards, J., and Pye, K.: Structure and development of shell cheniers in Essex, southeast England, investigated using high-frequency ground-penetrating radar, Marine Geology, 185, 435–469, doi:10.1016/S0025-3227(01)00239-0, 2002.

Neal, A., Richards, J., and Pye, K.: Sedimentology of coarse-clastic beach-ridge deposits, Essex, southeast England, Sedimentary Geology, 162, 167–198, doi:10.1016/S0037-0738(03)00136-2, 2003.

Otvos, E. G.: Cheniers, in: Encyclopedia of Coastal Science, edited by Finkl, C. W. and Makowski, C., pp. 1–5, Springer Nature Switzerland, doi:10.1007/978-3-319-48657-4_67-5, 2019.

Otvos, E. G. and Price, W. A.: Problems of chenier genesis and terminology - An overview, Marine Geology, 31, 251–263, doi:10.1016/0025-3227(79)90036-7, 1979.

Park, Y. A., Chang, J. H., Lee, C. H., and Han, S. J.: Controls of Storms and Typhoons on Chenier Formation in Komso Bay, Western Korea, Journal of Coastal Research, 12, 817–822, URL https://www.jstor.org/stable/4298531, 1996.

Parker, G. and Muto, T.: 1D numerical model of delta reponse to rising sea level, in: 3rd IAHR Symposium on River, Coastal and Estuarine Morphodynamics (RCEM), edited by Sánchez-Arcilla, A. and Bateman, A., pp. 1–10, International Association of Hydraulic Engineering and Research, Barcelona, Spain, 2003.

Partheniades, E.: Erosion and deposition of cohesive soils, Journal of the Hydraulics Division, 91, 105–139, doi:https://doi.org/10.1061/JYCEAJ.0001165, 1965.

Peel, M. C., Finlayson, B. L., and Mcmahon, T. A.: Updated world map of the Köppen-Geiger climate classification, Hydrology and Earth System Sciences, 11, 1633–1644, doi:10.5194/hess-11-1633-2007, 2007.

Penland, S. and Suter, J. R.: The geomorphology of the Mississippi River Chenier Plain, Marine Geology, 90, 231–258, doi:10.1016/0025-3227(89)90127-8, 1989.

Phan, L. K., van Thiel de Vries, J. S. M., and Stive, M. J. F.: Coastal mangrove squeeze in the Mekong Delta, Journal of Coastal Research, 31, 233–243, doi:10.2112/JCOASTRES-D-14-00049.1, 2015.

Pontee, N. I., Tastet, J.-P., and Masse, L.: Morpho-sedimentary evidence of Holocene coastal changes near the mouth of the Gironde and on the Medoc Peninsula, SW France, Oceanologica Acta, 21, 243–261, doi:10.1016/S0399-1784(98)80012-1, 1998.

Proisy, C., Gratiot, N., Anthony, E. J., Gardel, A., Fromard, F., and Heuret, P.: Mud bank colonization by opportunistic mangroves: A case study from French Guiana using lidar data, Continental Shelf Research, 29, 632–641, doi:10.1016/j.csr.2008.09.017, 2009.

Prost, M. T.: Coastal dynamics and chenier sands in French Guiana, Marine Geology, 90, 259–267, doi:10.1016/0025-3227(89)90128-X, 1989.

Pugh, D. T.: Tides, Surges and Mean Sea-Level, John Wiley & Sons Ltd., Chippenham, Wiltshire, UK, reprinted with corrections june 1996 edn., URL http://eprints.soton.ac.uk/id/eprint/19157, 1987.

Pujos, M., Pons, J.-C., and Parra, M.: Les minéraux lourds des sables du littoral de la Guyane française: bilan sur l'origine des dépôts de la plate-forme des Guyanes, Oceanologica Acta, 24, doi:10.1016/s0399-1784(01)00093-7, 2001.

Putranto, T. T. and Rüde, T. R.: Hydrogeological Model of an Urban City in a Coastal Area, Case study: Semarang, Indonesia, Indonesian Journal on Geoscience, 3, 17–27, doi:10.17014/ijog.3.1.17-27, 2016.

Quaresma, V. d. S., Bastos, A. C., and Amos, C. L.: Sedimentary processes over an intertidal flat: A field investigation at Hythe flats, Southampton Water (UK), Marine Geology, 241, 117–136, doi:10.1016/j.margeo.2007.03.009, 2007.

Quartel, S., Kroon, A., Augustinus, P. G. E. F., Van Santen, P., and Tri, N. H.: Wave attenuation in coastal mangroves in the Red River Delta, Vietnam, Journal of Asian Earth Sciences, 29, 576–584, doi:10.1016/j.jseaes.2006.05.008, 2007.

Reniers, A. J. H. M. and Gijón Mancheño, A.: XMgrove: Morphodynamic Mangrove Profile Modeling, manuscript in preparation, in prep.

Reniers, A. J. H. M., Roelvink, J. A., and Thornton, E. B.: Morphodynamic modeling of an embayed beach under wave group forcing, Journal of Geophysical Research, 109, doi:10.1029/2002jc001586, 2004.

Rhodes, E. G.: Depositional model for a chenier plain, Gulf of Carpentaria, Australia, Sedimentology, 29, 201–221, doi:10.1111/j.1365-3091.1982.tb01719.x, 1982.

Richards, D. R. and Friess, D. A.: Rates and drivers of mangrove deforestation in Southeast Asia, 2000-2012, Proceedings of the National Academy of Sciences of the United States of America, 113, 344–349, doi:10.1073/pnas.1510272113, 2016.

Robertson, B., Hall, K., Zytner, R., and Nistor, I.: Breaking waves: Review of characteristic relations, Coastal Engineering Journal, 55, doi:10.1142/S0578563413500022, 2013.

Rodríguez-Ramírez, A. and Yáñez-Camacho, C. M.: Formation of chenier plain of the Doñana marshland (SW Spain): Observations and geomorphic model, Marine Geology, 254, 187–196, doi:10.1016/j.margeo.2008.06.006, 2008.

Roelvink, J. A. and Stive, M. J. F.: Bar-Generating Flow Mechanisms on a Beach, Journal of Geophysical Research, 94, 4785–4800, doi:10.1029/JC094iC04p04785, 1989.

Romme, W. H., Everham, E. H., Frelich, L. E., Moritz, M. A., and Sparks, R. E.:

Are large, infrequent disturbances qualitatively different from small, frequent disturbances?, Ecosystems, 1, 524–534, doi:10.1007/s100219900048, 1998.

Rosen, T. and Xu, Y. J.: Riverine sediment inflow to Louisiana Chenier Plain in the Northern Gulf of Mexico, Estuarine, Coastal and Shelf Science, 95, 279–288, doi:10.1016/j.ecss.2011.09.013, 2011.

Ruessink, B. G., Wijnberg, K. M., Holman, R. A., Kuriyama, Y., and van Enckevort, I. M. J.: Intersite comparison of interannual nearshore bar behavior, Journal of Geophysical Research, 108, doi:10.1029/2002JC001505, 2003.

Ruessink, B. G., Kuriyama, Y., Reniers, A. J. H. M., Roelvink, J. A., and Walstra, D. J. R.: Modeling cross-shore sandbar behavior on the timescale of weeks, Journal of Geophysical Research, 112, doi:10.1029/2006JF000730, 2007.

Russell, R. J. and Howe, H. V.: Cheniers of Southwestern Louisiana, Geographical Review, 25, 449–461, URL https://www.jstor.org/stable/209313, 1935.

Ryu, J.-H., Kim, C.-H., Lee, Y.-K., Won, J.-S., Chun, S.-S., and Lee, S.: Detecting the intertidal morphologic change using satellite data, Estuarine, Coastal and Shelf Science, 78, 623–632, doi:10.1016/j.ecss.2008.01.020, 2008.

Saito, Y., Wei, H., Zhou, Y., Nishimura, A., and Sato, Y.: Delta progradation and chenier formation in the Huanghe (Yellow River) delta , China, Journal of Asian Earth Sciences, 18, 489–497, doi:10.1016/S1367-9120(99)00080-2, 2000.

Schofield, J. C.: Sea level fluctuations during the last 4,000 years as recorded by a chenier plain, Firth of Thames, New Zealand, New Zealand Journal of Geology and Geophysics, 3, 467—-485, doi:10.1080/00288306.1960.10422089, 1960.

Schulz, K., Klingbeil, K., Morys, C., and Gerkema, T.: The Fate of Mud Nourishment in Response to Short-Term Wind Forcing, Estuaries and Coasts, 44, 88–102, doi:10.1007/s12237-020-00767-4, 2021.

Shinn, E. A.: Carbonate Coastal Accretion in an Area of Longshore Transport, NE Qatar, Persian Gulf, in: The Persian Gulf, edited by Purser, B. H., pp. 179–191, Springer, Berlin, Heidelberg, doi:10.1007/978-3-642-65545-6_10, 1973.

Short, A. D.: Chenier research on the Australian coast, Marine Geology, 90, 345–351, doi:10.1016/0025-3227(89)90136-9, 1989.

Short, A. D.: Macro-Meso Tidal Beach Morphodynamics - An Overview, Journal of Coastal Research, 7, 417–436, URL https://www.jstor.org/stable/4297847, 1991.

Soulsby, R. L.: Dynamics of marine sands, Thomas Telford, London, URL http://www.icevirtuallibrary.com/content/book/100318, 1997.

Soulsby, R. L., Hamm, L., Klopman, G., Myrhaug, D., Simons, R. R., and Thomas, G. P.: Wave-current interaction within and outside the bottom boundary layer, Coastal Engineering, 21, 41–69, doi:10.1016/0378-3839(93)90045-A, 1993.

Soulsby, R. L., Manning, A. J., Spearman, J., and Whitehouse, R. J. S.: Settling velocity and mass settling flux of flocculated estuarine sediments, Marine Geology, 339, 1–12, doi:10.1016/j.margeo.2013.04.006, 2013.

Spaans, L.: Cross-shore morphodynamics of intertidal sandbars, Msc thesis, Faculty

of Civil Engineering and Geosciences, Delft University of Technology, URL http://resolver.tudelft.nl/uuid:7f0fe44f-4f8a-44b7-9bbd-23043e1a8e68, 2019.

Stronkhorst, J., Huisman, B., Giardino, A., Santinelli, G., and Duarte Santos, F.: Sand nourishment strategies to mitigate coastal erosion and sea level rise at the coasts of Holland (The Netherlands) and Aveiro (Portugal) in the 21st century, Ocean and Coastal Management, 156, 266–276, doi:10.1016/j.ocecoaman.2017.11.017, 2018.

Svendsen, I. A.: Wave heights and set-up in a surf zone, Coastal Engineering, 8, 303–329, doi:10.1016/0378-3839(84)90028-0, 1984.

Swart, D. H.: Offshore sediment transport and equilibrium beach profiles, Phd thesis, Faculty of Civil Engineering and Geosciences, Delft University of Technology, URL http://resolver.tudelft.nl/uuid:057cb136-5f5b-484a-878d-5616fbaeda4e, 1974.

Tamura, T., Horaguchi, K., Saito, Y., Nguyen, V. L., Tateishi, M., Ta, T. K. O., Nanayama, F., and Watanabe, K.: Monsoon-influenced variations in morphology and sediment of a mesotidal beach on the Mekong River delta coast, Geomorphology, 116, 11–23, doi:10.1016/j.geomorph.2009.10.003, 2010.

Tas, S. A. J., van Maren, D. S., and Reniers, A. J. H. M.: Observations of Cross-Shore Chenier Dynamics in Demak , Indonesia, Journal of Marine Science and Engineering, 8, doi:10.3390/jmse8120972, 2020.

Tas, S. A. J., van Maren, D. S., Helmi, M., and Reniers, A. J. H. M.: Drivers of cross-shore chenier dynamics off a drowning coastal plain, Marine Geology, 445, doi:10.1016/j.margeo.2022.106753, 2022.

Taylor, M. and Stone, G. W.: Beach-Ridges: A Review, Journal of Coastal Research, 12, 612–621, URL https://www.jstor.org/stable/4298509, 1996.

Temmerman, S., Bouma, T. J., Govers, G., Wang, Z. B., de Vries, M. B., and Herman, P. M. J.: Impact of vegetation on flow routing and sedimentation patterns: Three-dimensional modeling for a tidal marsh, Journal of Geophysical Research: Earth Surface, 110, doi:10.1029/2005JF000301, 2005.

Temmerman, S., Meire, P., Bouma, T. J., Herman, P. M. J., Ysebaert, T., and De Vriend, H. J.: Ecosystem-based coastal defence in the face of global change, Nature, 504, 79–83, doi:10.1038/nature12859, 2013.

The WAVEWATCH III Development Group: User manual and system documentation of WAVEWATCH III version 6.07, Tech. rep., NOAA/NWS/NCEP/MMAB, College Park, MD, USA, 2019.

Thomas, N., Lucas, R., Bunting, P., Hardy, A., Rosenqvist, A., and Simard, M.: Distribution and drivers of global mangrove forest change, 1996-2010, PLoS ONE, 12, doi:10.1371/journal.pone.0179302, 2017.

Thompson, R. W.: Tidal Flat Sedimentation on the Colorado River Delta, Northwestern Gulf of California, Geological Society of America, 107, doi:10.1130/MEM107-p1, 1968.

Thornton, E. B., Humiston, R. T., and Birkemeier, W.: Bar/trough generation on a natural beach, Journal of Geophysical Research, 101, 12 097–12 110,

doi:10.1029/96JC00209, 1996.

Toorman, E. A., Anthony, E. J., Augustinus, P. G. E. F., Gardel, A., Gratiot, N., Homenauth, O., Huybrechts, N., Monbaliu, J., Moseley, K., and Naipal, S.: Interaction of Mangroves, Coastal Hydrodynamics, and Morphodynamics Along the Coastal Fringes of the Guianas, in: Threats to Mangrove Forests, edited by Makowski, C. and Finkl, C. W., chap. 20, pp. 429–473, Springer, doi:10.1007/978-3-319-73016-5_20, 2018.

van Bijsterveldt, C. E. J.: Natural mangrove restoration: how can it be induced?, Master thesis, Utrecht University, 2015.

van Bijsterveldt, C. E. J.: Mangrove restoration for coastal protection, Phd thesis, Department of Physical Geography, Faculty of Geosciences, Utrecht University, in prep.

van Bijsterveldt, C. E. J., van Wesenbeeck, B. K., van der Wal, D., Afiati, N., Pribadi, R., Brown, B., and Bouma, T. J.: How to restore mangroves for greenbelt creation along eroding coasts with abandoned aquaculture ponds, Estuarine, Coastal and Shelf Science, 235, 106 576, doi:10.1016/j.ecss.2019.106576, 2020.

van Bijsterveldt, C. E. J., van Wesenbeeck, B. K., Ramadhani, S., Raven, O. V., van Gool, F. E., Pribadi, R., and Bouma, T. J.: Does plastic waste kill mangroves? A field experiment to assess the impact of macro plastics on mangrove growth, stress response and survival, Science of the Total Environment, 756, 143 826, doi:10.1016/j.scitotenv.2020.143826, 2021.

van Bijsterveldt, C. E. J., Debrot, A. O., Bouma, T. J., Maulana, M. B., Pribadi, R., Schop, J., Tonneijck, F. H., and van Wesenbeeck, B. K.: To Plant or Not to Plant: When can Planting Facilitate Mangrove Restoration?, Frontiers in Environmental Science, 9, 1–18, doi:10.3389/fenvs.2021.690011, 2022.

van Bijsterveldt, C. E. J., Herman, P. M. J., van Wesenbeeck, B. K., Ramadhani, S., van Starrenburg, C., Tas, S. A. J., Triyanti, A., Helmi, M., and Bouma, T. J.: Land subsidence of densely populated coasts protected by mangroves offers a preview of global sea level rise effects, manuscript in preparation, in prep.a.

van Bijsterveldt, C. E. J., van der Wal, D., Gijón Mancheño, A., Fivash, G., Helmi, M., and Bouma, T. J.: Can cheniers protect mangroves along eroding coastlines? The effect of contrasting foreshore-types on mangrove stability, manuscript submitted for publication, in prep.b.

van Duin, M. J. P., Wiersma, N. R., Walstra, D. J. R., van Rijn, L. C., and Stive, M. J. F.: Nourishing the shoreface: observations and hindcasting of the Egmond case, The Netherlands, Coastal Engineering, 51, 813–837, doi:10.1016/j.coastaleng.2004.07.011, 2004.

van Ledden, M., van Kesteren, W. G. M., and Winterwerp, J. C.: A conceptual framework for the erosion behaviour of sand-mud mixtures, Continental Shelf Research, 24, 1–11, doi:10.1016/j.csr.2003.09.002, 2004.

van Leussen, W. and Cornelisse, J. M.: The determination of the sizes and settling velocities of estuarine flocs by an underwater video system, Netherlands Journal

of Sea Research, 31, 231–241, doi:10.1016/0077-7579(93)90024-M, 1993.

van Maren, D. S.: Barrier formation on an actively prograding delta system: The Red River Delta, Vietnam, Marine Geology, 224, 123–143, doi:10.1016/j.margeo.2005.07.008, 2005.

van Maren, D. S. and Gerritsen, H.: Residual flow and tidal asymmetry in the Singapore Strait, with implications for resuspension and residual transport of sediment, Journal of Geophysical Research, 117, 1–18, doi:10.1029/2011JC007615, 2012.

van Maren, D. S., van Kessel, T., Cronin, K., and Sittoni, L.: The impact of channel deepening and dredging on estuarine sediment concentration, Continental Shelf Research, 95, 1–14, doi:10.1016/j.csr.2014.12.010, 2015a.

van Maren, D. S., Winterwerp, J. C., and Vroom, J.: Fine sediment transport into the hyper-turbid lower Ems River: the role of channel deepening and sediment-induced drag reduction, in: 12th International Conference on Cohesive Sediment Transport, edited by Harris, C. K., Springer, doi:10.1007/s10236-015-0821-2, 2015b.

van Rijn, L. C.: Principles of sediment transport in rivers, estuaries and coastal seas, Aqua Publications, Amsterdam, the Netherlands, 1993.

van Rijn, L. C.: Erodibility of Mud–Sand Bed Mixtures, Journal of Hydraulic Engineering, 146, 04019 050, doi:10.1061/(asce)hy.1943-7900.0001677, 2020.

van Rijn, L. C., Roelvink, J. A., and ter Horst, W.: Approximation formulae for sand transport by currents and waves and implementation in in DELFT-MOR, Tech. rep., WL — Delft Hydraulics, Delft, the Netherlands, URL http://resolver.tudelft.nl/uuid:c226bf0a-79d6-4357-80ff-c68c4d5f0416, 2001.

van Santen, P., Augustinus, P. G. E. F., Janssen-Stelder, B. M., Quartel, S., and Tri, N. H.: Sedimentation in an estuarine mangrove system, Journal of Asian Earth Sciences, 29, 566–575, doi:10.1016/j.jseaes.2006.05.011, 2007.

Vilas, F. E., Arche, A., Ferrero, M., and Isla, F. I.: Subantarctic macrotidal flats, cheniers and beaches in San Sebastian Bay, Tierra Del Fuego, Argentina, Marine Geology, 160, 301–326, doi:10.1016/S0025-3227(99)00021-3, 1999.

Vos, S., Spaans, L., Reniers, A. J. H. M., Holman, R. A., McCall, R., and de Vries, S.: Cross-shore intertidal bar behavior along the Dutch coast: Laser measurements and conceptual model, Journal of Marine Science and Engineering, 8, 1–21, doi:10.3390/jmse8110864, 2020.

Walstra, D. J. R., Reniers, A. J. H. M., Ranasinghe, R., Roelvink, J. A., and Ruessink, B. G.: On bar growth and decay during interannual net offshore migration, Coastal Engineering, 60, 190–200, doi:10.1016/j.coastaleng.2011.10.002, 2012.

Wang, W., Li, P., and Tan, H.: A Bayhead Chenier, Chengwan Bay, South China, Journal of Coastal Research, pp. 212–222, URL https://www.jstor.org/stable/25737036, 2004.

Wang, Y. and Ke, X.: Cheniers on the east coastal plain of China, Marine Geology, 90, 321–335, doi:10.1016/0025-3227(89)90134-5, 1989.

Weill, P., Tessier, B., Mouazé, D., Bonnot-Courtois, C., and Norgeot, C.: Shelly cheniers on a modern macrotidal flat (Mont-Saint-Michel bay, France) - Internal architecture revealed by ground-penetrating radar, Sedimentary Geology, 279, 173–186, doi:10.1016/j.sedgeo.2010.12.002, 2012.

Winterwerp, J. C.: On the sedimentation rate of cohesive sediment, in: Estuarine and Coastal Fine Sediments Dynamics: Intercoh 2003, edited by Maa, J. P. Y., Sanford, L. P., and Schoellhamer, D. H., vol. 8, pp. 209–226, Elsevier B.V., doi:10.1016/S1568-2692(07)80014-3, 2007.

Winterwerp, J. C., Erftemeijer, P. L. A., Suryadiputra, N., van Eijk, P., and Zhang, L.: Defining eco-morphodynamic requirements for rehabilitating eroding mangrove-mud coasts, Wetlands, 33, 515–526, doi:10.1007/s13157-013-0409-x, 2013.

Winterwerp, J. C., Albers, T., Anthony, E. J., Friess, D. A., Gijón Mancheño, A., Moseley, K., Muhari, A., Naipal, S., Noordermeer, J., Oost, A., Saengsupavanich, C., Tas, S. A. J., Tonneijck, F. H., Wilms, T., van Bijsterveldt, C. E. J., van Eijk, P., van Lavieren, E., and van Wesenbeeck, B. K.: Managing erosion of mangrove-mud coasts with permeable dams – lessons learned, Ecological Engineering, 158, 106 078, doi:10.1016/j.ecoleng.2020.106078, 2020.

Wodehouse, D. C. J. and Rayment, M. B.: Mangrove area and propagule number planting targets produce sub-optimal rehabilitation and afforestation outcomes, Estuarine, Coastal and Shelf Science, 222, 91–102, doi:10.1016/j.ecss.2019.04.003, 2019.

Woodroffe, C. D. and Grime, D.: Storm impact and evolution of a mangrove-fringed chenier plain, Shoal Bay, Darwin, Australia, Marine Geology, 159, 303–321, doi:10.1016/S0025-3227(99)00006-7, 1999.

Woodroffe, C. D., Curtis, R. J., and Mclean, R. F.: Development of a chenier plain, Firth of Thames, New Zealand, Marine Geology, 53, 1–22, doi:https://doi.org/10.1016/0025-3227(83)90031-2, 1983.

Worthington, T. A., Andradi-Brown, D. A., Bhargava, R., Buelow, C., Bunting, P., Duncan, C., Fatoyinbo, L., Friess, D. A., Goldberg, L., Hilarides, L., Lagomasino, D., Landis, E., Longley-Wood, K., Lovelock, C. E., Murray, N. J., Narayan, S., Rosenqvist, A., Sievers, M., Simard, M., Thomas, N., van Eijk, P., Zganjar, C., and Spalding, M.: Harnessing Big Data to Support the Conservation and Rehabilitation of Mangrove Forests Globally, One Earth, 2, 429–443, doi:10.1016/j.oneear.2020.04.018, 2020.

Wright, L. D. and Short, A. D.: Morphodynamic variability of surf zones and beaches: A synthesis, Marine Geology, 56, 93–118, doi:10.1016/0025-3227(84)90008-2, 1984.

Xie, D., Schwarz, C., Brückner, M. Z. M., Kleinhans, M. G., Urrego, D. H., Zhou, Z., and van Maanen, B.: Mangrove diversity loss under sea-level rise triggered by bio-morphodynamic feedbacks and anthropogenic pressures, Environmental Research Letters, 15, 114 033, doi:10.1088/1748-9326/abc122, 2020.

Xie, D., Schwarz, C., Kleinhans, M. G., Zhou, Z., and van Maanen, B.: Implications of Coastal Conditions and Sea-Level Rise on Mangrove Vulnerability: A

Bio-Morphodynamic Modeling Study, Journal of Geophysical Research: Earth Surface, 127, e2021JF006 301, doi:10.1029/2021JF006301, 2022.

Yan, Q., Xu, S., and Shao, X.: Holocene cheniers in the Yangtze Delta, China, Marine Geology, 90, 337–343, doi:10.1016/0025-3227(89)90135-7, 1989.

Yang, B. C., Dalrymple, R. W., and Chun, S.-S.: Sedimentation on a wave-dominated , open-coast tidal flat, south- western Korea: summer tidal flat – winter shoreface, Sedimentology, 52, 235–252, doi:10.1111/j.1365-3091.2004.00692.x, 2005.

Zhao, X.: Cheniers in China: An overview, Marine Geology, 90, 311–320, doi:10.1016/0025-3227(89)90133-3, 1989.

List of symbols

Roman letters

A	orbital excursion length [m]
a	wave amplitude [m]
C	Chézy coefficient [$m^{1/2}/s$]
c	sediment concentration [kg/m^3]
D	depositional flux [$kg/m/^2/s$]
D_p	peak wave direction [degree]
D_{50}	median sediment diameter [m]
D_{90}	90th percentile sediment diameter [m]
E	erosion flux [$kg/m/^2/s$]
f_{SUSW}	user-defined tuning parameter for suspended sediment transport due to wave asymmetry effects in Delft3D [-]
f_w	wave friction factor [-]
g	gravitational acceleration [m/s^2]
H	height of chenier crest [m]
H_{rms}	root-mean-square wave height [m]
H_s	significant wave height [m]
h	water depth [m]
h_{top}	water depth on top of the chenier crest [m]
k	wave number [m^{-1}]
k_s	Nikuradse roughness height [m]
M	sediment mobility number [-]
M_e	excess sediment mobility number [-]
M_{ero}	erosion parameter [$kg/m/^2/s$]
p	pressure [Pa]
S_b	bed load transport [kg/m/s]
$S_{b,c}$	bed load transport due to currents alone [kg/m/s]
$S_{b,w}$	bed load transport due to waves alone [kg/m/s]
S_s	suspended sediment load [kg/m/s]
$S_{s,w}$	suspended sediment transport due to wave asymmetry effects [kg/m/s]
$S(\tau_{\text{cw}}, \tau_{\text{cr,e}})$	erosion function [-]
s	relative sediment density [-]
T	frequency-dependent transfer function [-]
T_p	peak wave period [s]

t	time [s]
U	depth-averaged velocity in x-direction [m/s]
U_A	velocity asymmetry value [m/s]
U_{off}	offshore-directed, high-frequency near-bed orbital velocity [m/s]
U_{on}	onshore-directed, high-frequency near-bed orbital velocity [m/s]
u	instantaneous velocity (in x-direction) [m/s]
$\overline{u}$	time-averaged velocity [m/s]
$\widetilde{u}$	velocity due to short wave motion [m/s]
u_{ig}	velocity due to infragravity waves [m/s]
u_{orb}	peak orbital velocity [m/s]
u_{10}	wind speed at 10m elevation [m/s]
v	instantaneous velocity (in y-direction) [m/s]
v_{cr}	critical velocity for the initiation of motion [m/s]
v_{eff}	effective velocity due to waves and currents [m/s]
v_{R}	magnitude of the depth-averaged current velocity [m/s]
w_s	settling velocity [m/s]
x	x-coordinate [m]
x_B	x-coordinate of back-barrier face [m]
x_C	x-coordinate of chenier center [m]
x_S	x-coordinate of beachface toe [m]
x_T	x-coordinate of chenier toe [m]
y	y-coordinate [m]
z	z-coordinate [m]
z_B	z-coordinate of back-barrier face [m]
z_C	z-coordinate of chenier center [m]
z_S	z-coordinate of beachface toe [m]
z_T	z-coordinate of chenier toe [m]

Greek letters

α	chenier toe slope [-]
β	offshore shoreface slope [-]
γ	phase lag coefficient [-]
Δx	horizontal displacement chenier center [m]
Δx_{st}	seaward displacement as result of storm season [m]
Δz	vertical displacement chenier center [m]
$\epsilon_{s,x}$	horizontal eddy diffusivity [m^2/s]
η	water surface elevation [m]
θ	tidal phase lag [min]
ρ_s	sediment density [kg/m^3]
ρ_w	water density [kg/m^3]
τ_c	bed shear stress due to current alone [N/m^2]
$\tau_{\text{cr,e}}$	critical bed shear stress for erosion [N/m^2]
τ_{cw}	maximum bed shear stress due to currents and waves [N/m^2]

τ_w	bed shear stress due to waves alone [N/m^2]
φ	angle between current direction and direction of wave propagation [-]
ϕ_p	pressure phase shift [-]
ϕ_u	velocity phase shift [-]
ω	wave angular frequency [s^{-2}]

Abbreviations

ADV	Acoustic Doppler Velocimeter
DGPS	Differential Global Positioning System
D3D	Delft3D
FFT	Fast Fourier Transform
MSL	Mean Sea Level
N	North
NW	North West
pdf	probability density function
RMSE	Root Mean Square Error
SE	South East
S#	location of frame with instruments, with frame number #

Acknowledgements

Over the last five years, there have been moments where I really didn't think I would ever reach this point. It is thanks to many wonderful people that I am writing these very last words of my dissertation today. I will be forever grateful for their support.

First and foremost, thank you to my supervisors Ad, Bas and Han. Although the title page shows only one promotor, I definitely consider all three my promotors. Bas, you taught me so much. Your questions always lead to significant improvements and you helped me with my first steps toward becoming an independent researcher. The way you were always able to reduce my extremely long and way too descriptive sentences to short and to the point messages was a big help. I can only wish to approach your writing skills one day. Ad, your endless ideas and inspiration kept me going even after I was truly convinced we had exhausted all options. But even more important, your care for the wellbeing of everyone around you is incredible. You helped me through the difficult patches of not only the typical PhD roller coaster ride, but also an unprecedented and at times overwhelming pandemic. Han, thank you for initiating the BioManCO project and bringing us all together. This thesis may have turned out completely different to what you had in mind at the start (the word 'chenier' wasn't even mentioned in the entire proposal and there's definitely more sand than mud in my chapters), but you fully supported me and believed in me. Together, you were truly complementary and the best supervisory team I could have asked for. Thank you so much!

While a PhD can seem a very lonely task, I was immeasurably lucky to have two amazing colleagues by my side: Alejandra and Celine. From our first steps in Indonesia ('there are no mosquitoes here'), through countless hoops for the research permit ('smile and wave'), to field work fails (broken instruments, absent waves, missing trees) but also field work triumphs (celebrated with pizza from Trattoria or homemade pancakes in Timbulsloko), and back to our desks in the Netherlands (and the shared struggle of finishing our PhDs), you were with me at every step along the road and I couldn't have done it without you. It makes me really happy that you'll be the paranymphs at my defence. Thanks for this unforgettable journey!

I also would like to thank all other people involved in the BioManCO project. The rest of the BioManCO team (Wim, Tjeerd, Peter, Bregje), our monthly meetings often lead to fruitful discussions, benefiting from the different backgrounds and expertise. Our colleagues at UNDIP, with special thanks to Pak Helmi, for his supervision, translation of the summary to Bahasa Indonesia and his endless

efforts in making this collaboration successful, as well as Pak Max, Pak Rudhi, Aris, Ibu Tita for their advice and support, and the many students who helped us in the field. I would like to thank the families of Pak Slamet and Pak Saeri for hosting us during the field work, Pak Muis for helping us communicate, and all the fishermen who accompanied and assisted us in the field.
At TU Delft, I was surrounded by a great group of colleagues. Special thanks go to our Covid-coffee-Skype crew (Carine, Sotiria, Marion, Lennart and Floris): our Skype sessions were a true beacon of joy in those weird and difficult lockdown months. Sabine, Irene, Alejandra, it was a pleasure sharing 2.94 with you, the milk frother and the almost-dead tree. Anne, BwN-buddy, grading assignments became much more enjoyable with you. The CEG PhD council, for being a group of like-minded people wanting to make our faculty an even better place. I also want to thank all other HE PhDs, postdocs and staff with whom I crossed paths these last five years, be it over drinks at PSOR, during lunch or random coffee breaks: it was always interesting to learn about your research, share highlights and moments of misery, or hear about your weekend exploits. Thank you for providing such a welcoming atmosphere!
Tenslotte wil ik ook graag alle vrienden bedanken die me hebben gesteund de afgelopen jaren. MGLD, hard trainen en gezellig chillen (incl. thee, puzzels en spelletjes) bleken het ideale tegengif voor PhD-stress. Mama, papa, Gilles en Jana, jullie zijn de definitie van onvoorwaardelijke liefde. Dankjewel.

Silke Tas
Delft, May 2022

List of Publications

Journal articles

Tas, S.A.J., van Maren, D.S. and Reniers, A.J.H.M. (2020). Observations of Cross-Shore Chenier Dynamics in Demak, Indonesia. *Journal of Marine Science and Engineering*, 8(972).

Parts of this manuscript are discussed in Chapter 3

Tas, S.A.J., van Maren, D.S., Helmi, M. and Reniers, A.J.H.M. (2022). Drivers of cross-shore chenier dynamics off a drowning coastal plain. *Marine Geology*, 445(106753).

Parts of this manuscript are discussed in Chapter 4

Winterwerp, J.C., Albers, T., Anthony, E.J., Friess, D.A., Gijón Mancheño, A., Moseley, K., Muhari, A., Naipal, S., Noordermeer, J., Oost, A., Saengsupavanich, C., **Tas, S.A.J.**, Tonneijck, F.H., Wilms, T., van Bijsterveldt, C.E.J., van Eijk, P., van Lavieren, E. and van Wesenbeeck, B.K. (2020). Managing erosion of mangrove-mud coasts with permeable dams - lessons learned. *Ecological Engineering*, 158(106078).

Conferences

Tas, S.A.J., Gijón Mancheño, A., Herman, P.M.J., Reniers, A.J.H.M., Uijttewaal, W.S.J. and Winterwerp, J.C. (2017). Wave transformation on the mangrove-mud coast of Demak, Indonesia. Poster presented at *14th International Conference on Cohesive Sediment Transport (INTERCOH 2017)* in Montevideo, Uruguay, 13-17 November 2017 (3rd place poster award).

Gijòn Mancheño, A., **Tas, S.A.J.**, Herman, P.M.J., Reniers, A.J.H.M., Uijttewaal, W.S.J. and Winterwerp, J.C. (2017). Wave attenuation by brushwood dams in a mud-mangrove coast. Poster presented at *14th International Conference on Cohesive Sediment Transport (INTERCOH 2017)* in Montevideo, Uruguay, 13-17 November 2017 (3rd place poster award).

Tas, S.A.J., van Bijsterveldt, C.E.J., Reniers, A.J.H.M. and van Maren, D.S. (2019). Chenier dynamics on an eroding mangrove-mud coast in Demak, Indonesia. Poster presented at *NCK days 2019 (Netherlands Centre for Coastal Research)* in Enkhuizen, the Netherlands, 20-23 March 2019 (voted best poster of the day).

Tas, S.A.J., van Maren, D.S. and Reniers, A.J.H.M. (2019). Chenier dynamics at an eroding mangrove-mud coastline in Demak, Indonesia. Oral presentation at *11th River, Coastal and Estuarine Morphodynamics Symposium (RCEM 2019)* in Auckland, New Zealand, 16-21 November 2019.

Tas, S.A.J., Helmi, M., van Maren, D.S. and Reniers, A.J.H.M. (2019). Restoring mangroves in Demak: The role of cheniers. Online oral presentation at *6th International Conference on Tropical and Coastal Region Eco-Development (ICTCRED 2020)* in Semarang, Indonesia, 27-28 October 2020.

Tas, S.A.J., Gijón Mancheño, A., van Bijsterveldt, C.E.J., Helmi, M., Winterwerp, J.C., van Maren, D.S. and Reniers, A.J.H.M. (2021). Modelling cross-shore chenier dynamics on a drowning coastal plain. Online oral presentation at *8th edition of the Coastal Dynamics Conference* in Delft, the Netherlands, 28 June-2 July 2021.

Curriculum Vitae

May 13, 1993 Born in Ghent, Belgium

Education

2005 - 2011 Algemeen Secundair Onderwijs, richting Latijn-wiskunde
Koninklijk Atheneum Voskenslaan, Ghent, Belgium

2011 - 2014 Bachelor of Science in Civil Engineering (cum laude)
Delft University of Technology, the Netherlands
Minor in Mathematics and Modeling at Virginia Tech, USA
BSc thesis ”The influence of depth on a ROFI”

2014 - 2016 Master of Science in Civil Engineering (cum laude)
Delft University of Technology, the Netherlands
MSc thesis ”Coastal protection in the Mekong Delta” in Vietnam, in collaboration with University of Danang and GIZ, funded by an EMMA scholarship

2016 - present PhD candidate at section of Environmental Fluid Mechanics
Delft University of Technology, the Netherlands

Awards and scholarships

2015 Nomination Student Inspiration Award
Delft University of Technology, the Netherlands

2016 Erasmus Mundus Mobility with Asia (EMMA) scholarship
European Education and Culture Executive Agency (EACEA)

Over the last decades, mangrove forests have suffered immense and rapid losses worldwide. Unfortunately, many rehabilitation attempts have failed, lacking a thorough system understanding of mangrove-mud coasts. Some mangrove-mud coasts are protected on their seaward side by sandy ridges (called 'cheniers'). In order to sustainably restore mangrove-mud coasts, chenier dynamics need to be understood at the temporal and spatial scales relevant for mangrove establishment (daily to yearly variability driven by waves and tides). This dissertation aims to advance our understanding of chenier dynamics within the context of an eroding mangrove-mud coast.

